The Role of Large Woody Debris on Sandy Beach-Dune Morphodynamics

by

Michael J. Grilliot

B.Sc., Ohio University, 2007

M.Sc., Western Washington University, 2009

A Dissertation Submitted in Partial Fulfillment of the

Requirements for the Degree of

DOCTOR OF PHILOSOPHY

in the Department of Geography

The Role of Large Woody Debris on Sandy Beach-Dune Morphodynamics

by

Michael J. Grilliot

B.Sc., Ohio University, 2007

M.Sc., Western Washington University, 2009

Supervisory Committee

Dr. Ian J. Walker, Supervisor

Adjunct Professor, Department of Geography, University of Victoria

Professor, School of Geographical Sciences & Urban Planning, Arizona State University

Professor, School of Earth & Space Exploration, Arizona State University

Dr. Bernard O. Bauer, Member

Adjunct Professor, Department of Geography, University of Victoria

Professor, School of Arts and Sciences, University of British Columbia Okanagan

Dr. James V. Barrie, Outside Member

Professor, School of Earth and Ocean Sciences, University of Victoria

Abstract

Coastal foredune evolution involves complex processes and controls. Although a great deal is known about the effects of vegetation cover, moisture, and fetch distance on sediment supply, and of topographic forcing on airflow dynamics, the role of large woody debris (LWD) as a modulator of sediment supply and a control on foredune growth is understudied. Large assemblages of LWD are common on beaches near forested watersheds and collectively have a degree of porosity that increases aerodynamic roughness and provides substantial sand trapping volume. To date, no research has attempted to understand the geomorphic role that LWD matrices, as a whole, have as roughness elements affecting airflow and sediment transport across a beach-dune system, or, what the long-term implications of these impacts are on beach and foredune erosion recovery and evolution. This four-year research initiative investigated the role of a LWD matrix on beach-dune morphodynamics on West Beach, Calvert Island on the central coast of British Columbia, Canada.

This study integrated data from research that spanned three temporal scales, 1) event-scale (10 min) flow and sediment transport patterns, 2) daily frequency and relative magnitude of landscape changing events, 3) seasonal to interannual-scale volumetric and LWD changes. An event-scale experiment to characterise airflow dynamics and related sand transport patterns showed that LWD distinctly alters wind flow patterns and turbulence levels from that of incoming flow over a flat beach. Overall, mean wind speed and fluctuating flow properties declined as wind transitioned across the LWD. Streamwise mean energy was converted to turbulent energy, however, the reductions in mean flow properties were too great for the increased streamwise turbulence to have an effect on transport. In response to these flow alterations and more limited sand transport pathways to the foredune, sediment flux was reduced by 99% in the LWD compared to the open beach, thereby reducing sand supply to the foredune. Sand grains rebounding off of the LWD were carried higher into the flow field resulting in greater mass flux recorded at 20-50 cm in the LWD as opposed to the flat beach. This effect was only recorded 6 m into the LWD. As such, LWD has the potential to modulate rates of foredune recovery, growth, and evolution.

Time-lapse photography collected at 15 min intervals during the study revealed that storm events lead to wave-induced erosion of the backshore and reworking of the LWD matrix. The exposed LWD matrix subsequently traps aeolian sediment that leads to rapid burial of the LWD and building of a raised platform for emergent vegetation. However, infilling of the accommodation space within the LWD matrix is so rapid, that sediment starvation of the foredune is short-lived. While the LWD at this site does trap sediment in the backshore, helping to protect the dune from scarping, LWD at this study site maintains an overall lower impact on transport to the foredune. Critical to this relationship is the frequency and magnitude of nearshore events that erode the beach periodically and re-organize the LWD matrix, which directly impacts the ability of LWD to store sediment and modulate transport to the foredune. A conceptual model exploring these relationships is presented.

Contents

List of Figures

List of Tables

List of Equations

List of Appendices

Acknowledgments

The author is grateful for the opportunity and recognizes that the study took place on the traditional territory of the Heiltsuk First Nation and Wuikinuxv Nation.

I would like to acknowledge the Hakai Institute, notably Eric Peterson and Christina Munck, as research partners and for providing logistical support. I cannot thank the Hakai Institute and all of its staff enough for the opportunity to study one of the earth's true wilderness treasures. I encourage anyone reading this to explore www.hakai.org to discover a wealth of science and knowledge openly available on British Columbia's coastal margin.

This research was supported financially by the Tula Foundation through a Hakai Ph.D. Fellowship, the University of Victoria Geography Department, University of Victoria Scholarships, Derek Sewell Scholarships, University of Victoria Graduate Student Society Travel Grants, and from NSERC Discovery and Canadian Foundation for Innovation Leaders Opportunity Fund grants to Ian Walker.

Special thanks are reserved for the staff of the Hakai Institute's Calvert Ecological Observatory without whom this research would not be possible. Your generosity and friendship over the years has left a lasting impression upon my soul, and I thank you for all of your hard work and dedication. I owe a sincere debt of gratitude to Derek Heathfield, my fieldwork brother, with whom I would fight a dragon. I could not ask for a better companion to explore the beaches of Calvert Island and conduct fieldwork; your dedication to the task at hand, whether that is carrying a laser scanner through muck and rain or sharing a laugh, is forever appreciated and never undervalued. A special thanks to: Alana Rader and Felipe Gomez for their friendship, assistance in the field, and for creating unforgettable memories in one of the most beautiful places on earth; the Hakai Geospatial team: notably Keith Holmes, Luba Reshitnyk, and Will McInnes for your field assistance, and technical guidance; my lab mates and friends at the University of Victoria, Georgia Clyde, Ian Darke, Jordan Eamer, Steffi Rohland, Robin Kite, Alex Lausanne, and Dr. Dan Shugar for their comradery and support; and

undergraduates Nhan Nguyen and Jessica MacLean for staring at seemingly endless hours of time-lapse footage for me.

I wish to thank all of my committee members who were instrumental partners on this journey, providing direction and encouragement. I would like to say a special thanks to my advisor, Dr. Ian Walker, whose guidance and professionalism cannot be overstated. Thank you for accepting me into your dune family, always having an open door, and challenging me to become a better researcher. Also, thanks to Dr. Bernie Bauer for his expert assistance in the field and whose coastal knowledge is unparalleled. I have learned so much from you that without your guidance on experiment design, setup, implementation, data processing, and critical thinking, this work would not be of the quality it is.

I would like to thank previous influential educators for inspiring me in various ways; Dan Smith (Lancaster High School) for feeding my curiosity and passion of the cosmos and all things science, Dr. Dorothy Sack (Ohio University) for challenging me to take the leap to the west coast, Dr. Tom Terich (Western Washington University) for introducing me to the splendor of beaches, and Dr. Chris Suczek (Western Washington University) for showing me that sediments are exciting.

Most importantly, I want to thank my family who supported me during this journey. My wife Sarah, for her unwavering love and support through these trials. She is my best friend and confidant, offering emotional support and encouragement when the task ahead seemed insurmountable. She has been infinitely patient and understanding of my struggles and deserves the excitement and joy of completing this degree as much as I do. I thank you from the bottom of my heart. My parents, Chris and Jim, for instilling in me a passion for learning and challenging me to be the best I can. My brother, Matt and his family, for taking the time to create memories and reminding me that family always comes first. I love you all, and thank you.

Dedication

To all those who seek to protect this planet.

“It has been said that astronomy is a humbling and character-building experience. There is perhaps no better demonstration of the folly of human conceits than this distant image of our tiny world. To me, it underscores our responsibility to deal more kindly with one another, and to preserve and cherish the pale blue dot, the only home we've ever known.”

— Carl Sagan, Pale Blue Dot: A Vision of the Human Future in Space

1. Introduction

1.1 Investigating the geomorphic role of beached large woody debris (LWD): an opportunity to better understand beach-dune systems.

Beached LWD[1] (colloquially known as driftwood) has been an ever present part of Canadian west coastal ecosystems since forest stands began to recolonize during the last deglaciation (Stembridge, 1979; Eamer et al., 2017). Recent research has shown that at least parts of British Columbian coastal islands have been ice free since at least 14,500 cal yr BP (McLaren et al., 2014; Shugar et al., 2014). Pollen data shows that sparse stands of shore pine (*Pinus contorta*) dominated the first forests in British Columbia following deglaciation, with expanding western hemlock (*Tsuga heterophylla*) creating mixed-conifer and red alder (*Alnus rubra*) dominated forests by the early Holocene (Eamer et al., 2017). The cypress family (Cupressaceae) has dominated since 8.3 ka cal B.P. with the western red cedar (*Thuja plicata*) population migrating north from stands in Washington State and Oregon, USA (Hebda and Mathewes, 1984; Eamer et al., 2017). The highly productive forest growth on the coast of British Columbia has provided the main source of wood that enters the marine environment, a portion of which comes to rest on the shoreline. Although, it also possible for decay and insect resistant logs to travel vast distances and even across oceans, depositing non-native wood on the shore (Adams et al., 2000).

LWD can enter the marine environment in many ways. The steep slopes of many British Columbia shorelines afford the potential for landslide deposits to enter the ocean, delivering vast quantities of LWD in episodic events (West et al., 2011; Ruiz-Villanueva et al., 2014). Subaerial landslides entering the ocean, along with submarine landslides, displacement by submarine earthquakes, or the impact of bodies in the ocean can also cause tsunamis that can strip the ground bare, washing extensive forest stands into the ocean (Clague et al., 2003; Hara et al., 2016; Tomita et al., 2016; Higman et al., 2018). Terrestrial landslides can also deliver

[1] LWD is classified as dead wood in many stages of decomposition and generally defined as having a minimum diameter of 0.1 m and length of 1 m (Harmon and Hua, 1991; Marshall and Davis, 2002; Wallerstein and Thorne, 2004; Marburg et al., 2006).

mass quantities of LWD to streams and rivers that can find their way to the ocean during anomalously high flows or outburst floods caused by temporary damming by sediment or logjams (Nakamura et al., 2000; Gomi et al., 2001; May and Gresswell, 2003a, 2003b; Reeves et al., 2003; West et al., 2011). Forest fires, pest infestations, and logging, can also provide large amounts of dead trees or slash and expose soil that increase short-term erosion rates and recruitment of LWD to river channels and, eventually, the ocean (Wells, 1987; Jakob, 2000; Guthrie, 2002; Roberts et al., 2004; Sidle et al., 2006; Hassan et al., 2008; Wolter et al., 2010; Langhans et al., 2017; Parise and Cannon, 2017). Industrial scale logging since the mid 1800's has increased the amount of LWD appearing in the marine environment due to shipwrecks, escapement from log booms, and decreased recruitment and residency in river channels (Edgell and Ross, 1983; Gonor et al., 1988; Bilby and Ward, 1991; Ralph et al., 1994; Green et al., 2014; Scott and Wohl, 2018).

In the 1800s, many rivers in the Pacific Northwest were documented to have multiple driftwood jams blocking river flows with one to two times as much LWD than present amounts (Sedell et al., 1988; Collins et al., 2002). LWD in logjams on rivers and in estuaries was systematically removed to improve navigation up until the late 1980s substantially reducing the amount of wood in waterways (Gonor et al., 1988; Sedell et al., 1988, 1991). While natural wood in rivers decreased as a result, cut log abundance on marine shorelines increased due to escapement from log transport (Waelti and MacCleod, 1971; Edgell and Ross, 1983; Sedell et al., 1991). In the 1970's, shorelines near logging transport operations held approximately 50 % cut logs and only 15 % natural sourced (with root wads) and the rest undistinguishable (Dayton, 1971; Gonor et al., 1988). A more recent report showed approximately 60 to 90 % of LWD volume on sample shorelines near Vancouver, BC, Canada, was comprised of cut logs, depending on distance to log transporting routes (Williams and Cooper, 2000). Even though cut log abundance is increasing, the total volume of wood on shorelines has generally decreased since the mid 1900s due to logging, and direct harvesting (Terich and Milne, 1977; Bilby and Ward, 1991; Maclennan, 2005; Heathfield and Walker, 2011).

Logs that enter the marine environment can be colonized and dissolved by organisms, transported vast distances, and possibly washed ashore to rest on the coastal margin. Many

marine species of worms (e.g., *Teredo navalis*) and isopods (native: *Limnoria lignorum*, invasive: *L. tripunctata*) in the Pacific Northwest are capable of deteriorating log mass in short (days) timespans to the effect of breakup and disintegration or becoming waterlogged and sunk (Gonor et al., 1988; Ray, 2005). Logs that are not degraded or sunk can travel vast distances, carried by ocean currents that are primarily responsible for LWD transport (Strong and Skolmen, 1963; Adams et al., 2000). Whether the log is from a local or distant source, there is a good chance the log would be deposited on a shoreline. In the Pacific Northwest, logs can be thrown onto rocky shorelines by high wave events, deposited in estuaries and marshes during high tide events or storm surges, left stranded on steep gravel beaches, or delivered to sandy beach-dune ecosystems (Gonor et al., 1988; Walker and Barrie, 2006). The latter are the focus of this dissertation and are important and rare environments in BC as they support rare and listed, under the Species at Risk Act, flora and fauna, and are threatened by invasive species, habitat loss, and climate change (Page et al., 2011).

The geomorphic role of LWD in sandy beach-dune coastal ecosystems has been largely understudied compared to fluvial and lake systems (Keller and Swanson, 1979; Maser et al., 1988; Sedell et al., 1988; Nakamura and Swanson, 1993; Christensen et al., 1996; Kail, 2003; Wallerstein and Thorne, 2004; Walker and Barrie, 2006; Brauns et al., 2007; Eamer and Walker, 2010; Heathfield and Walker, 2011). Initial research from the 1970's and 80's suggested that LWD could potentially stabilize beaches and capture sediment (Stembridge, 1975, 1979; Terich and Milne, 1977), while more recent investigations have attempted to quantify this potential impact (Eamer and Walker, 2010; Heathfield and Walker, 2011). To date, no research has attempted to understand the geomorphic role that LWD matrices, as a whole, have as roughness elements affecting airflow and sediment transport across a beach-dune system, or, what the long-term implications of these impacts are on beach and foredune erosion recovery and evolution. Thus, a timely opportunity exists to explore the broader geomorphic role of LWD on Pacific Northwest sandy beaches through the following research objectives:

1) Quantify the effects of LWD on near-surface airflow fronting a coastal foredune. The purpose of this objective was to improve our understanding of LWD matrices as a roughness element and modifier of flow dynamics over the beach fronting a scarped foredune. Three-

dimensional airflow and turbulence properties were characterized during event-scale sand transport using sonic anemometry. This objective is addressed in Section 2.

2) Quantify the effects of LWD on sediment transport and morphology fronting a coastal foredune. The purpose of this objective was to improve our understanding of the impact of LWD matrices on event-based sediment transport and explore the implications for scarped dune recovery and rebuilding. Sediment transport patterns are closely coupled with alterations to the turbulent boundary layer in section 2. The implications of the sediment transport patterns are explored by measuring volumes and resulting morphology of the event-based study area over many months using independent terrestrial laser scan (TLS) surveys. This objective is addressed in Section 3.

3) Determine the long-term impacts of the presence of a LWD matrix on a beach-dune system. The purpose of this objective was to evaluate the long-term impact of the event-based experiment results within the overall wave and wind transport regime. To this end, the frequency and magnitude of morphology changing events was recorded over four years in an effort to better understand the effects of LWD on beach-dune processes. From these data, a conceptual model is presented describing the various morphological states of a beach-dune system fronted with LWD. This objective is addressed in Section 3.

Addressing these objectives together will help describe the role of LWD in altering beach-dune morphodynamics.

1.2 Research Context

1.2.1 The geomorphic role of LWD in the Pacific Northwest

LWD has a unique position amongst ecosystem function providers because it provides a critical link between the aquatic and terrestrial ecosystems (Marburg et al., 2006). LWD is well documented in forest, lake, riparian, and fluvial environments providing various ecosystem functions, including: creating unique substrate, reducing erosion, providing shade and habitat for many decomposers and heterotrophs, affecting soil development, increasing biodiversity, storing nutrients (namely carbon) and water, and serving as seedbeds (Keller and Swanson, 1979; Sedell et al., 1988; Maser et al., 1988; Harmon and Hua, 1991; Nakamura and Swanson,

1993; Christensen et al., 1996; Gurnell et al., 2002; Kail, 2003; Wallerstein and Thorne, 2004; Brauns et al., 2007; Herrero et al., 2013; Kramer and Wohl, 2015; Wohl, 2017). Fluvial literature holds the most extensive documentation of the geomorphic role of LWD in the Pacific Northwest due to the vital role of LWD in forming and maintaining salmon-bearing river and stream morphology (Le Lay et al., 2013; Wohl, 2017). Some pieces of LWD have been dendrochronologically dated showing their active presence in a riparian channel for over 200 years (Sedell et al., 1988). LWD in fluvial systems has been shown to affect hydraulic roughness (Manga and Kirchner, 2000; Hygelund and Manga, 2003; Manners et al., 2007), modify streamflow (Gregory et al., 2002; Gurnell et al., 2002; Curran and Wohl, 2003; Andreoli et al., 2007), affect channel morphology (Kail, 2003; Atha, 2013), create turbulence (Smith et al., 1993; Wallerstein and Thorne, 2004), and promote scour and deposition features (Keller and Swanson, 1979; Nakamura and Swanson, 1993).

The extensive fluvial literature can provide parallel insight to the beach-dune environment that experiences both hydraulic and aeolian activity (Smith et al., 1993; Gurnell et al., 2002). LWD in water has been shown to deflect flow direction, reduce flow velocity and elevate the water surface profile due to drag induced by the LWD (Gippel, 1995; Hygelund and Manga, 2003). As a result, in a river with a bank-full width to depth ratio of 50, critical bed-load transport shear stresses were not reached even though flow is near bank-full conditions (Manga and Kirchner, 2000). The removal of LWD in a channel increased boundary shear stress influencing bed slope, bedload transport, grain-size distribution, and bar-pool topography (Smith et al., 1993). It is safe to presume that the presence or removal of LWD could have a similar effect on subaerial flow across a beach.

Geomorphic impacts of LWD on lakeshore environments is not well documented. A study in the Canadian Arctic documents driftwood collections known by the neologism, “driftcretions,” that stabilize, persist on the shore, and become vegetated (Kramer and Wohl, 2015). Driftcretions exist in various forms and are created by the disconnection of driftwood with shore processes, by changes in water level, waves or ice pushing the driftwood ashore, or by promoting sedimentation and shoreline progradation. Kramer and Wohl (2015) suggest that decreasing supplies of driftwood to the lake will increase erosion. They also note the similarity

of driftcretions in the arctic to landforms on the coast of Haida Gwaii described in Walker and Barrie (2006) suggesting that they may serve a similar function.

The function of LWD in the coastal environment is suggested to play a key role in sandy beach morphodynamics by trapping windblown sand, providing a nuclei for vegetation growth, and helping to stabilize the backshore (Walker and Barrie, 2006). To understand the potential that a LWD matrix has in trapping sand, Eamer and Walker (2010) used airborne LiDAR and high resolution digital aerial photography to quantify sand storage capacity. The authors found sizeable amounts of sand in storage by the LWD matrix, about 1.14 m to 1.60 m storage depth, and potential capacity to hold an additional depth of 0.2 m (Eamer and Walker, 2010). Heathfield and Walker (2011) noted evidence of historic LWD buried by pioneer plant communities and Sitka Spruce (*Picea sitchensis*) landward of the beach, although investigations using an auger to probe at depth were unsuccessful in locating LWD buried within historical dune deposits. Vegetation using LWD as a nurse location in the backshore documented by Heathfield and Walker (2011) is consistent with findings from the arctic (Kramer and Wohl, 2015) although the different bio-geomorphic setting could lead to variations in function. Kennedy and Woods (2012) also found LWD to have backshore stabilizing properties on reflective gravel beaches. While the clast size is vastly larger than coastal sand ecosystems, the primary function of storing sediment seems to be the same, with the larger clast sizes leading to steeper shoreface as opposed to the relatively shallow and wide storage experienced by Eamer and Walker (2010).

1.2.2 Boundary layer development

In order to explore the effect of LWD on airflow over beaches and dunes, an understanding of how air flow interacts with the surface (via the boundary layer) is required. The boundary layer is a region of lower velocity flow of a viscous fluid (e.g., air) that is in contact with a surface, and exists from the surface up to the point of 99% free-stream velocity (Kuethe, 1971; Bauer, 2013). The boundary layer exhibits a vertical velocity profile gradient with slowest flow near the surface (Pethick, 1984; Bauer, 2013). The molecules in contact with the surface are considered to be stationary, in a no-slip condition, while fluid layers above the

surface slide past each other in laminar (viscous forces dominating) or turbulent (inertial forces dominating) motion characterized by the Reynolds number (Pye and Tsoar, 1990; Bauer, 2013):

$$Re = \frac{LU}{v} \quad [1]$$

L is the roughness length parameter, U is the velocity, v is the kinematic viscosity.

Because air has such a low viscosity it can assume turbulent flow at low velocities (> 0.1 m s^{-1} at low roughness lengths) causing almost all natural flows linked to aeolian transport to be turbulent (Pye and Tsoar, 1990). Fully developed turbulent flow in thermally neutral conditions over rough surfaces is described by the von Karman - Prandtl log velocity profile, or law of the wall (Perry et al., 1969; Goldsmith, 1985; Nickling and Davidson-Arnott, 1990; Pye and Tsoar, 1990; Lancaster, 1995; Sherman, 1995; Bauer, 2013):

$$\frac{u}{u_*} = \frac{1}{k} ln \frac{z}{z_0} \quad [2]$$

μ is the velocity at height z, μ_* is the shear velocity, z_0 is the aerodynamic roughness length (equal to d/30, where d is the diameter of the sand grains on the surface), k is the von Karman constant (approximately 0.4). The log velocity profile relates the fluid velocity at height with both the surface roughness and critical shear stress(via shear velocity) at the surface (Goldsmith, 1985; Bauer, 2013):

$$\tau_{cr} = \rho u_*^2 \quad [3]$$

τ_{cr} is the critical shear stress, ρ is the air density of 1.225 kg m^{-3}. Shear stress along with pressure, drag, lift, and motion opposing forces are important factors in sand grain entrainment and thus dune building (Pye and Tsoar, 1990). Our understanding of these interactions is largely based on time-averaged wind and particle interactions that require boundary-layer conditions to remain constant, which is unlikely in the natural environment (Sherman and Bauer, 1993; Sherman, 1995; Bauer, 2013).

1.2.3 Airflow and sediment transport over beaches and foredunes

Coastal dunes are formed by the interaction of oceanic and atmospheric processes mobilizing beach sediment and depositing it in the backshore where pioneer plants colonize and maintain overall stability (Pye and Tsoar, 1990; Arens et al., 1995; Arens, 1996; Huggett,

2007; Hesp, 2011; Hesp and Walker, 2013). Mass and energy transfer drive the evolution of coastal dunes through complex process-form interactions and controls on the system (Walker and Hesp, 2013). Process-form interactions can create secondary flow patterns over dunes that are critical to dune maintenance (Arens et al., 1995; Wiggs et al., 1996; Walker, 1999; Tsoar, 2001; Walker et al., 2009b; Baddock et al., 2011; Weaver and Wiggs, 2011; Bauer et al., 2012; Hesp et al., 2015). Secondary flow patterns of concern to this dissertation include those leading up to the crest of the dune: 1) flow deceleration at the dune toe, 2) flow steering, acceleration, and sand transport decoupling by a scarp, 3) streamline compression and flow acceleration up the stoss slope, 4) and flow steering near the crest (Hesp et al., 2009; Bauer et al., 2012; Walker and Hesp, 2013). These flow patterns along with sediment characteristics, topography, roughness elements (e.g. vegetation, wrack, LWD), and surface cohesion (moisture content, salt crusting, lag) control on sediment transport over the beach and foredune (Sherman, 1995; Bauer, 2013; Houser and Ellis, 2013; Walker and Hesp, 2013).

Changes in surface slope from the beach to the foredune crest have a pronounced effect on sediment transport. Beach slopes (the primary sediment source for foredunes) are typically too shallow to have any effect on deposition. However, as flow approaches the foredune (assuming onshore normal flow direction) the presence of the dune creates a variety of flow patterns that affect sediment transport (White and Tsoar, 1998). The rapid increase in slope at the dune toe creates a positive pressure gradient reducing wind speeds and shear stresses and promoting deposition (Carter et al., 1990; Robertson-Rintoul, 1990; Wiggs et al., 1996; Walker and Nickling, 2002; Walker and Hesp, 2013). The reduced shear stress and flow velocity may cause some sorting of coarser sediments at the dune toe versus finer sediments closer to the crest (White and Tsoar, 1998).

The presence of a wave-formed scarp at the toe of the dune can alter flow patterns depending on the scarp slope gradient and incoming flow angle. For direct onshore flow, basal flow separation does not occur on slopes shallower than 60°, while the flow is accelerated up to the scarp crest with increased turbulence and lower speeds immediately downwind of the scarp crest (Bowen and Lindley, 1974, 1977; Tsoar, 1983). Flow separation occurring on slopes steeper than 60° occurs at an upwind distance from the scarp approximately equal to 3h, where

h is the height of the scarp (Tsoar, 1983; Qian et al., 2011; Piscioneri et al., 2019). Onshore flow over steep (>60°) scarps will form roller vorticies at the base of the scarp while oblique incoming flow can be deflected towards crest-parallel alignment forming a region of pronounced turbulence and alongshore helicoidal flow (Tsoar, 1983; Tsoar and Blumberg, 2011; Piscioneri et al., 2019). This alongshore flow can potentially transport sediment along the beach, decreasing the amount of sediment reaching the foredune (Bauer et al., 2012). However, Piscioneri et al. (2019) noted that sand could be transported over a scarp by helicoidal flow.

As flow begins to pass over the dune it is continually accelerated up the stoss slope with maximum velocity reached at the crest as a result of streamline compression and the laws of conservation of mass and energy (Arens et al., 1995; Wiggs et al., 1996; Walker and Hesp, 2013). The law of conservation of mass and energy maintains that a volume of air passing over the dune at the stoss toe with velocity u_1 must equal the volume passing the crest with velocity u_2 (Pye and Tsoar, 1990). The velocity at the crest must therefore be higher so the same volume can pass through the smaller space (because of streamline compression) in the same amount of time. This corresponds to a drop in pressure coincident with the increase in velocity because the increased kinetic energy must be balanced by a decrease in static pressure according to Bernoulli's principle (Walker and Nickling, 2002; Hesp et al., 2015). Dune crest wind speeds have been measured over five times higher than speeds immediately upwind of the dune with speed increases following the increasing slope (Lancaster, 1995; Hesp et al., 2009; Hesp and Smyth, 2016; Yuxiang et al., 2017).

Oblique wind flow over the stoss slope of a dune can also result in topographically steered flow (Hesp et al., 2015). Oblique flows between 30^o and 60^o (90^o is onshore) are deflected strongly toward crest-normal, flow > 60^o is only slightly deflected toward crest-normal (declining toward directly onshore), while flow < 30^o is deflected parallel to the crestline (Svasek and Terwindt, 1974; Arens et al., 1995; Hesp and Pringle, 2001; Walker et al., 2006, 2009b; Bauer et al., 2012). Flow steering near the dune crest is the result of lower pressure at the crest having a greater influence on air closer to the crest (Hesp et al., 2015). The most pronounced steering occurs close to the surface at the crest where flow acceleration

effects are strongest (Arens et al., 1995; Walker et al., 2006, 2009a; Hesp et al., 2015). Steering as great as 37^{o} from the incident flow has been observed (Walker et al., 2009a). All flows lee of the crest decelerate due to flow expansion (Walker and Hesp, 2013). As onshore and slightly oblique flows (>70^{o} from crest parallel) cross the crest, they separate, creating a roller vortex (Sweet and Kocurek, 1990; Walker, 2005). Highly oblique flow (< 70^{o} from crest parallel) crossing the crest does not separate and does not decelerate as much as onshore flows due to the lower aspect ratio imposed by the dune (Bauer et al., 2012; Walker et al., 2017).

Sand transport over a beach and foredune is affected by topographic flow modifications caused by changes in slope, vegetation cover, and the presence of a scarp. (Bauer et al., 2012). During transport enabling winds, sand transport increases downwind from the limit of swash run-up (wet-dry line) toward the upper beach (Nordstrom and Jackson, 1992; Bauer et al., 2009; de Vries et al., 2014a). Sand transport then declines at the dune toe due to the previously mentioned positive pressure gradient. The presence of a vertical scarp or dense vegetation at the dune toe stops nearly all sand from reaching the stoss slope (Arens, 1996; Bauer et al., 2012; Walker et al., 2017). In the absence of dense vegetation, flow acceleration up the stoss slope can initialize transport that reaches maximum flux towards the crest, potentially eroding the stoss slope (Walker et al., 2017). Steeper stoss slopes enhance streamline compression and flow acceleration, and thus sediment transport, but steeper slopes also increase the internal friction angle requiring greater shear velocities and wind speeds to entrain sediment (Hardisty and Whitehouse, 1988a, 1988b). Sand deposition will occur on the stoss slope if dense vegetation is present, however, sand has been known to travel over dense vegetation by means of strong jet-like flows (Arens et al., 1995; Hesp et al., 2009; Hesp and Smyth, 2016).

1.2.4 Roughness elements modifying fluid flow and sediment transport over beaches

There is a growing volume of literature on the effects of solid roughness elements (i.e. objects having characteristics of height, porosity, shape, and spacing above the surface) on airflow and sedimentation patterns relevant to beach-dune systems (Iversen et al., 1990; Dong et al., 2007; Brown et al., 2008; Nordstrom et al., 2011; Luo et al., 2012; Bauer et al., 2013; Jackson and Nordstrom, 2013; Furieri et al., 2014). Typical roughness elements on beaches and

foredunes include large woody debris, wrack, and vegetation having non-porous and porous characteristics. There are three ways that roughness elements can control sediment transport to, on, and over a foredune: 1) extracting momentum from the air flow, 2) acting as an obstacle and physical barrier, and 3) reducing the sediment source area (Wolfe and Nickling, 1993).

Roughness elements critically modify the motion of fluids over surfaces causing flow deformation, secondary flow patterns, and a general loss of flow momentum that are similar to the effects previously described in the fluvial environment (Hesp, 2004; Chappell and Heritage, 2007; Smith, 2014). In this way, LWD is expected to generally reduce flow velocity near the surface, similar to other roughness arrays constructed of solid elements (cf., Gillies and Lancaster, 2013; Gillies et al., 2015). Although, Gillies et al. (2017) note that sand, accelerated around solid elements (see McKenna Neuman and Bédard, 2015), could slow the loss of energy with downwind distance as compared to a porous roughness element. Localized flow acceleration and shear stress around an object also increases with the size of the object, similar to the enhancement of secondary flow patterns over a dune as dune height increases (Finnigan, 2000; Brown et al., 2008; Vandenbruwaene et al., 2011; Bauer et al., 2013). Therefore, the larger the piece of LWD, the greater chance for local scour and erosion around the LWD. LWD does typically self organize with the long-axis parallel to the shore, so in many cases the LWD could act like the sand fences described in Gillies et al. (2017) in that they deflect flow upwards more so than around the object. Although, flow deflection around individual logs is dependant on many factors (i.e., size, shape, orientation to incoming flow, amount of burial), it is the combination of these effects within randomly arranged LWD matrices that greatly complicate flow across a beach with LWD.

Roughness elements can trap wind-transported sediment from reaching the foredune (Hesp, 1989, 2004; Nordstrom et al., 2011; Hesp and Walker, 2013; Jackson and Nordstrom, 2013). In turn, this newly captured sediment could act as nuclei for incipient dune formation by promoting vegetation colonization and offers an additional buffer of sediment to wave erosion (Stembridge, 1979; Walker and Barrie, 2006). Walker and Barrie (2006) and Eamer and Walker (2010) demonstrated how LWD matrices can capture vast quantities of sediment, storing it in the backshore before it reaches the foredune. Similar to LWD, research on artificial arrays of

solid roughness elements have also demonstrated a sediment modulating capacity where sand transport is decreased downwind within the array, promoting deposition in the upwind portions of the array (Gillies et al., 2006, 2015). However, the impact that the array had on sediment transport declined (i.e., increased flux over time) as the objects were buried. The same effect could occur with LWD matrices fronting a foredune.

Modified suspension of sand grains could transport sand farther into a LWD matrix. High velocity jet-like flow has been documented showing dense suspended sand clouds passing over heavily vegetated, steep foredunes, allowing sediment to reach beyond the foredune in rare cases (Arens, 1996; Hesp et al., 2009; Hesp and Smyth, 2016) The same could be true for LWD matrices, given a high enough wind speed for sand to be transported in modified suspension over a large matrix, especially if grains impact the logs in such a way that they bounce even higher into the boundary layer. Anderson and Walker (2006) documented sand transport downwind of a large and exposed LWD matrix and noted substantial infilling over several months. This mechanism could have an impact on sand ramp rebuilding after scarping events if enough sand is transported over the LWD matrix. The sediment transport patterns resulting from the presence of LWD are of primary importance to this dissertation and explored in greater detail in the following chapters.

2. Airflow dynamics over a beach and foredune system with large woody debris.

Michael J. Grilliot, Ian J. Walker, and Bernard O. Bauer

Published, 24 April 2018, in:
Geosciences 8, 147. https://doi.org/10.3390/geosciences8050147

2.1 Abstract

Airflow dynamics over beach-foredune systems can be complex. Although a great deal is known about the effects of topographic forcing and vegetation cover on wind-field modification, the role of large woody debris (LWD) as a roughness element and modifier of boundary layer flow is relatively understudied. Individual pieces of LWD are non-porous elements that impose bluff body effects and induce secondary flow circulation that varies with size, density, and arrangement. Large assemblages of LWD are common on beaches near forested watersheds and collectively have a degree of porosity that increases aerodynamic roughness in ways that are not fully understood. A field study on a mesotidal sandy beach with a scarped foredune (Calvert Island, British Columbia, Canada) shows that LWD influences flow patterns and turbulence levels. Overall mean and fluctuating energy decline as flow transitions across LWD, while mean energy is converted to turbulent energy. Such flow alterations have implications for sand transport pathways and resulting sedimentation patterns, primarily by inducing deposition within the LWD matrix.

Keywords: Aeolian Geomorphology; Large Woody Debris; Roughness Elements, Beach-Dune Morphodynamics; Foredune; Turbulence, Quadrant Events, Ultrasonic Anemometry

Introduction

2.2 Introduction

Natural roughness elements (e.g., plants, rocks, wrack, logs) protrude into the near-surface flow field, increasing aerodynamic drag and extracting momentum from the wind as well as acting as a physical barrier to aeolian sediment transport (Wolfe and Nickling, 1993; Hesp, 2002; Gillies et al., 2014; Mayaud et al., 2016a, 2016b). There are many studies on the effects of porous and pliable roughness elements (i.e., grassy vegetation) on flow interactions and sediment transport over coastal foredunes (Arens et al., 1995, 2004; Arens, 1996; Walker et al., 2006; Davidson-Arnott et al., 2012; Chapman et al., 2013; Keijsers et al., 2015; Hesp and Smyth, 2017), as well as around discrete, artificial non-porous roughness elements (e.g., Sutton and McKenna Neuman, 2008; Bauer et al., 2013; McKenna Neuman and Bédard, 2015; Hesp and Smyth, 2017) and roughness arrays (e.g., Gillies et al., 2006, 2015; Gillies and Lancaster, 2013). However, there remains a gap in understanding as to how natural non-porous objects, like fallen trees and large woody debris (LWD), affect flow and sedimentation on and in front of coastal foredunes (Walker and Barrie, 2006; Eamer and Walker, 2010; Bauer et al., 2013; Mayaud et al., 2016a).

Flow interactions around, isolated, non-porous objects with simple shapes are well-studied and relatively predictable (Lee and Soliman, 1977; Raupach, 1992; Raupach et al., 1993; Wiggs et al., 1996; Sutton and McKenna Neuman, 2008; Baddock et al., 2011; Mayaud et al., 2016a) (Figure 1), although the resulting topographic changes are less well understood (McKenna Neuman and Bédard, 2015). Unidirectional horizontal flow around a three-dimensional cylinder (most closely representing an upright tree stump) is characterized by flow separation, the creation of horseshoe vortices extending downwind near the surface, and flow reversals in the lee of the object (McKenna Neuman and Bédard, 2015). Lee flow reversals create an area of converging flow with reduced velocity where shadow dunes form (Iversen et al., 1990; Lancaster, 1995; Sutton and McKenna Neuman, 2008). McKenna Neuman and Bédard (2015) demonstrated that scour, caused by flow acceleration around the sides of the object, migrates windward as minor slope failures. Horseshoe vortices develop as the scoured regions grow and converge forming an erosional horseshoe-shaped trough (Sutton and McKenna Neuman, 2008; McKenna Neuman and Bédard, 2015). Leenders et al. (2007) measured a similar

increase in wind speed around the base of single tree trunks.

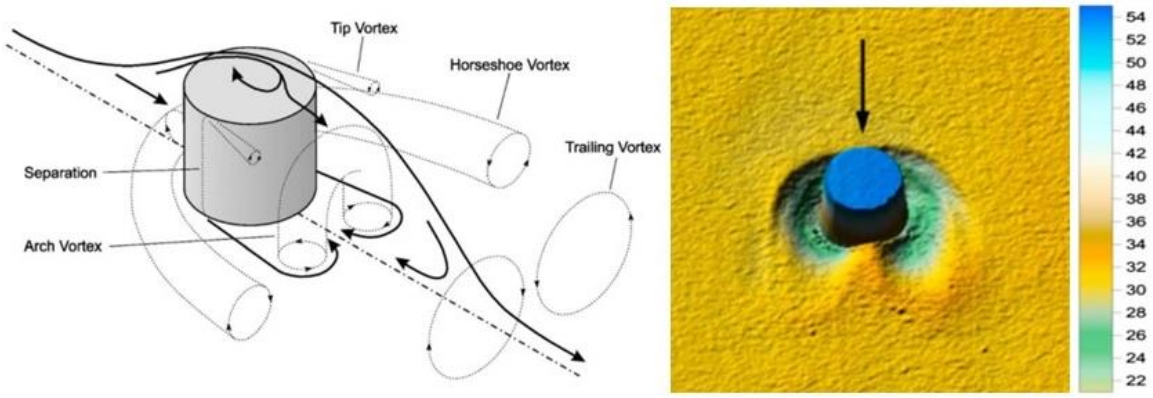

Figure 1 – (Left) Conceptualization of coherent flow structures surrounding a wall-mounted cylinder (Reproduced from McKenna Neuman and Bédard (2015) p. 1827, originally from Pattenden et al., 2005). Copyright 2005, with permission from Springer Nature. (Right) Resulting morphology after a transporting event with scale in mm (Reproduced from McKenna Neuman and Bédard (2015) p. 1829). Copyright 2015, with permission from John Wiley and Sons.

Research on arrays of non-porous roughness elements has revealed a complex relationship between flow characteristics, sediment transport, and roughness density (Lancaster and Baas, 1998; Gillies et al., 2006, 2007, 2015). Uniform roughness array densities > 44% (based on spacing pattern) can produce skimming flow (Lee and Soliman, 1977; Wolfe and Nickling, 1993) that has been shown to reduce the potential for sediment transport downwind of the array, in contrast to isolated roughness elements that have localized influences (Mayaud et al., 2016b) (Figure 2).

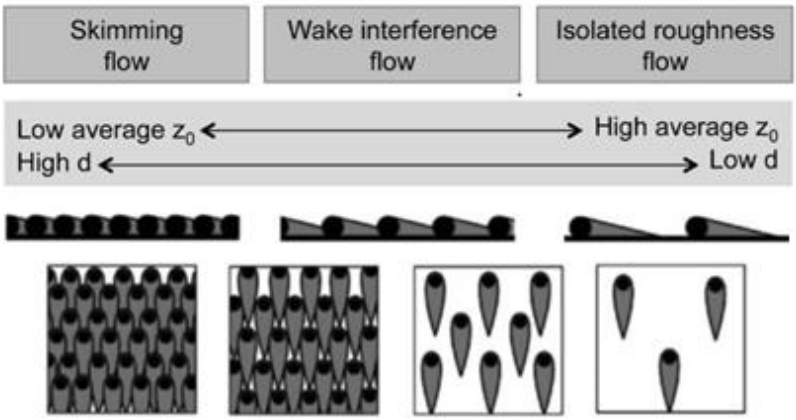

Figure 2 – Flow regimes and associated theoretical wake development, shown in schematic plan and side view. Shaded areas are wake regions. The effect of different flow regimes on average z_o (aerodynamic roughness) and d (displacement height) per plant unit is shown. (Modified and reproduced from Mayaud et al., 2016b, p. 142 under the Creative Commons attribution license).

Examples of the effects of LWD on aeolian sand transport and erosion/deposition patterns on beaches include extensive upwind and lateral horseshoe basal scour (cf., McKenna Neuman and Bédard 2015), which is common for highly exposed elements (Figure 3). However, accumulations of LWD in dense matrices are also common (Figure 4). Variations in LWD matrix shape, size, structure, density, orientation to incoming flow, height above the surface, and apparent porosity create complex flow-form interactions that alter flow characteristics and sediment transport pathways in unpredictable ways. Because of these effects, predicting flow patterns and sand supply to foredune systems laden with LWD becomes increasingly difficult. To date, there is no published research to quantify the impacts of a LWD matrix on airflow in the vicinity of a coastal foredune.

Figure 3 – Typical scour pattern due to horseshoe vortex around a piece of isolated LWD. Deflation hole is approximately 2 m in diameter. (photo credit: M. Grilliot)

Figure 4 – Photos of LWD deposits commonly found on beaches around the world. Photo (a) shows a partially buried log with up- and down-wind sand ramps: Stewart Island, New Zealand; (b) shows a dense matrix of logs with appreciable amounts of aeolian deposition common on open coasts in British Columbia, Canada; (c) shows a matrix of LWD with near complete aeolian infilling in front an established foredune that was scarped by as much as 1.5 m one year before the photo was taken. Photo credits: (a) B. Bauer, (b) and (c) I. Walker.

The overall purpose of this study was to improve our understanding of the effects of LWD on near-surface airflow fronting a coastal foredune. The approach used was to study the aggregate effect of the LWD deposit, rather than the properties and flow dynamics around

individual roughness elements. Three-dimensional airflow and turbulence properties were characterized during sand transport events along shore-perpendicular transects with and without LWD. This paper examines specifically the influence of a recently emplaced LWD matrix on the flow dynamics fronting an established, scarped foredune.

2.3 Methods

2.3.1 Study Site

The study site is located on Calvert Island, on the central coast of British Columbia, Canada (Figure 5). The study was part of a collaborative research program on Coastal Sand Ecosystems in partnership with the Hakai Institute. Weather data from a nearby meteorological station from 2012 to 2018 show prevailing winds from the SE (obliquely alongshore), a unimodal resultant drift potential (RDP) and a resultant drift direction of 322^{o} (Figure 5) derived using the Fryberger and Dean (1979) model and following the approach of Miot da Silva and Hesp (2010). The experiment was conducted on West Beach, a 1 km wide embayed, shallow sloping (1.8^{o} average intertidal slope), sandy beach bounded by rocky headlands with a SE aspect (Figure 6). The West Beach foredune on the north end of the beach is approximately 6.5 m tall and partially vegetated with stoss slope angles of 23° to 37° and a crestline orientation of SE - NW (128° | 308°). The foredune toe was incised by a 1 to 2 m scarp formed by a storm on March 10, 2016. The beach is macro-tidal with a spring tide range of >4 m and has a low tide width of 250 m and an effective fetch in the resultant drift direction of >500 m. D_{50} of beach-dune sediments is 0.198 mm with a calculated transport threshold wind speed measured at 10 m above ground level of 5.3 m s^{-1} (Eamer, 2017). The foredune is predominantly vegetated by *Elymus mollis* and fronted by accumulations of LWD.

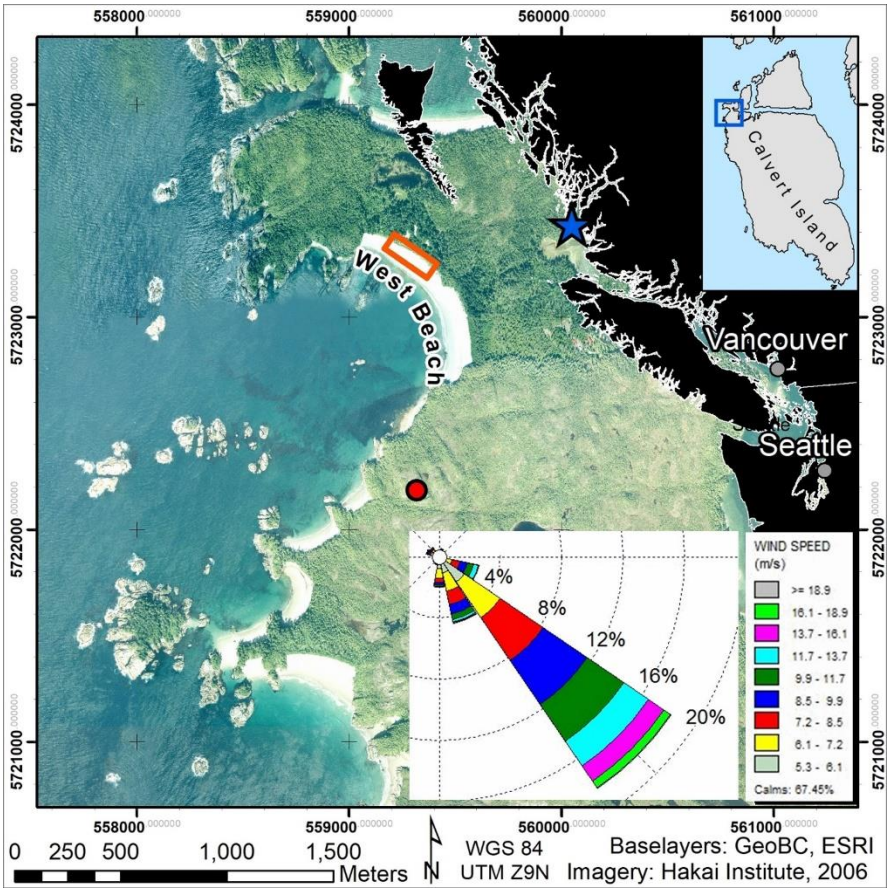

Figure 5 – Location of the study area (orange rectangle) on West Beach, Calvert Island, British Columbia, Canada. Black overlay on the right shows the location of Calvert Island (blue star) in British Columbia. The upper-right inset shows the location of orthophoto detail (blue square). The red dot shows the location of the weather station used for the wind rose and drift rose (Figure 6) calculations.

2.3.2 Experimental Setup

The experiment was conducted from 11 - 25 April 2016. Four shore-normal transects were established that remained fixed, but only the results from two transects are discussed (Figure 6) because the other two transects yielded flow data below the transport threshold and were therefore unfit for analysis. Shore-normal transects were established following convention for aeolian studies on coastal beaches and in anticipation of localized topographic steering of the regional wind field leading to oblique onshore winds. Transect (T1) was located within the LWD matrix, and Transect 2 (T2) was the reference transect, which was cleared of

LWD to 4 m on either side of the transect (Figure 5). Two instrument stations were situated on each transect, one on the flat upper beach and a second on the stoss slope of the foredune (Figure 7). The stoss slope stations at T1 and T2 were both positioned 3 m landward of the scarp. The upper beach stations were at 4.5 m seaward of the scarp along T1 but 7 m seaward of the scarp along T2 (the reference station). During the experiment, T1 had different upwind LWD coverage due to changes in the obliquity (165^{o} average) of the incoming wind direction (Table 1), whereas the beach station at T2 was not sufficiently far outside of the LWD to not be influenced by this altered roughness effect.

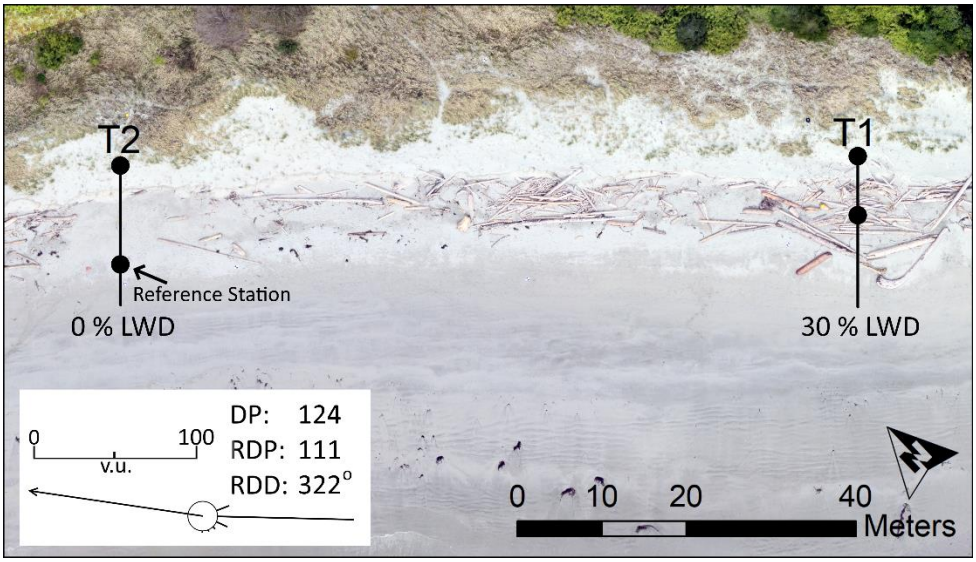

Figure 6 – Aerial photo showing the location of transects 1 and 2 (T1, T2) as black lines and associated LWD coverage. LWD coverage is defined as the amount of plan-view surface area covered by LWD, extending 1 m on either side of the transect and 20 m seaward from the dune station. The arrow next to the reference station (i.e., not under the influence of LWD) indicates the average incoming wind direction at 1.5 m.

Table 1 – Upwind LWD cover densities (%) based on average incoming wind direction of 28^{o} (relative to crestline) by transect (Figure 6 lines) and station location (Figure 6 dots).

Station location	Transect 1	Transect 2
Beach	13	0
Dune	27	1

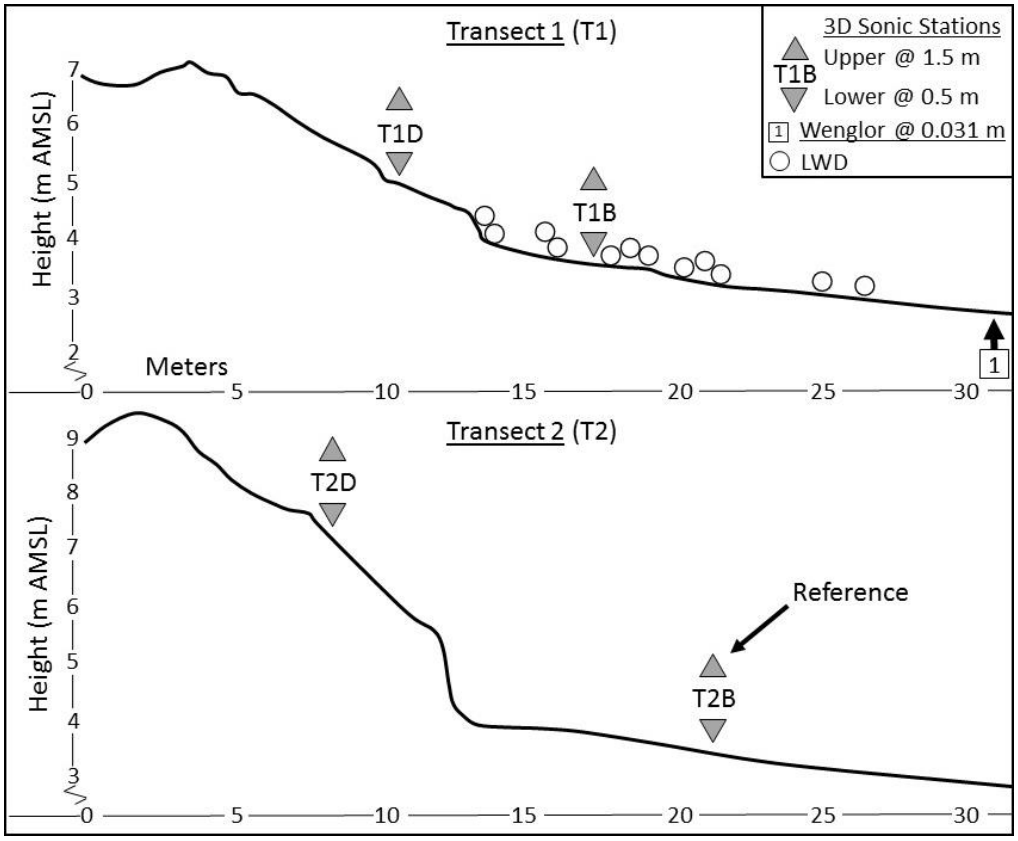

Figure 7 – Diagram of instrument locations along shore-normal transects T1 and T2. 3D sonic anemometer stations are labeled by transect number (T#) and beach (B) and dune (D) locations. Individual anemometers are referenced by downward-pointing triangles (0.5 m) and upward-pointing triangles (1.5 m).

Ultrasonic anemometers (3D Gill WindMaster) were used to sample wind velocity components (u, horizontal; v, spanwise; and w, vertical). Anemometers are referred to via the designations and heights in Figure 7, e.g. the Transect 1 anemometer on the beach at 0.5 m is referred to as "$T1B_{0.5}$". All instruments were horizontally-aligned with the $+u$ axis oriented offshore at 218° and $+v$ axis alongshore at 128° SE (relative to true north; Magnetic Declination of +17° 47' East). All flow directions are presented relative to the dune crestline (0° alongshore, 90° onshore) unless otherwise noted. Each instrument station consisted of two 3D sonics mounted on an aluminum frame at 0.5 m (inverted) and 1.5 m (upright) above the surface (Figure 8, a and b). The 0.5 m height placed the anemometer just above the average LWD height (approximately 0.25 m, measured from terrestrial laser scans) so as to avoid complex

eddy shedding in the wake of individual pieces of LWD. Care was taken to clean the sensor nodes throughout the day and between runs to reduce moisture and dust contamination.

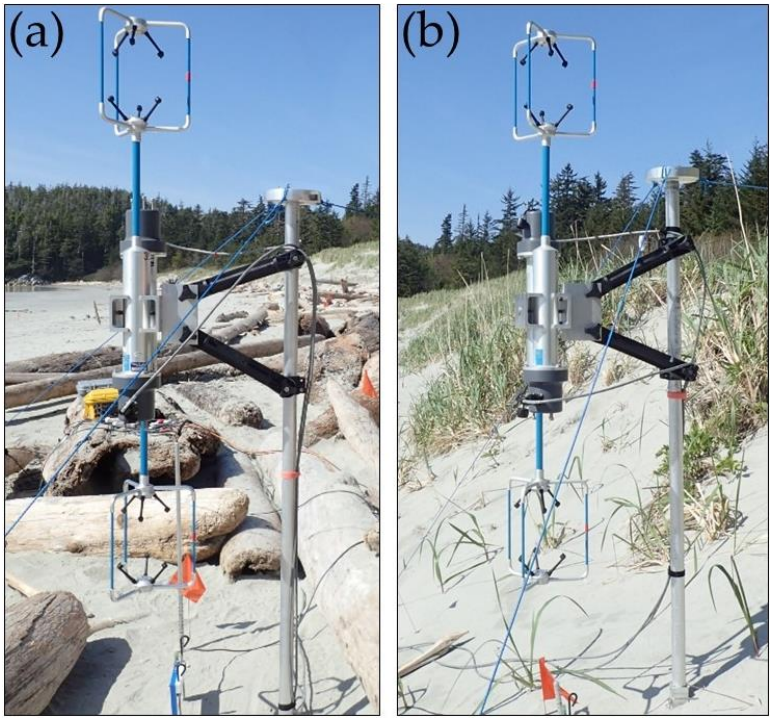

Figure 8 – Deployment of 3D anemometer flow measurement stations on T1 in the LWD on the beach (a) and dune (b), approximately 7.5 m apart. The upper anemometer is set at 1.5 m and the lower at 0.5 m.

All electronic instruments were hard-wired to Hobo® EnergyPro Data Loggers (Onset Computer Corporation® part # H22-001) housed in weather-resistant cases adjacent to the transects. All data were sampled and recorded at 1Hz. Standard data conversion routines were applied following manufacturers' recommended guidelines. A Wenglor (model YH08PCT8) laser particle counter (80 mm path length, 0.6 mm beam width, laser sampling beam was placed 0.031 m above the surface, located 5 m seaward from the LWD on T1, and aligned toward the incoming transport direction of 150^{o}) was used to measure saltation intensity (counts^{-1}).

2.3.3 Data Description and Analyses

The events examined in this study include a subset of eight 10-min runs from the April

13 and April 15 of 2016 (Figure 9). Runs were selected for analysis based on greatest sustained wind speeds, limited directional deviation, and presence of transport activity. Although the transport data are not described in this paper, the Wenglor activity records shown in Figure 9 were used solely in this paper to identify periods when transport was most active. All anemometer data were normalized by the data from $T2B_{1.5}$ to portray relative spatial trends (normalizing equations are found in the respective figure descriptions). Missing data during runs 6-8 are due to sensor malfunctions.

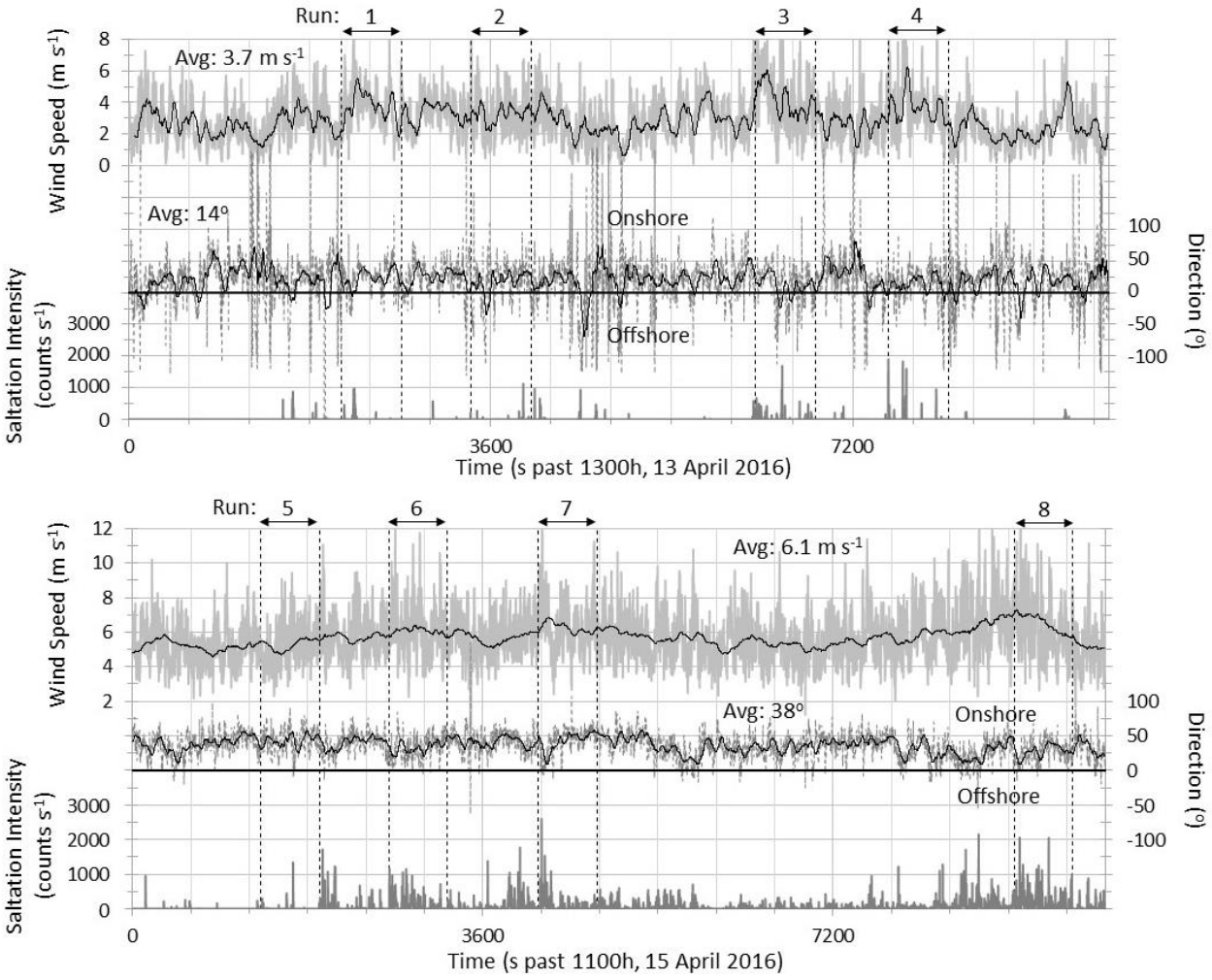

Figure 9 – Time series of incident wind speed (upper solid grey line with black 60 s running mean, upper left axis, m s^{-1}), direction (middle dashed grey line with black 60 s running mean, right axis, degrees), and saltation intensity (bottom grey bars, bottom left axis, counts s^{-1}) on 13 April (top graph) and 15 April (bottom graph). Wind speed and direction are from

$T2B_{1.5m}$ and Saltation Intensity is from W1 (Figure 7). Runs are indicated on the top of each graph.

Velocity data from the sonic anemometers were rotated to account for yaw and pitch alignments relative to the incident streamlines (van Boxel et al., 2004; Walker, 2005; Lee and Baas, 2012; Mayaud et al., 2016b). Yaw corrections used the following equations:

$$u_1 = u\,cos\,\alpha + v\,sin\,\alpha \quad [4]$$

$$v_c = -u\,sin\,\alpha + v\,cos\,\alpha \quad [5]$$

$$\alpha = tan^{-1}\left(\frac{V}{U}\right) \quad [6]$$

in which u_1 and v_c are yaw adjusted values, alpha (α) is the time-averaged angle derived from U and V, which are the time-averaged velocity vectors for the sampling interval.

The yaw rotation transforms the horizontal coordinates toward a resultant speed such that the spanwise signal has zero mean. Pitch rotations used the following equations:

$$u_c = u_1\,cos\,\varphi + w\,sin\,\varphi \quad [7]$$

$$w_c = u_1\,sin\,\varphi + w\,cos\,\varphi \quad [8]$$

$$\varphi = tan^{-1}\left(\frac{W}{U_1}\right) \quad [9]$$

in which u_c and w_c are pitch and yaw adjusted values. Phi (φ) is the angle of the incoming streamline relative to the sensor plane (mounted horizontally) derived from U_1, which is the mean horizontal velocity in the streamwise direction after yaw rotation, and W is the time-averaged vertical velocity vector from the original time series for the sampling interval. Fluctuating components (u', v', w') were calculated as follows:

$$u' = u_c - U_c \quad [10]$$

$$v' = v_c - V_c \quad [11]$$

$$w' = w_c - W_c \quad [12]$$

in which U_c, V_c, W_c are the time-averaged velocity vectors for the sampling interval derived from the yaw and pitch corrected data.

Turbulent stresses and other flow parameters were then calculated from the rotated component time series. Reynolds kinematic normal stresses ($\overline{u'^2}, \overline{v'^2}, \overline{w'^2}$) were calculated as the variance of the velocity components (u_c, v_c, w_c) using Eq [13] while the standard deviation was

calculated as the square root of the variance (*VAR*) using Eq [14]:

$$VAR(u_c) = \overline{(u_c - U_c)^2} = \overline{u'^2} \quad [13]$$

$$\sigma_{u_c} = \sqrt{VAR(u_c)} = \sqrt{\overline{u'^2}} \quad [14]$$

Turbulent Kinetic Energy (TKE) ($m^2 s^{-2}$) quantifies the total energy of the fluctuating flow, or how much the airflow deviates from its mean components, using Eq [15]:

$$\text{TKE} = \frac{1}{2}\left[\left(\overline{u'^2}\right) + \left(\overline{v'^2}\right) + \left(\overline{w'^2}\right)\right] \quad [15]$$

Kinematic Reynolds stress (RS_k) is the time-averaged covariance of the streamwise and vertical fluctuating components, which characterizes the average vertical flux of streamwise momentum, using Eq [16]:

$$RS_k = -\overline{u'w'} \quad [16]$$

The parameterization in Eq. 16 assumes that there is relatively little fluctuation in the spanwise direction (e.g., as in a wind tunnel), but with natural flows across LWD, there can be significant spanwise wind energy. The horizontal kinematic Reynolds stress (RS_{Hk}) captures the degree of correlation between the additional spanwise and vertical fluctuations using Eq [17] (Lee and Baas, 2012; Mayaud et al., 2016b):

$$RS_{Hk} = \sqrt{\overline{u'w'}^2 + \overline{v'w'}^2} \quad [17]$$

Turbulence Intensity (in the streamwise direction) is characterized by the coefficient of variation (CV_{u_c}), which assesses the magnitude of wind speed fluctuations relative to the mean flow using Eq [18]:

$$CV_{u_c} = \frac{\sigma_{u_c}}{U_c} \quad [18]$$

For the sake of simplicity, all future references to u, v, w and U, V, W in this paper should be considered as referring to the yaw and pitch adjusted values (with the subscripts dropped) unless specifically noted.

Fluctuating velocity components (u' and w') were used to produce quadrant plots that show the stress geometry of turbulent flow in graphical form (Figure 10). Quadrant activity was classified as 'significant' if the stress event exceeded one standard deviation (i.e., a hole size of H=1) (Lu and Willmarth, 1973). Thus, only large contributions to the Reynolds stress are considered significant and included in the analysis (e.g., Sarkar and Dey, 2010).

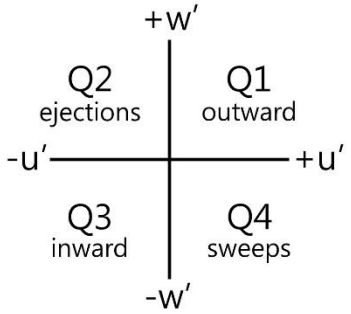

Figure 10 – Quadrant plot with $\pm u'$ and $\pm w'$ axes. Quadrant 1 (Q1) is associated with outward interactions (u'>0, w'>0), quadrant 2 (Q2) with ejections (u'<0, w'>0), quadrant 3 (Q3) with inward interactions (u'<0, w'<0), and quadrant 4 (Q4) with sweeps (u'>0, w'<0).

2.4 Results & Discussion

2.4.1 Flow Dynamics over LWD

Flow properties over the LWD are compared to conditions over the beach with no LWD using normalized quantities. All runs were averaged to establish a baseline from which to assess deviations from the mean (normalized) state. For example, differences in time between the various runs can be assessed relative to the overall mean for all runs, and similarly, the relative deviation of T1 away from T2 for all runs provides an indication of the influence of LWD on flow dynamics. A summary of observed flow properties averaged over the eight selected runs (Figure 9) is provided in Table 2 and a complete list of flow properties for individual 10-minute runs is found in the Appendix. Average incoming wind speed at the reference station for all eight runs was 4.8 m s^{-1} (σ = 1.2) while average incoming wind direction was 28^o (σ = 10.6). Figure 11 and Figure 13 are based on the data in Table 2 and portray graphically the quantities at T1 (LWD) in terms of the percent difference from T2 (the reference site with no LWD). Percentages indicate a relative decrease (negative) or increase (positive) of flow quantities.

Table 2 – Average flow properties for all runs including surface slope angle and incident flow angle (degrees), resultant 3D wind speed (S, m s^{-1}), flow streamline angles (degrees), Normal Reynolds stresses ($\overline{u'^2}, \overline{v'^2}, \overline{w'^2}$, m^2 s^{-2}), turbulent kinetic energy (*TKE*, m^2 s^{-2}), Horizontal kinematic Reynolds stress (RS_{Hk}, m^2 s^{-2}), and coefficient of variation (CV_u). Flow angle is relative to crestline (0° alongshore, 90° onshore). Streamline angles and surface slope angles are relative to horizontal (0°).

	T1 (LWD)				T2 (No LWD)			
	Beach lower (0.5 m)	Beach upper (1.5 m)	Stoss lower (0.5 m)	Stoss upper (1.5 m)	Beach lower (0.5 m)	Beach upper (1.5 m)	Stoss lower (0.5 m)	Stoss upper (1.5 m)
surface slope angle (o)	-4	-4	-23	-23	-4	-4	-37	-37
Flow angle (o)	24.5	29.8	24.6	28.6	26.8	28.2	32.7	30.1
Streamline angle (o)	-3.6	-4.0	-8.7	-10.0	-0.3	-2.6	-16.3	-15.4
S	2.99	4.20	3.15	3.62	4.41	4.87	3.50	4.14
$\overline{u'^2}$	1.72	2.45	1.58	1.81	2.15	2.46	1.69	2.03
$\overline{v'^2}$	1.05	2.25	1.68	1.86	2.21	2.47	1.92	2.32
$\overline{w'^2}$	0.11	0.18	0.25	0.32	0.04	0.12	0.36	0.50
TKE	1.44	2.45	1.76	2.00	2.20	2.52	1.99	2.38
RS_{Hk}	0.16	0.17	0.49	0.47	0.16	0.22	0.72	0.78
CVu	0.56	0.47	0.53	0.46	0.38	0.37	0.46	0.41

LWD fronting the foredune had a clear and measurable effect on flow over the upper beach and was highly effective at altering flow characteristics measured at both 1.5 and 0.5 m (Figure 11). Overall, there were consistent decreases in mean wind speed (S), spanwise normal stress ($\overline{v'^2}$), turbulent kinetic energy (*TKE*) at T1 (with LWD) relative to T2 (without LWD). Similarly, there was a consistent increase in turbulence intensity (CV_u) at T1. These differences in flow dynamics in the presence of LWD indicate that the enhanced roughness exerts additional drag on the flow field, extracting energy from the mean flow (i.e., decrease in S and *TKE*) and converting it to enhanced turbulent motion (i.e., increase in CV_u). Also noteworthy is the near 60% increase in $\overline{w'^2}$ on the beach resulting from flow deflection up and over the LWD, despite the small magnitude of the vertical motions relative to the horizontal components.

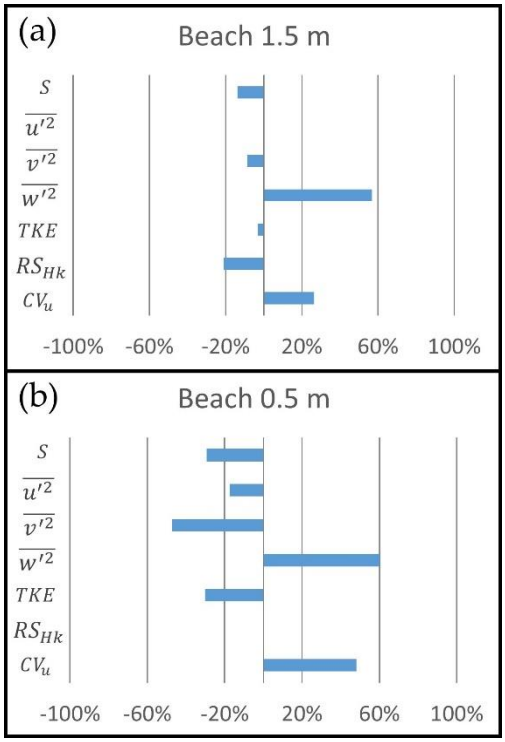

Figure 11 – Percent difference in normalized flow quantities over the beach (calculated as: (T1 - T2)/T2B$_{1.5}$) between similar anemometer locations on T1 (LWD) and T2 (no LWD) over all runs and flow quantities: resultant 3D wind speed (S, m s^{-1}), normal kinematic Reynolds stresses ($\overline{u'^2}$, $\overline{v'^2}$, $\overline{w'^2}$, m^2 s^{-2}), turbulent kinetic energy (TKE, m^2 s^{-2}), horizontal kinematic Reynolds stress (RS_{Hk}, m^2 s^{-2}), and the coefficient of variation (CV_u). (a) Beach 1.5 m, (b) Beach 0.5 m.

The 50% reduction in $\overline{v'^2}$ at T1B$_{0.5}$ can be attributed to two primary factors. First, the LWD-induced drag close to the sand surface reduces overall mean and fluctuating energy because the wind slows down within the LWD matrix (Table 2). Second, spanwise fluctuations are subdued because the individual logs act as physical barriers to lateral flow, and therefore the wind is directed up and over the LWD. In this way, spanwise fluctuating energy is transformed into vertical fluctuating energy. The strong increase in $\overline{w'^2}$ at T1B$_{0.5}$ (Figure 12, bottom) supports this assertion.

The roughness drag induced by the LWD matrix created a strongly sheared flow zone between the sand surface and the flow layer above the LWD matrix. However, net RS_{Hk} remained nearly the same at T1 and T2 (Figure 11b). Wind speed and TKE were smaller at T1 by

about 30%, indicating an extraction of mean energy from the flow (Figure 11b). The quadrant plots (Figure 12) show that the magnitude of w' occurrences at $T1B_{0.5}$, remained relatively small compared to the magnitude of u', despite a 60% increase in the absolute value of $\overline{w'^2}$ from T2 to T1. Even though the increase in w' is relatively small, it is visible on the $T1B_{0.5}$ quadrant plot, which shows an orientation favoring a Q2:Q4 alignment. In contrast, RS_{Hk} is not affected as much as the other quantities at $T1B_{0.5}$. The actual w' values are simply so small relative to u' that the contribution to RS_{Hk} from the increase in $\overline{w'^2}$ is minor and nearly balanced by the -13% decrease in $\overline{u'^2}$. Net RS_{Hk} therefore remains nearly unchanged despite the increased drag and shear, and conversion of mean to turbulent energy.

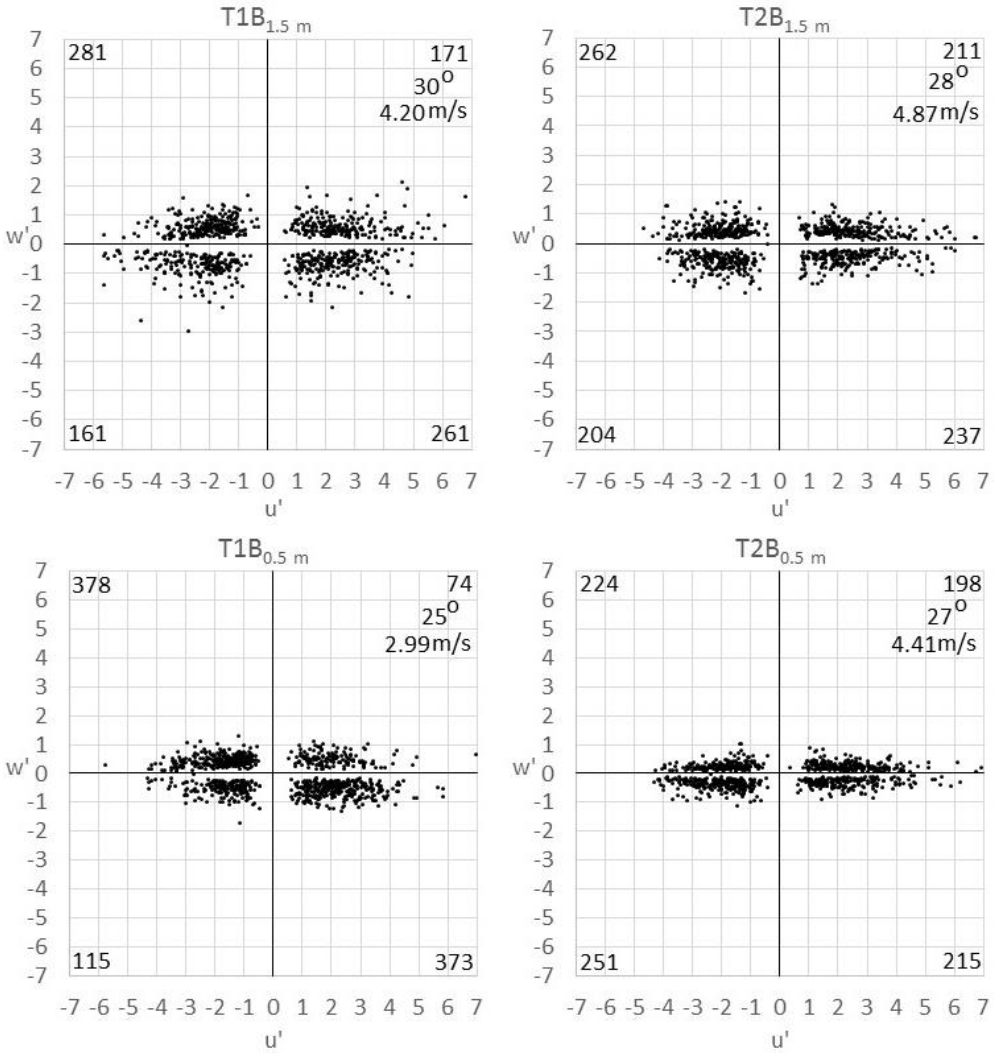

Figure 12 – Beach (T1B and T2B) Quadrant plots (1 Hz) for all runs (80 min, n=4800). Each plot includes data from all eight runs to better visualize the gross distribution of RS_{Hk} components in the quadrant plots. However, only those fluctuations deemed to be significant (> 1 standard deviation) are shown in the plots (total number in each quadrant is indicated by the values in the corners). The top right-hand corner also displays the mean incident flow angle (0^o is alongshore, 90^o is onshore), and wind speed (S) for all eight runs.

LWD did not have the same effect on flow over the stoss slope of the dune. The majority of changes on the dune are within 10 % of the reference values and are generally less pronounced than over the beach (Figure 13). Notable reductions in $\overline{w'^2}$ and RS_{Hk} are most likely the result of the presence of a 1.8 m tall scarp on T2, rather than the influence of LWD. The larger scarp on T2 generates greater vertical fluctuations (w', Figure 14) and disrupts flow modulations (e.g., topographically forced flow compression, acceleration, and streamline curvature) that inhibit turbulent motions (Frank and Kocurek, 1996; Wiggs et al., 1996; Walker et al., 2009b; Bauer, 2013). This influence makes attributing changes to flow properties on the dune to the presence of upwind LWD problematic, and should not be interpreted as absolute, but rather as a general characterization. Still, the minimal change to all other flow properties suggests that characteristic flow modulations that occur in the presence of large dunes are pronounced and dominate flow characteristics, regardless of the presence of LWD upwind of the dune.

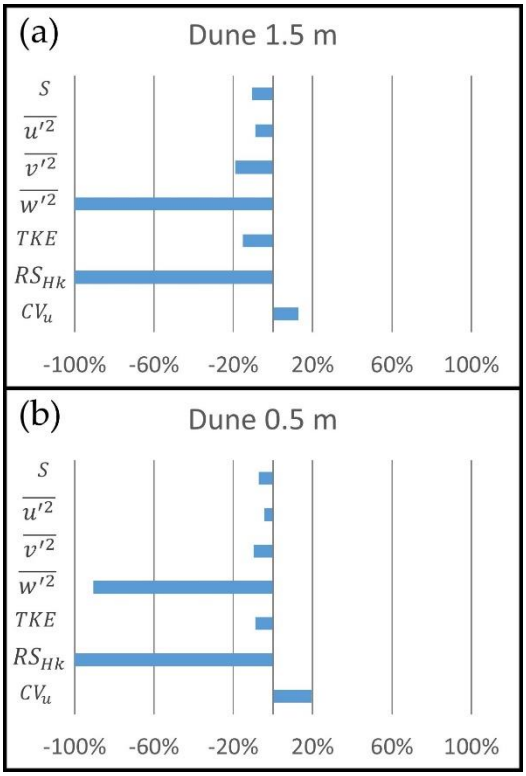

Figure 13 – Percent difference in normalized flow quantities over the stoss slope of the foredune (calculated as: (T1 – T2)/T2$B_{1.5}$) between similar anemometer locations on T1 (LWD) and T2 (no LWD) over all runs and flow quantities: resultant 3D wind speed (S, m s^{-1}), normal kinematic Reynolds stresses ($\overline{u'^2}$, $\overline{v'^2}$, $\overline{w'^2}$, m^2 s^{-2}), turbulent kinetic energy (TKE, m^2 s^{-2}), horizontal kinematic Reynolds stress (RS_{Hk}, m^2 s^{-2}), and the coefficient of variation (CV_u). Top: Dune-1.5 m (excludes incomplete datasets from runs 6-8), Bottom: Dune-0.5 m.

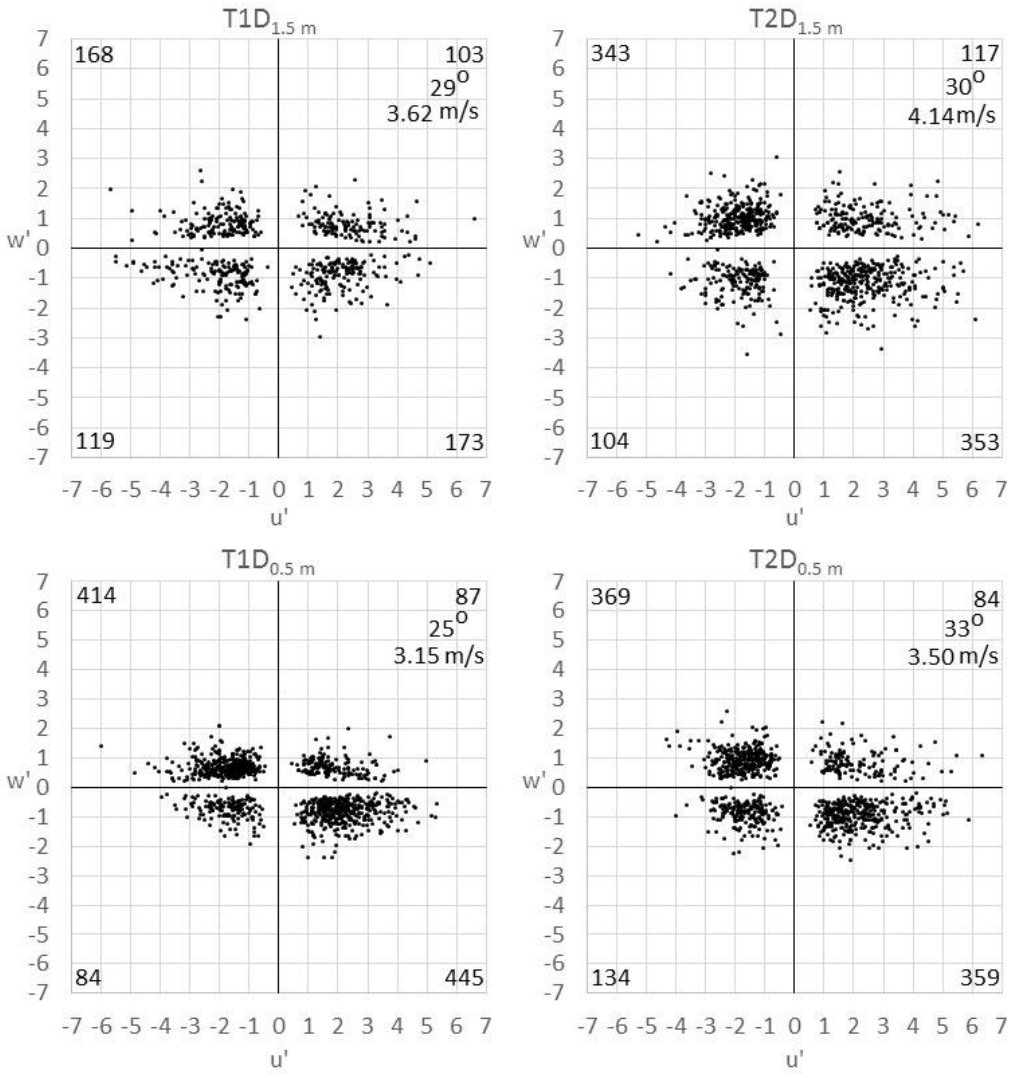

Figure 14 – Dune (T1D and T2D) Quadrant plots (1 Hz) for all runs (80 min, n=4800). For each quadrant, values for significant activity (> 1 standard deviation) are shown in the corner. The top right-hand corner also displays the incident flow angle (0^o is alongshore, 90^o is onshore), and wind speed (S).

The LWD had a more pronounced effect on the flow closer to the beach surface (at 0.5 m) than immediately above the LWD matrix (at 1.5 m). Figure 15 shows the deviation of the change between the $T1_{0.5}$ and $T1_{1.5}$ anemometers at the beach and dune stations relative to those on T2. A value of zero (negative; positive) indicates the change between the $T1_{0.5}$ and $T1_{1.5}$ anemometers was the same as (greater than; less than) the change between the $T2_{0.5}$ and $T2_{1.5}$ anemometers, even if the absolute values between transects varied. Reductions in S, $\overline{u'^2}$,

$\overline{v'^2}$, and TKE on the beach (shown in Figure 15) indicate that the drag effect induced by LWD is stronger closer to the surface. The LWD was also effective at converting mean energy to streamwise turbulent energy at 0.5 m, based on the increase in CV_u. On the dune, all of the flow quantities increased, supporting the observation that flow adjustments at 0.5 m were dominated by the presence of the dune and not the upwind LWD.

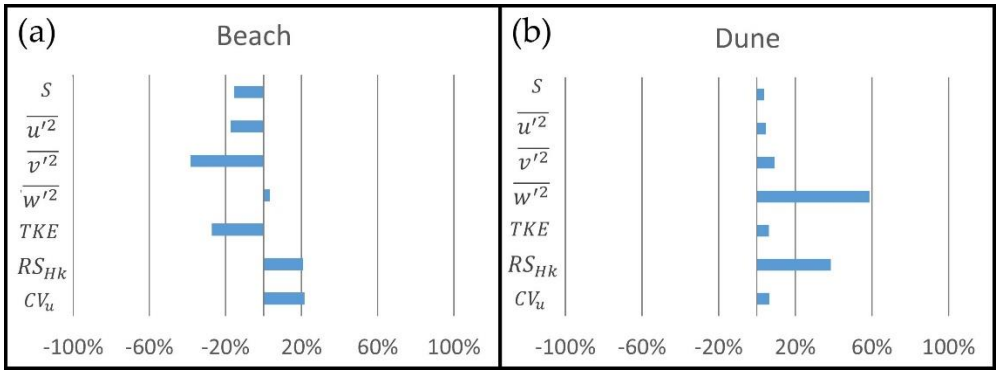

Figure 15 – Average normalized difference in flow quantities (calculated as: {(((T1$_{0.5}$ – T1$_{1.5}$) – (T2$_{0.5}$ – T2$_{1.5}$))/T2B$_{1.5}$)} at height (0.5 m and 1.5 m) between T1 and T2 at the beach (left) and dune (right) using the same flow quantities as in Figure 11. Data were normalized to the 1.5 m beach anemometer on T2 (T2B$_{1.5}$) for each run. The dune values (b) exclude incomplete datasets from runs 6-8.

2.4.2 Flow Steering over LWD

Flow direction on the reference transect at the beach station (T2B$_{0.5}$) shows minimal deviation from the reference condition at T2B$_{1.5}$ (Table 3). Flow across the dune profile along T2, however, was steered towards crest-normal, in agreement with previous research on oblique flow over a stoss slope (Walker et al., 2006, 2009b, 2017; Bauer et al., 2012; Hesp et al., 2015). In contrast, flow direction on T1, with LWD, was altered to a much greater degree than along the reference transect with no LWD (

Table 3). Results over T1 at both the beach and dune locations varied by run and day. Runs 1-4 (April 13), with a mean wind angle of 14^{o}, recorded mostly onshore steering, while runs 5-8 (April 15), with mean wind angle of 38^{o} (0^{o} alongshore, 90^{o} onshore), recorded alongshore steering at the same locations. So, the predominantly onshore flow was steered alongshore in a manner similar to deflection in the presence of a scarp (Hesp et al., 2015), whereas the oblique alongshore flow was steered towards the dune, similar to findings from other studies of flow over foredunes (Svasek and Terwindt, 1974; Arens et al., 1995; Hesp et al., 2005; Walker et al., 2006, 2009b).

It is possible that LWD on the beach contributed to the observed flow steering patterns, however, the presence of a larger scarp and taller dune on T2 complicates any causal association. The LWD matrix as arranged during this study was fairly low in height (< 0.5 m) with few stacked logs resulting in mostly shore-parallel or acute alignments (see Figure 6Figure 8a), thus providing a short, non-porous physical barrier that could steer flow alongshore. The drag-induced flow speed reduction over the LWD at 0.5 m could create a pressure differential between the faster flow observed on the stoss slope, thus steering alongshore flow toward the faster and lower pressure flow on the dune. However, T1B was placed 3.5 m closer to the dune crest than the reference station T2B, which was intentionally placed farther seaward to avoid effects of the taller scarp (+1 m) and dune (+2.5 m). As a result, the flow steering over the LWD cannot be conclusively linked to the presence of LWD since the effects of T1B being placed closer to the dune are unknown. Unfortunately, the incident flow angle for this study did not vary more than 30^{o} and additional data from multiple and highly variable wind approach angles with similar landward dune characteristics is necessary to fully realize the effects of LWD matrices and LWD orientation on flow steering.

Table 3 – Average flow direction deviation (degrees) by anemometer relative to $T2B_{1.5}$. Negative values indicate a more alongshore flow while positive values indicate a more onshore flow. $T1D_{1.5}$ is missing for runs 6-8 due to a sensor malfunction. † $T2B_{1.5}$ shows the deviation of the average incoming approach angle relative to the dune crest to show the obliquity of flow (bold italicized = reference).

	T1 (LWD)				T2 (No LWD)			
	Beach (0.5 m)	Beach (1.5 m)	Dune (0.5 m)	Dune (1.5 m)	Beach (0.5 m)	***Beach† (1.5 m)***	Dune (0.5 m)	Dune (1.5 m)
Run 1	-1	1	-8	-5	0	***25***	7	2
Run 2	10	11	12	9	0	***23***	4	0
Run 3	10	14	8	6	0	***17***	11	7
Run 4	14	16	11	10	-1	***15***	7	3
Run 5	-20	-10	-15	-12	-2	***44***	2	1
Run 6	-13	-5	-12		-3	***33***	2	1
Run 7	-10	-2	-10		-2	***26***	1	1
Run 8	-20	-11	-14		-2	***42***	3	1

2.4.3 Implications of Flow over LWD for Beach-Dune System Morphodynamics

Analysis of turbulent flow properties over LWD on the beach and on the dune stoss slope provides the basis for a discussion of the potential implications for sand transport and dune morphodynamics. The overall effect of the LWD matrix was to reduce near-surface wind speed, Reynolds Normal Stress, and turbulent energy while simultaneously transferring energy from the mean flow field to the fluctuating components, as shown by increases in CV_u. The increased CV_u demonstrates that the LWD matrix facilitates a transfer of energy from the mean flow to the turbulent fluctuations. This cascade of energy toward enhanced turbulence might suggest an increased capacity to transport sediment, but values such as $\overline{u'^2}$, which have been shown to have a stronger role in sediment transport than CV_u (Bauer et al., 1998, 2013; Sterk et al., 1998; Weaver and Wiggs, 2011; Bauer, 2013; Chapman et al., 2013), decreased over the LWD (Table 2). Similarly, the absolute reduction in streamwise fluctuations relative to the increase in vertical fluctuations results in RS_{Hk} remaining nearly static. Therefore the LWD matrix acts effectively as a pseudo-stagnation zone in front of the dune, which can serve as a sink for sediment deposition.

Changes to flow quantities downwind of the LWD indicate the potential for sediment transport on the stoss slope of the dune despite the flow alterations caused by LWD on the beach. The increase in $\overline{w'^2}$ and RS_{Hk} (Figure 15b) as well as Q2 and Q4 occurrences at $T1D_{0.5}$ compared to $T1D_{1.5}$ (Figure 14) confirm that turbulent structures are conveyed toward the bed. The quadrant occurrences are consistent with the increase in RS_{Hk} as the Q2 and Q4 interactions contribute positively to Reynolds stress. Turbulent structures conveyed toward the bed are the result of topographic forcing (i.e., flow compression and streamline concavity) (Chapman et al., 2012). Thus, transport could still be active on the stoss slope of the foredune (e.g., Chapman et al., 2013), downwind of the LWD.

2.4.4 Limitations

As LWD matrices are inherently diverse and complex, and since the data collected during this study span a relatively limited range of conditions, the conclusions are necessarily site and event specific. It is important to remember that this study monitored wind speeds over a fairly limited range, averaging 3.7 and 6.1 m s^{-1} gusting to 11.0 and 12.2 m s^{-1}, which produced highly intermittent and spatially variable sand transport that may not be representative of conditions during sustained winds with greater energy. Further research is needed to fully capture the range of conditions that may prove the importance of LWD in modifying wind and transport conditions across beach-dune systems. In particular, variations in LWD matrix height, depth, density, and stage of infilling should be measured to ascertain their effect on flow alterations.

Comparing flow over LWD to flow over a reference transect with no LWD is desirable, but difficult to achieve in the field. Variations in dune height and topography, presence of a scarp (and scarp height), vegetation density and variability, and the ability to clear the LWD make comparing different locations on the beach problematic. Indeed, this study refers to T2 as the reference transect, yet the highly alongshore nature of flow resulted in the T2 dune station being influenced slightly by LWD, as evidenced by the coverage density in Table 1. Future experiments would likely benefit from locating additional instrumentation within, up-, and down-wind of the matrix while referencing changes in flow conditions relative to fully

developed boundary-layer flow over the beach, thus eliminating impacts from variable morphology and the need for a transect with no LWD present.

2.5 Conclusions

The effects of LWD on turbulent airflow over an embayed sandy beach-dune system were investigated. Sonic 3D anemometry was used to quantify flow and turbulence quantities over and through a LWD matrix (approximately 12 m wide and < 0.5 m in height) fronting the foredune during highly oblique alongshore flow and a limited wind speed range. The main findings are:

- LWD acted as a highly effective flow modifier over the beach by inducing roughness drag that served to deflect the incoming flow upward and away from the surface. The absolute magnitude of near-surface mean wind speed, turbulent kinetic energy, and Reynolds stress were reduced in the presence of a LWD matrix. In addition, there was a transfer of energy from the mean flow field to the turbulent fluctuations, such that the overall turbulence intensity increased along with a slight shift in the quadrant geometry toward Q2/Q4 event activity. These flow modifications would seem to favor sediment transport potential, but this was not the case due to the overall reduction in the mean energy of the flow field. The effect of the LWD matrix on flow considered in this paper did not include the localized flow patterns around individual pieces of LWD nor its effect on sand transport due to the substantial physical barrier LWD presents to saltating grains.
- Shore-parallel aligned LWD has the potential to cause alongshore flow steering of obliquely onshore winds, although this depends on incoming flow angle. An alongshore flow steering effect of highly oblique incident winds could enhance the decoupling effect of beach and dune sediment transport pathways described by Bauer et al. (2012) minimizing landward transport (Ollerhead et al., 2013).
- Downwind of the LWD, on the stoss slope of the dune, there was evidence of flow compression and streamline concavity that conveys turbulent flow structures toward the bed. The presence of these flow patterns suggests that flow downwind of a LWD

matrix responds characteristically to topographic forcing as would be expected in the absence of LWD, thus providing the potential for sediment transport on the stoss slope of the dune.

3. Aeolian sand transport and deposition patterns within a large woody debris matrix fronting a foredune.

Michael J. Grilliot, Ian J. Walker, and Bernard O. Bauer

Published, 10 April 2019, in:
Geomorphology 338C. https://doi.org/10.1016/j.geomorph.2019.04.010

3.1 Abstract

Sediment transport pathways and resulting erosion-deposition patterns across beach-foredune systems can be complex. Although a great deal is known about the effects of wind fetch, surface moisture, topographic forcing, and vegetation cover, the role of large woody debris (LWD) as a control on sediment redistribution across beaches is relatively understudied. Pieces of LWD act as non-porous roughness elements that induce secondary flow circulation, thereby creating unique sedimentation patterns that differ markedly from those over a flat beach. Large accumulations of LWD collectively have a bulk porosity that provides substantial sand trapping volume, yet, no studies to date have quantified the effect of LWD on aeolian sand transport. Results from a field study on a macrotidal beach on Calvert Island, British Columbia, Canada, show that the LWD matrix alters the character of the turbulent boundary layer in a way that reduces sediment flux by 99%. Sand is trapped within the LWD matrix, thereby interrupting sediment delivery from the nearshore to the foredune. As such, LWD has the potential to modulate rates of foredune recovery, growth, and evolution. The relative importance of this effect depends on the density and arrangement of LWD as a fundamental control on aeolian sediment transport, as well as on the magnitude and frequency of events that erode the beach periodically and re-organize the LWD matrix.

Keywords: Beach-Dune systems; Sediment Transport; Coastal Erosion; Roughness Elements.

3.2 Introduction

Roughness elements on beaches and coastal dunes (i.e., vegetation, beach wrack, large woody debris) play an important role in beach-dune morphodynamics by acting as an accretion anchor for aeolian sediment, modulating sand transport to foredunes, and providing substrate for incipient dune development (Walker and Barrie, 2006; Nordstrom et al., 2007, 2011; Heathfield and Walker, 2011; Bauer et al., 2013; Eamer and Walker, 2013; Hesp and Walker, 2013). Porous vegetation, for example, has been identified as a key control on sedimentation patterns and foredune growth because the enhanced roughness extracts momentum from wind and induces deposition (Hesp, 1989; Wolfe and Nickling, 1993; Arens, 1996; Hesp and Walker, 2013; Gillies et al., 2014; Keijsers et al., 2015; Hesp et al., 2016). Large Woody Debris (LWD), in contrast, is a non-porous roughness element that is relatively understudied in coastal sand transport and sedimentation research (Walker and Barrie, 2006; Eamer and Walker, 2010). This paper addresses this knowledge gap by exploring the geomorphic role of LWD on beach-dune sediment transport.

A LWD matrix is a collection of solid roughness elements arranged in an array with a density that depends on the packing and arrangement of the LWD elements, analogous to other solid roughness arrays (Lancaster and Baas, 1998; Gillies et al., 2006, 2007, 2015; Gillies and Lancaster, 2013). Variations in LWD size, shape, structure, density, apparent porosity, orientation to incoming air flow, and height above the surface create complex flow-form interactions that alter aeolian sediment transport pathways in sometimes unpredictable ways (Figure 16). Unlike sand fences, which are linear 2D forms that have been studied extensively (Hotta and Horikawa, 1990; Li and Sherman, 2015; Gillies et al., 2017), LWD matrices are three-dimensional roughness arrays with varying porosity and accommodation space for sediment deposition about which relatively little is known.

Figure 16 – Photos of LWD deposits on West Beach, Calvert Island, British Columbia, Canada. (a) Partially buried log with up- and down-wind sand ramp; (b) Dense matrix of logs; (c) Matrix of LWD with near complete aeolian in-filling in front an established foredune.

LWD is acted upon by littoral and aeolian processes that change its function in the coastal backshore environment. Kennedy and Woods (2012) found that the presence of LWD on gravel beaches helped dissipate wave energy, resulting in gravel deposition in the LWD matrix that led to taller and steeper storm berms. Some studies noted that LWD could be rafted during high water events and act like battering rams to expose more dune area to erosion by ripping up berm and foredune deposits (Stembridge, 1979; Finlayson, 2006; Johannessen and Maclennan, 2007; Heathfield and Walker, 2015). Aeolian accretion within a LWD matrix was identified as key to several geomorphic roles, including damming backshore rivers to create ephemeral pond systems, helping rebuild eroded dune sediment by trapping and storing sediment to be reworked during high water levels, and acting as a nuclei for vegetation establishment and incipient dune formation (Komar and Rea, 1976; Walker and Barrie, 2006;

Eamer and Walker, 2010). While every possible function is compelling in its own right, there is a clear knowledge gap in quantifying the impact that a LWD matrix, as a whole, can have on aeolian sand transport and deposition to a coastal foredune (Gonor et al., 1988; Walker and Barrie, 2006; Eamer and Walker, 2013).

The purpose of this study was to identify the effects of a recently reworked LWD matrix on aeolian sand transport and deposition on a high energy, macro-tidal beach. The results from a short-term sediment transport experiment comprising several individual events are placed in the context of seasonal measurements quantifying long-term, post-event volumetric and morphological changes using terrestrial laser scanning (TLS). Sediment transport during a typical transporting wind event was measured along shore-perpendicular transects with varying concentrations of LWD. Event-based sediment transport patterns are linked to alterations to the turbulent boundary layer over the LWD, which were described in Grilliot et al. (2018).

3.3 Methods

3.3.1 Study Site

The study site is located on Calvert Island, on the central coast of British Columbia, Canada (Figure 5). The experiment was conducted on West Beach, a 1-km wide embayed beach bounded by rocky headlands with a SW aspect and relatively open exposure to the Pacific Ocean. The foredune is found on the north end of the beach and is approximately 6.5 m tall and partially vegetated by native dune grass (*Leymus mollis*). The foredune has stoss (seaward) slope angles of 23° to 37° and a crestline orientation of SE - NW (128° - 308°). A storm on 10 March 2016, incised the foredune toe creating a 1 to 2 m high scarp that remained near vertical with some slump blocks at the time of the experiment. The beach is macro-tidal with a spring tide range of >4 m, a low tide width of 250 m, and an effective fetch >500 m in the obliquely alongshore resultant sand drift direction. Data from a nearby meteorological station for 2012 to 2018 show prevailing winds from the SE (obliquely alongshore). Median grain size (D_{50}) of the beach-dune sediments was 0.198 mm (Eamer, 2017) and the aeolian sand transport potential regime (see Fig. 3 inset) is unimodal with a resultant drift potential (RDP) of 111 vector units (vu) toward a resultant drift direction of 322^{o} as derived using the Fryberger and Dean (1979)

model per the approach of Miot da Silva and Hesp (2010).

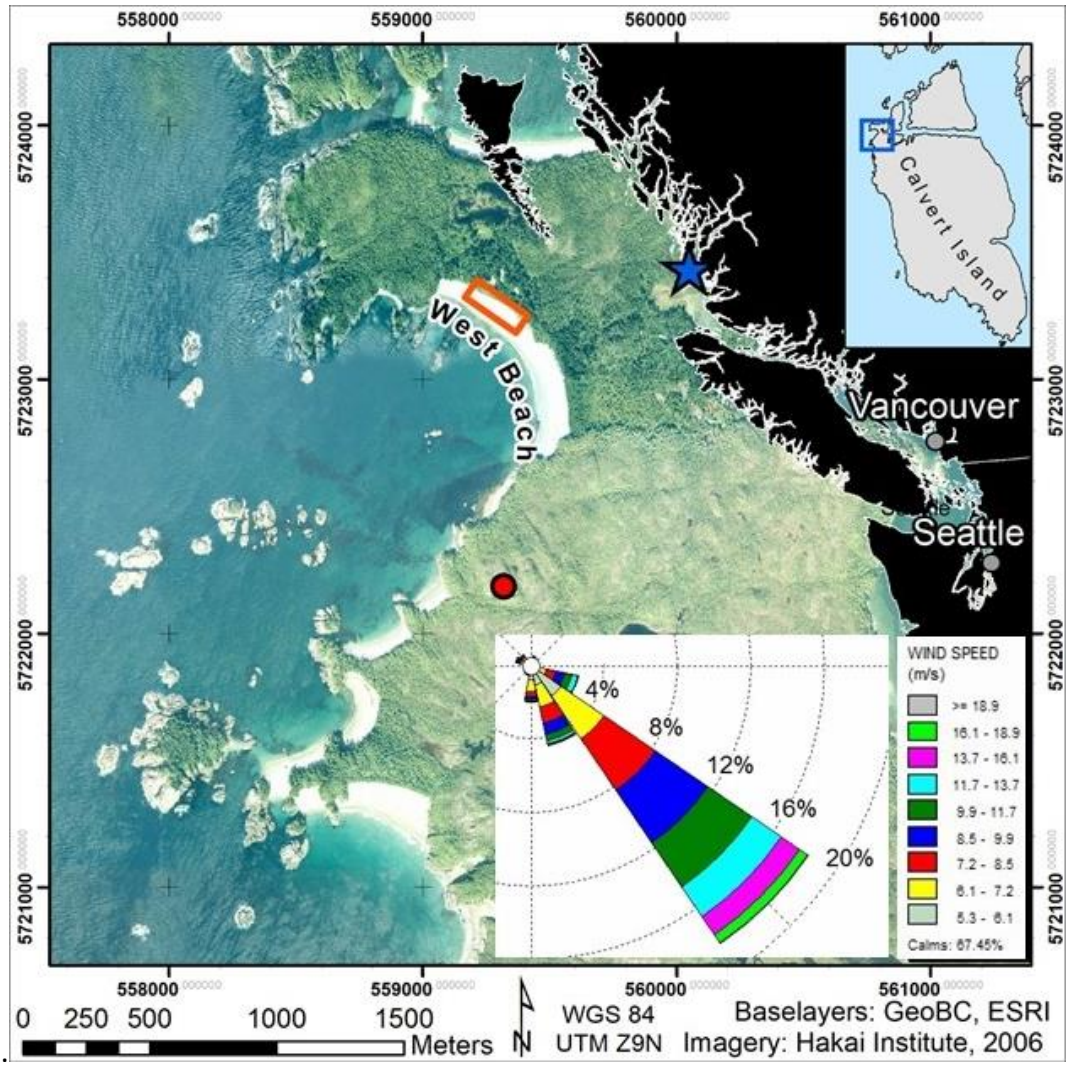

Figure 17 – Location of the study area (orange rectangle) on West Beach, Calvert Island, British Columbia, Canada. The red dot shows the location of the weather station used for drift rose calculations (Figure 3).

3.3.2 Experimental Setup

The experiment was conducted from 11 - 25 April 2016 along three shore-normal transects that were instrumented and monitored (Figure 18 and Figure 19). Transect 1 (T1) was located through an array of dense LWD; Transect 2 (T2) in sparser LWD; whereas Transect 3 (T3) served as the 'control' transect, which was cleared of LWD to 4 m on either side. Eighteen 0.3 m long aluminum erosion pins (6 per transect) were installed along each transect in the

same locations relative to the scarp base (negative = landward, on the foredune) at -3.3, -1.3, 1.7, 4.2, 7.7, and 13.7 m (Figure 73). Boundary-layer flow information was measuring coincidentally and discussed in detail by Grilliot et al. (2018).

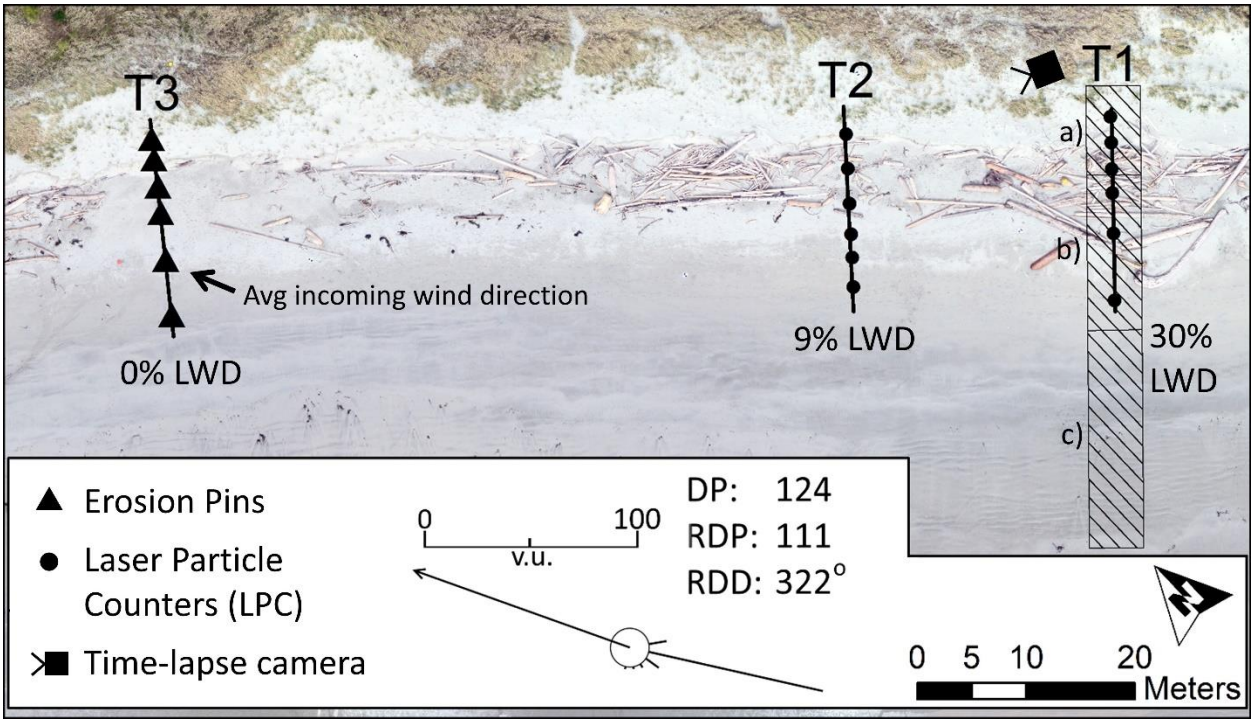

Figure 18 – Aerial photograph (11 April 2018) showing the location of Transects 1 through 3 (T1-T3) as black lines. T3 is the control transect with minimal LWD cover. The hashed rectangles show the location of the TLS morphological units a) foredune (37 m^2), b) backshore (71 m^2), c) foreshore (100 m^2). The black dots on T1 and T2 show the locations of LPCs. No LPCs were installed along T3. Erosion pins were installed on all transects at the same relative locations as on T3.

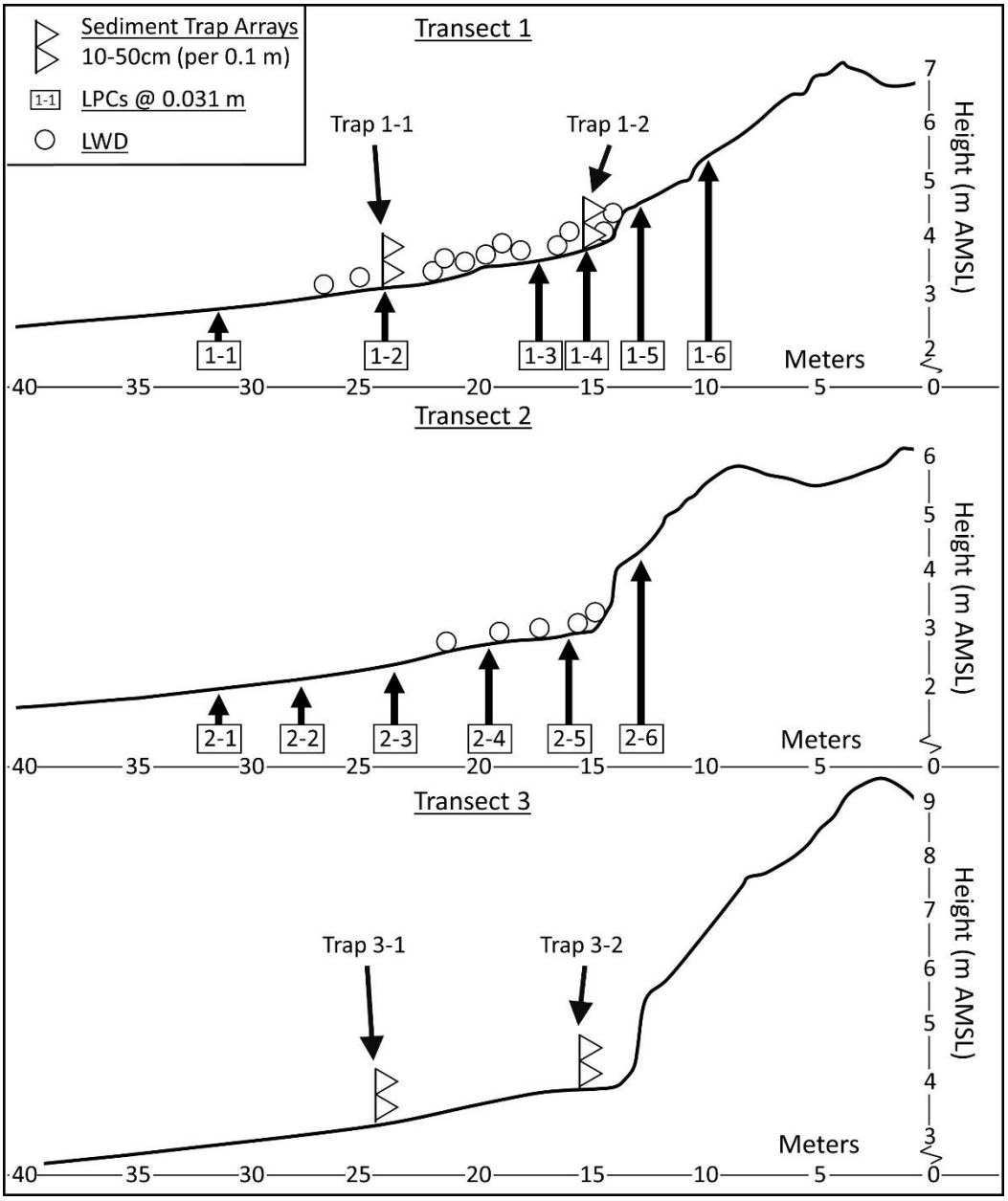

Figure 19 – Diagram of instrument locations on Transects 1 through 3. LPCs and Sediment Trap arrays are named by Transect # and closest seaward position (e.g., LPC 2-4 is on T2 and is the fourth sensor from the seaward-most sensor).

Hilton-style aeolian sediment traps with a sampling orifice of 4 cm^2 (Hilton et al., 2017) were installed in four vertical arrays on aluminum rods on each transect with sampling heights of 10, 20, 30, 40, and 50 cm at the center of the traps (Figure 20). The arrays were co-located with laser particle counters (LPCs) to measure sand transport intensity at locations 1-2 and 1-4

(7.7 and 1.7 m seaward of the scarp, respectively) on T1 and 3.7 m and 8.5 m seaward of the scarp on T3 (Figure 19). The landward T3 trap array location was altered slightly from T1 because of a larger dune ramp and to avoid interference with other instruments. Sediment trap arrays were installed for 5 hours from 11:00 to 16:00 on 15 April 2016 only. Trap samples were dried, weighed, and reported as mass flux (kg m^{-2} day^{-1}) and as a percent of the total mass collected at the coincident Trap 3-1 height.

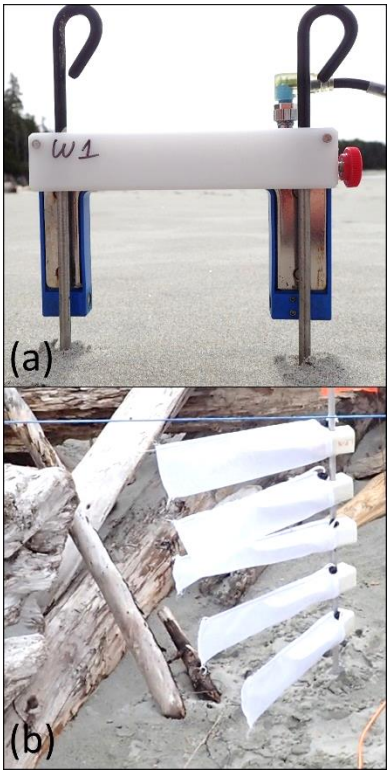

Figure 20 – (a) Wenglor LPC, and (b) Hilton-style sediment trap array (Hilton et al., 2017).

Sand transport intensity (grain counts s^{-1}, hereafter referred to as 'counts') was measured using LPCs (Wenglor model YH08PCT8) with 80 mm path lengths and a beam width of 0.6 mm. Each LPC was set to the maximum sensitivity, which has the advantage of recording large transport rates (1000 counts per second, i.e., Hz) before significant increases in error arise. For further details on LPC operation and performance see Barchyn et al., 2014; Hugenholtz and Barchyn, 2011; and Bauer et al., 2018. LPCs were placed with the laser

sampling beam 0.031 m above the sand surface. Transport directions were variable within the LWD matrix and no cosine adjustments were applied to adjust for wind angle variations relative to the path length of the laser beam. Although these sensors were aligned approximately perpendicular to the incoming wind, count data should be interpreted as relative transport intensity only.

LPCs were hard-wired to Onset® EnergyPro Data Loggers housed in weather-resistant cases. Each data logger had six analog channels for recording anemometer outputs and six digital pulse channels to record LPC counts. All data were sampled and recorded at 1Hz. Standard data conversion routines were applied following manufacturers' guidelines. Care was taken to clean LPC lenses throughout the day and between runs to reduce moisture and dust contamination.

Surface elevation change measurements were collected at five seasonal intervals (Apr 2016, Jul 2016, Sep 2016, Apr 2017, Aug 2017) using a Riegl VZ-1000 TLS with a precision of 8 mm at 100 m distance. Environmental conditions (visibility, temperature, relative humidity, and barometric pressure) are parameterized on the scanner during the time of measurement to account for atmospheric variability in scan accuracy (Wang et al., 2014; Fabbri et al., 2017). Post-processing was completed in RiScan Pro© software. Individual scan positions were initially registered using stationary targets (10 cm diameter cylindrical reflectors) sited over benchmarks or using a top-mounted Trimble R10 GNSS receiver in Real Time Kinematic (RTK) mode linked to a network-surveyed base station. Individual scan registration was refined using the Multi-Station Adjustment (MSA) tool in RiScan Pro that matches similar points and features between scans to improve accuracy. Relative registration of all scans to the July 2016 survey was completed to eliminate possible GNSS errors and the need for repeat RTK ground-truthing surveys. Final registration accuracy for each survey date was less than 1 cm RMSE. Vegetation and LWD were removed from the TLS point clouds using the vegetation filter in RiScan Pro and an iterative refinement method developed by Riegl (2010). A conservative absolute accuracy for each survey was set at 2 cm to account for potential inaccuracies associated with vegetation and LWD removal for digital terrain model (DTM) creation. DTMs were created in Quick Terrain Modeler (QTM) version 8.0.7 using adaptive triangulation at 5 cm^2 raster size. Volumetric

analysis was performed in Geomorphic Change Detection (GCD) 7.0 software plugin for ArcGIS (Wheaton et al., 2010) using the spatially uniform student's t-test to determine significant volumetric change (p-value of 0.05).

To monitor geomorphic changes to the beach and dune between volumetric surveys a RECONYX™ HC500 HyperFire™ camera was installed on the dune (location shown in Figure 3) looking west-northwest. Images were taken every 15 minutes from 7 am to 7 pm local time.

3.4 Results

3.4.1 Transport Intensity and Activity

Sand transport events considered in this study represent a subset of eight 10-min runs from the 13 and 15 of April 2016 (Figure 21). Transport was highly intermittent during the experiment and only those periods with significant transport activity and limited directional deviation in the wind field were selected for analysis. Due to limited data logger capacity, LPC counts were collected only along T1 on 15 April 2016 and only along T2 on 13 April 2016, although both days had similar wind conditions. Raw LPC counts were compared directly and also using an Activity Parameter that defines the proportion of time in a sampling interval that active transport is recorded (Davidson-Arnott et al., 2012; Smyth et al., 2014). An Activity Parameter value of zero reflects no transport recorded while a value of one reflects sediment transport in all of the records of the sampling interval. This is the inverse of the intermittency parameter proposed by Stout and Zobeck (1997).

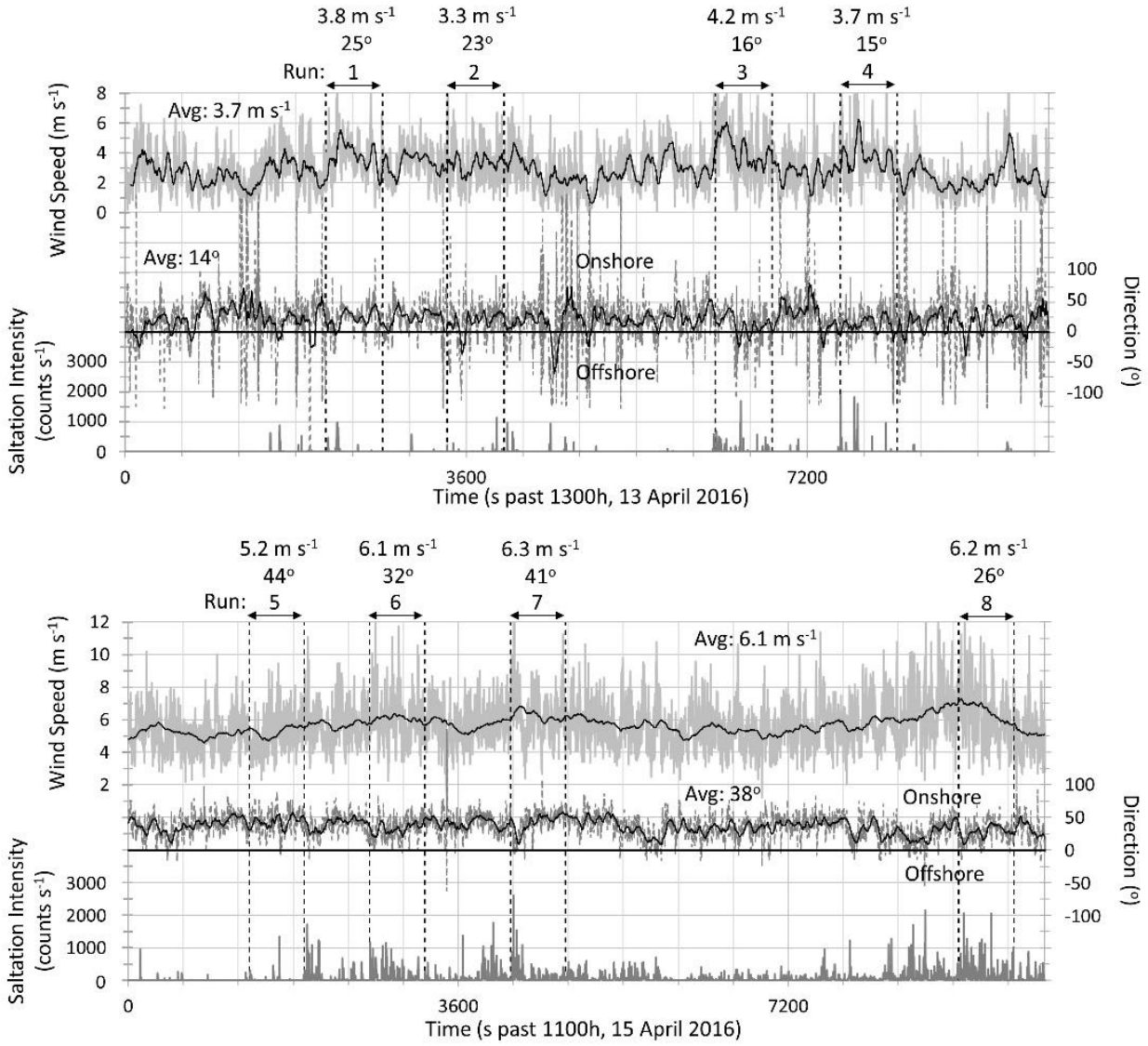

Figure 21 - Time series of incident wind speed (upper solid grey line) with 60 s running mean (black solid line) and values indicated by upper left axis (m s^{-1}), wind direction (middle dashed grey line) with 60 s running mean (black solid line) and values indicated by right axis (degrees), and saltation intensity (bottom grey bars) with values indicated along bottom left axis (counts s^{-1}) on 13 April (top graph) and 15 April (bottom graph). Wind speed and direction are from a Gill Instruments 3D sonic anemometer on the beach (7 m seaward of the scarp) on T3 at 1.5 m height. Saltation Intensity is from W1 on T1 (Figures 4, 5). Selected runs are indicated by the number on the top of each graph with average speed and direction values above.

LWD had a clear and measurable effect on sediment transport processes across the backshore. Absolute particle counts and the Activity Parameters downwind of the LWD were much smaller than the unimpeded transport across the beach during all runs (Table 4 and Table 5; Figure 22). LPC counts were reduced by at least an order of magnitude at the first sensor inside the LWD matrix (LPC1-2 on T1; LPC2-4 on T2). The decline in counts was maintained onto the stoss slope (LPC1-5 on T1; LPC2-6 on T2) along both transects. The trends in Activity Parameter were similar, with reductions at the first sensor downwind of the LWD, especially along T1 with a more densely packed LWD matrix. The decline in Activity Parameter was maintained onto the stoss slope of the foredune. The sensors below the foredune scarp and on the stoss slope recorded a 99-100% decrease in counts and Activity Parameters relative to the beach. These observations are consistent with other research showing sand transport decreasing with downwind distance in a roughness array (e.g., Gillies and Lancaster, 2013; Gillies et al., 2015).

Table 4 – LPC counts for all 10-min runs. Runs 1-4 were located on T2 and runs 5-8 were located on T1. The transect average of all runs per LPC location is shown normalized as a percent of the LPC 1-1 and 2-1 average respectively (i.e., $Average_N$). Cell shading indicates sensor position: no shading shows LPC's seaward (upwind) of the LWD; Light gray shading shows LPC's within the LWD matrix, and dark gray shows LPCs on the stoss slope of the foredune. See Figure 19 for LPC locations relative to the LWD and scarp.

	LPC 1-1	LPC 1-2	LPC 1-3	LPC 1-4	LPC 1-5	LPC 1-6
T1: Run 5	7282	24	6	1	3	2
T1: Run 6	59811	332	57	1	0	7
T1: Run 7	101359	2699	220	60	40	40
T1: Run 8	5420	758	45	14	4	44
T1: AverageN	**100%**	**1.71%**	**0.15%**	**0.03%**	**0.02%**	**0.04%**
	LPC 2-1	LPC 2-2	LPC 2-3	LPC 2-4	LPC 2-5	LPC 2-6
T2: Run 1	12861	6605	5656	268	0	0
T2: Run 2	4394	2404	1682	197	1	0
T2: Run 3	24299	14314	8621	488	2	0
T2: Run 4	21613	18644	11789	897	2	0
T2: AverageN	**100%**	**66.44%**	**43.93%**	**2.93%**	**0.01%**	**0.00%**

Table 5 – LPC 10-min Activity Parameters for all 10-min runs. Runs 1-4 were located on T2 and runs 5-8 were located on T1. The transect average of all runs per LPC location is shown normalized as a percent of the LPC 1-1 and 2-1 average respectively. Cell shading indicates sensor position: see Table 4 for details. See Figure 19 for LPC locations relative to the LWD and scarp.

	LPC 1-1	LPC 1-2	LPC 1-3	LPC 1-4	LPC 1-5	LPC 1-6
T1: Run 5	0.20	0.01	0.01	0.00	0.01	0.00
T1: Run 6	0.68	0.12	0.05	0.00	0.00	0.01
T1: Run 7	0.65	0.12	0.07	0.03	0.00	0.00
T1: Run 8	0.67	0.08	0.02	0.01	0.01	0.02
T1: AverageN	**100%**	**13.2%**	**6.6%**	**1.7%**	**0.9%**	**1.8%**
	LPC 2-1	LPC 2-2	LPC 2-3	LPC 2-4	LPC 2-5	LPC 2-6
T2: Run 1	0.13	0.12	0.17	0.08	0.00	0.00
T2: Run 2	0.09	0.07	0.09	0.06	0.00	0.00
T2: Run 3	0.33	0.28	0.29	0.14	0.00	0.00
T2: Run 4	0.18	0.15	0.18	0.11	0.00	0.00
T2: AverageN	**100%**	**83.8%**	**101.3%**	**56.2%**	**1.2%**	**0.0%**

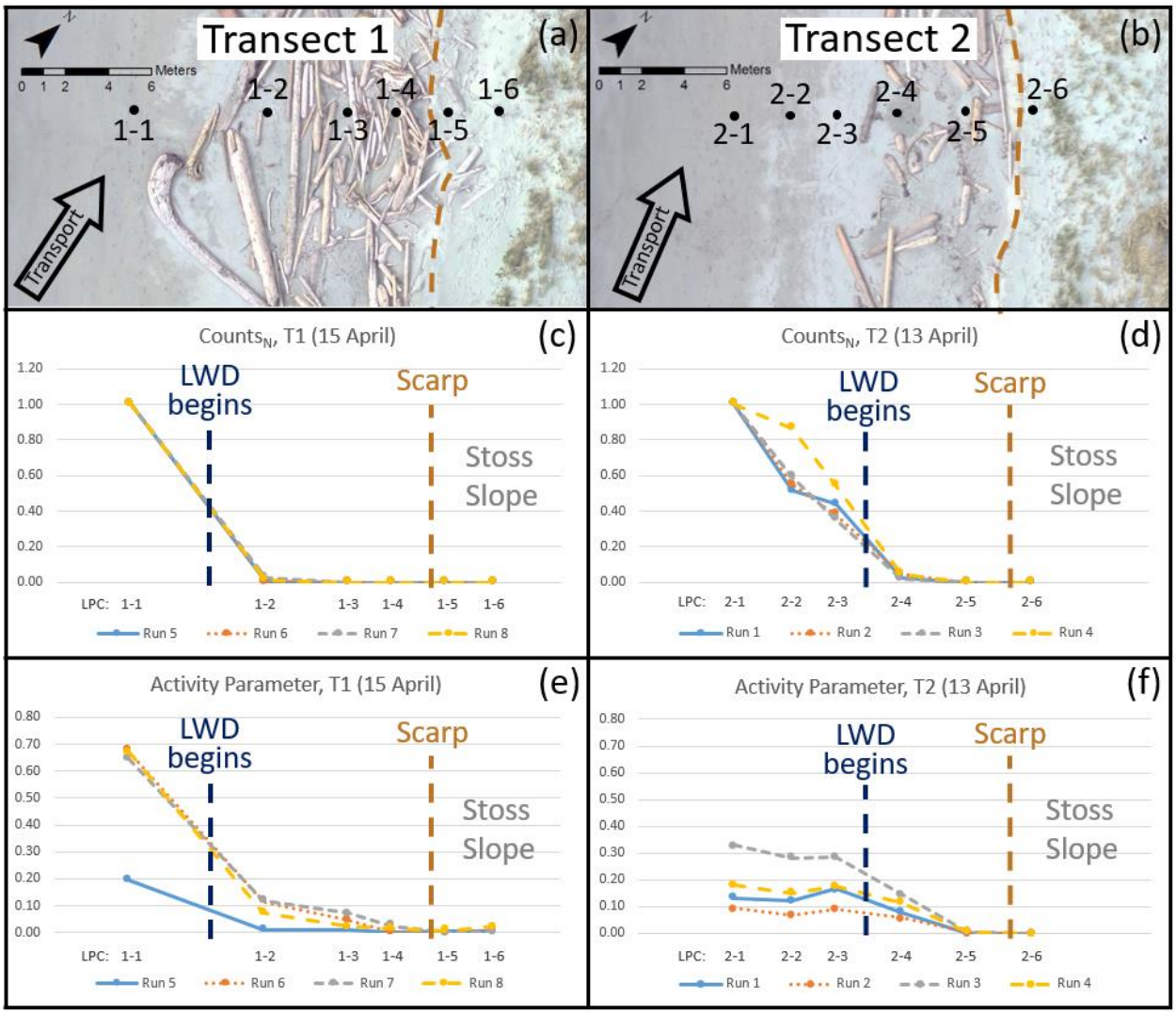

Figure 22 – Summary of transport intensity data showing: LPC locations and average incoming wind direction (a, b); counts$_N$, which shows the absolute values normalized by LPC 1-1 and 2-1 on each transect by run (c, d); and 10 min Activity Parameter (e, f) for runs 5-8 on T1 (a, c, e,) and Runs 1-4 on T2 (b, d, f).

Along T2 there were three LPCs on the unimpeded beach upwind of the LWD matrix, and they measured a progressive decline in particle counts across the beach. The most likely explanation is that these LPCs were positioned in the lee of the LWD along T1 given the oblique flow directions (Figure 22d, Figure 22f). Nevertheless, there was still an abrupt decline in sediment transport between LPC2-3 and LPC2-4, which coincides with the transition from an open sand surface to the LWD matrix. At the landward extent of the LWD (immediately

seaward of the foredune scarp), LPC1-4 and LPC2-5 recorded little to no counts and therefore zero Activity Parameter. The same is true for the stoss slope (LPC1-5, LPC1-6, and LPC2-6), except during runs 7 and 8 when only a few tens of counts were recorded. These comprise less than 1% of transport observed on the beach for each run.

The sharp decline in counts and Activity Parameters on both transects just downwind of the transition from open beach to LWD (at LPC1-2 and LPC2-4) is attributed to the roughness effect of the LWD matrix on the turbulent boundary layer. Grilliot et al. (2018) demonstrated that there was an abrupt decrease in mean near-surface wind speed, turbulent kinetic energy, and Reynolds shear stress at the transition into the LWD matrix, as well as a flow steering effect that re-orients the incident wind depending on the stacking orientation of the LWD. Differences in LWD coverage and arrangement along T1 and T2 therefore yielded different transport trends. Figure 22 illustrates how normalized grain counts ($counts_N$) and Activity Parameters decreased within the LWD matrix as a function of downwind distance for all eight runs. The decline in $counts_N$ and Activity Parameters on T2 downwind of the LWD was not as great as on T1 likely because of less LWD surface cover (Figure 18) as well as the size and arrangement of the LWD immediately upwind of LPC1-2 and LPC2-4. While there was active sand transport during the experiment there was no substantial erosion or deposition. The three seaward most erosion pins recorded < 0.5 cm basal scour on April 13th. Otherwise, no change was recorded at any of the erosion pins during the experiment, and they were removed in April 2016.

3.4.2 Sediment Flux

Measured sediment flux data from the Hilton-style traps (Figure 19) are summarized according to transect (T1 and T3) and height above the surface (10, 20, 30, 40, 50 cm) in Table 6. The vertical array of five traps along the control transect (T3) at location 3-1, which was the most seaward position on the unimpeded beach, accounted for 76% of the total mass collected from all traps, at all locations, because of its unobstructed exposure to uniform streamer activity over most of the beach (Figure 23). Both traps on Transect 3 were in locations that were distant from the influence of LWD, so the reduced transport at location 3-2 relative to 3-1 likely reflects subtle differences in saltation dynamics as wind moved across the beach closer to the

dune scarp. The vertical array of traps at location 1-1 (5 m inside the LWD) and 1-2 (12 m inside the LWD) recorded reductions of 89% and 96%, respectively, of the flux trapped along Transect 3 at the same relative location from the scarp. It is reassuring that the LPCs co-located with the Hilton-style traps on Transect 1 showed similar reductions in transport intensity as a proportion of LPC 1-1 on the unimpeded beach (Table 4). Thus, the spatial trends in sediment transport are real rather than due to measurement uncertainty inherent to the manual versus electronic technologies. In general, the trap data indicate that most of the sediment flux moves close to the bed with variable rates of transport higher in the profile. Traps at location 1-1 recorded slightly elevated mass fluxes at the 20-50 cm trap heights compared to the same trap heights at location 3-1. The differences in flux can be attributed to grains rebounding off the LWD, therefore being launched higher into the flow field than might normally be true for streamers. This will depend on the position of the traps relative to the nature of the LWD immediately upwind. In some instances, trap opening may be sheltered completely whereas in other cases the traps will be within highly turbulent wakes and eddy recirculation zones downwind of large logs.

Table 6 – Sediment trap mass flux density (g m^{-2} min^{-1}). Total sediment trap array (10 – 50 cm) data are also shown.

	T1 (with LWD)		T3 (No LWD)	
Trap Height (cm)	location 1-1	location 1-2	location 3-1	location 3-2
10	9.38	0.63	156.67	27.92
20	4.17	0.42	1.25	2.29
30	1.67	0.21	0.00	0.21
40	1.25	0.00	0.63	0.42
50	1.67	0.00	0.21	0.21
Total	18.13	1.25	158.75	31.04

Figure 23 – Image showing distribution of streamers on the beach moving toward the observer (looking upwind to the southeast) during run 6 on 15 April 2016.

3.4.3 Geomorphic and Volumetric Changes

Net morphological change was minimal during the transport experiments, and sand surface elevation fluctuations were within the accuracy of measurement of the erosion pins (approximately ± 5 mm). Transport fluxes were rather small and highly intermittent, which accounts for the small degree of morphologic change during the individual events monitored during the short-term experiments. However, seasonal changes as measured by TLS scans reveal significant morphologic change driven by the relative impacts of aeolian versus nearshore transport activity. Figure 24 - Figure 26 suggest that there is a beach-dune erosion and rebuilding cycle that mimics the classic summer-winter beach profile model first developed for the beaches of Southern California (Shepard, 1950). The TLS scans show that there was foreshore accretion in the summer (approx. +0.5 m), followed by erosion in the winter (approx. -0.6 m). However, the signal is less clear on West Beach because of the macro-tidal context, which influences the geomorphic effectiveness of storms depending on their timing relative to tidal phases. A major storm may only have a minimal impact on the beach in terms of wave

erosion if it occurs during low tide and is short-lived, but this same storm may be accompanied with substantial aeolian redistribution of sediment depending on wind speed and direction.

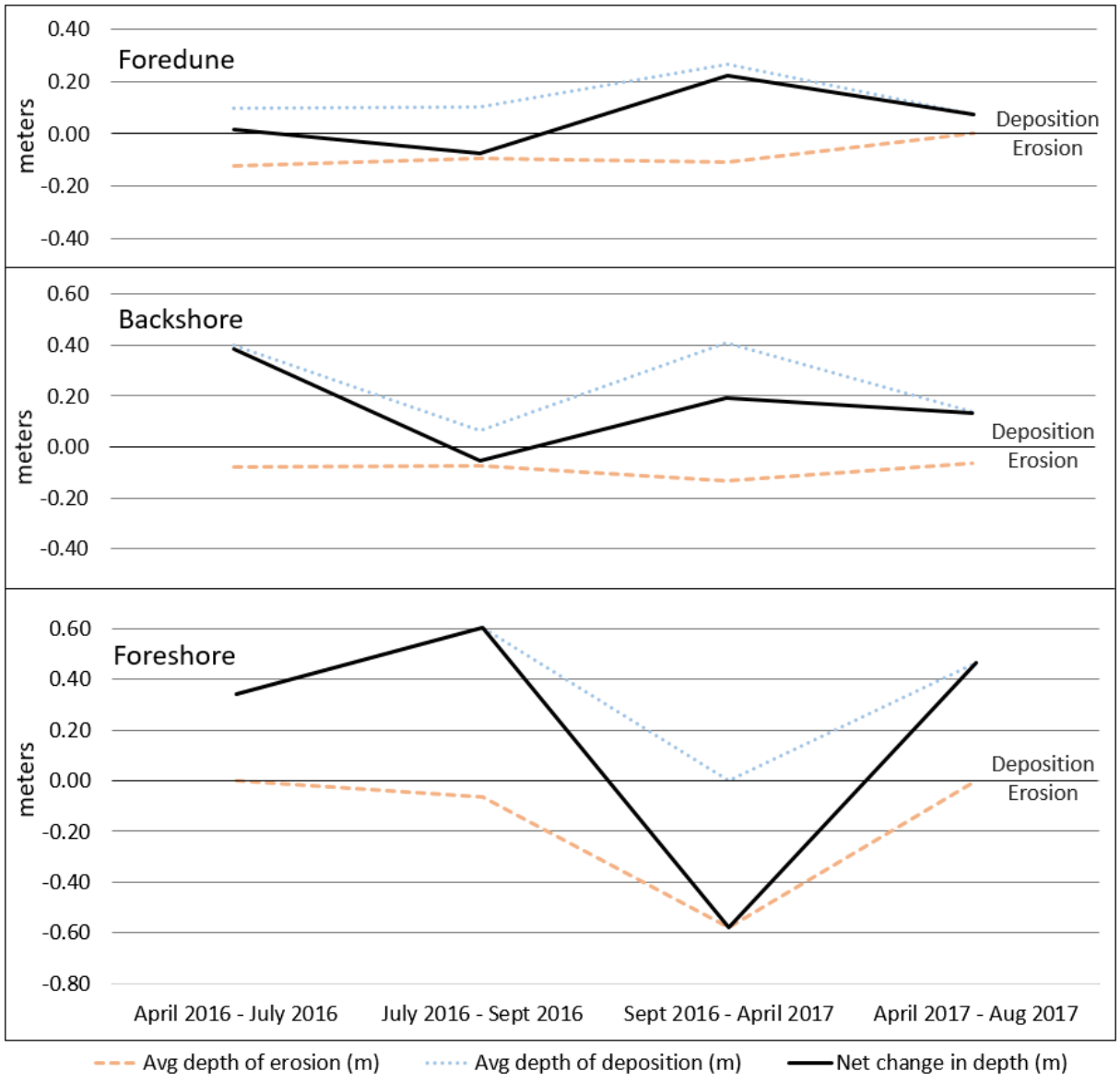

Figure 24 – Graphs showing changes in average depths of erosion and deposition during TLS scan intervals for each morphological unit over the area of detectable change (See Figure 18 for unit areas).

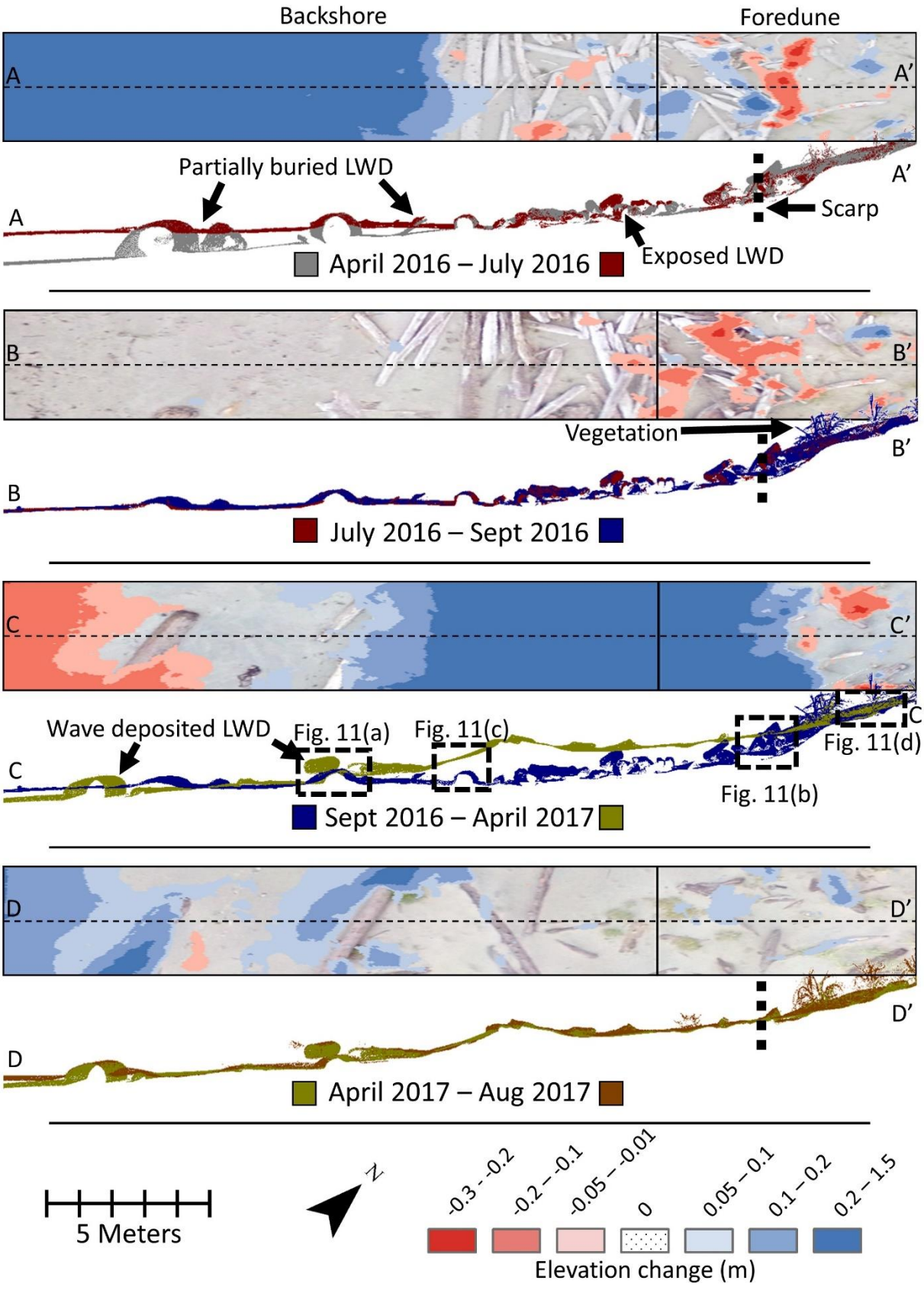
Backshore
Foredune
A
A'
Partially buried LWD
A'
A
Scarp
Exposed LWD
April 2016 – July 2016
B
B'
Vegetation
B'
B
July 2016 – Sept 2016
C
C'
Wave deposited LWD
Fig. 11(a)
Fig. 11(c)
C'
Fig. 11(d)
C
Fig. 11(b)
Sept 2016 – April 2017
D
D'
D'
D
April 2017 – Aug 2017
5 Meters
N
-0.3 – -0.2
-0.2 – -0.1
-0.05 – -0.01
0
0.05 – 0.1
0.1 – 0.2
0.2 – 1.5
Elevation change (m)

Figure 25 – Volumetric and profile changes between TLS surveys in the study area; April 2016 – July 2016, July 2016 – Sept 2016, Sept 2016 – April 2017, and April 2017 – Aug 2017. Plan view raster maps: The study area (see figure 3 for location) is divided into three morphological units; foreshore (not shown), backshore, and foredune. Significant volumetric changes (p = 0.05) to the study area are reported as deposition (blue) and erosion (red), see legend bottom-right. Underlying orthoimagery is from the later date in the date range. Dashed lines indicate the location of the TLS profiles. The short (y) axis of the raster is condensed to fit the figure and is actually 5 m wide. The long (x) axis is to scale, spanning a total beach width of 22.5 m. The foreshore is approximately 20 m in length. Profiles: Extracted TLS profiles include points within 1 m on either side of the profile line. Locations of LWD, vegetation, and the scarp are indicated on the figure. The crest of the scarp is 3.7 m AMSL (CGVD28). Dashed rectangles on profile A - A' show locations of the detail in Figure 26. The profile is to scale with no vertical exaggeration.

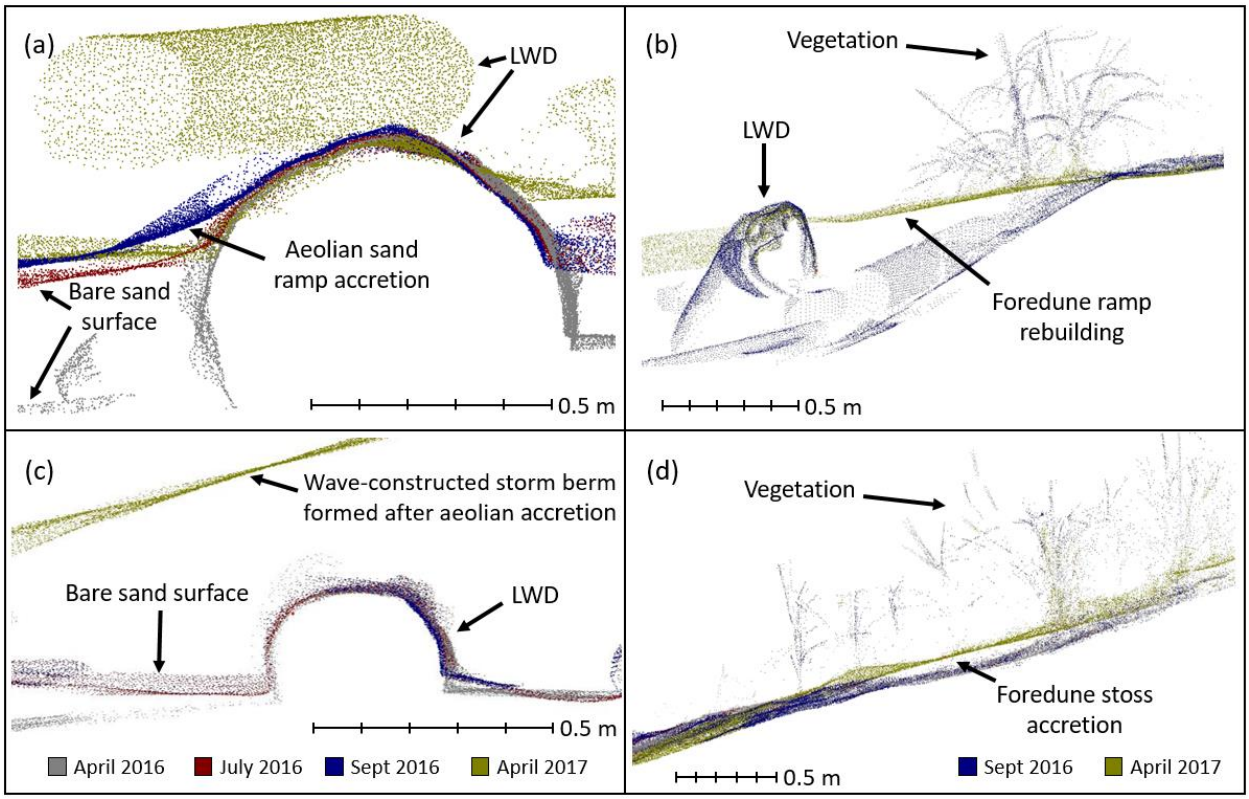

Figure 26 – TLS point cloud profiles (1 m wide) showing surface elevation changes between April 2016, July 2016, Sept 2016, and April 2017. (a) shows sand progressively

deposited around a large piece of LWD with an additional smaller piece of LWD deposited on top by wave action between Sept 2016 and April 2017. (b) shows the foredune ramp being rebuilt between Sept 2016 and April 2017. (c) shows aeolian deposition around LWD that is eventually buried between Sept 2016 and April 2017. (d) shows minor accretion on the stoss slope amongst vegetation between Sept 2016 and April 2017. Each panels scale is shown while (b) shows the legend for (a) and (b), and (d) shows the legend for (c) and (d).

Following a major wave event in March 2016 that scarped the foredune, minor readjustments on the scarp face and lower foredune slope were evident by April 2016 in the form of block slumping and grain fall deposits at the base of the scarp (Figure 28). Figure 25 shows that erosion of the dune decreased over time as the sand ramp fronting the foredune redeveloped.

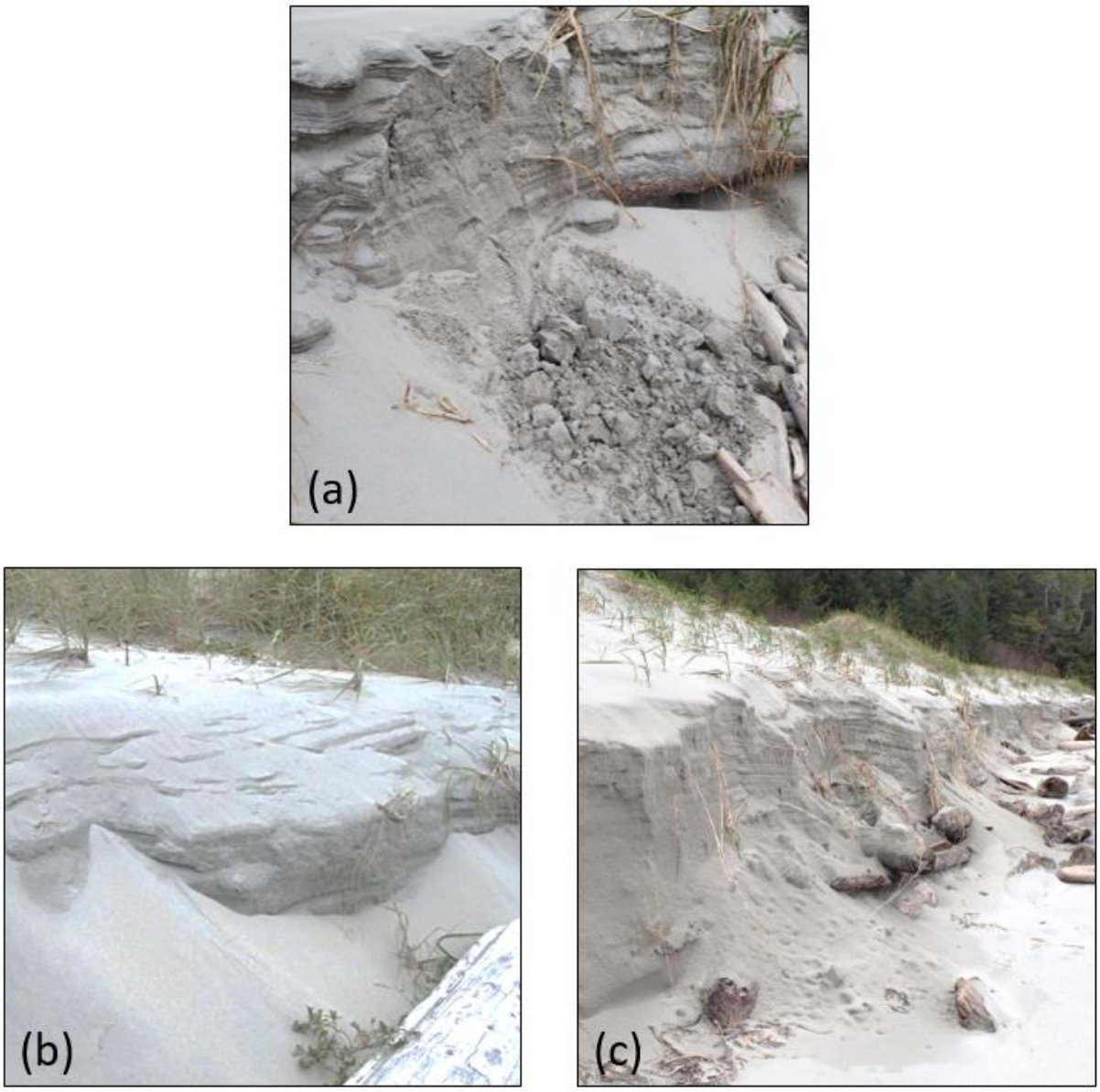

Figure 27 - Examples from the study site showing (a) blockfall, (b) grainflows, (c) combination of blockfalls, grainflows, and slumping partially burying LWD and beginning to rebuild the foredune ramp (April 2016).

From April to Sept 2016, wave-deposited sediments on the foreshore and backshore partially buried some of the LWD by an average of 0.4 m (Figure 25, profile A-A' and Figure 26a). As the beach aggraded and the storm season subsided, wave runup events became less effective in reaching the backbeach zone, leaving it exposed to aeolian transport. However,

generally calm winds during this period resulted in only minor aeolian accretion (Figure 24). Even so, the detail shown in Figure 26 shows localized aeolian deposits occurring as small sand ramps on the windward (Figure 26a) and leeward sides (Figure 26b) of individual pieces of LWD, reinforcing the importance of the LWD matrix in inducing aeolian sediment deposition.

The Fall and Winter months (September 2016 – April 2017) revealed significant aeolian deposition within the LWD matrix, as well as the formation of a fully developed aeolian sand ramp at the base of the foredune (Figure 26b). The sum of net volumetric changes in the backshore was 0.66 m^3 m^{-2} (Figure 24). Despite significant rainfall during the fall and winter, aeolian deposition in the LWD matrix zone was pronounced because of increased mean wind speed relative to summer. This created a situation where sediment delivered to the foreshore in the summer, building the beach, occurred during a different season than peak aeolian activity building the dune. Similar findings have been reported on the Pacific coast in Washington State where sediment delivery to the beach by waves is out of phase (occur at different times of the year) with peak aeolian activity to the foredune zone (Cohn et al., 2018).

Time-lapse imagery (Figure 28) revealed that most of the aeolian deposition in the LWD matrix was largely the result of a single wind storm in early November 2016, which lasted several days. Pre-event conditions are shown in Figure 28c, whereas post-event conditions are shown in Figure 28d, indicating complete burial of the LWD matrix (Figure 26b and Figure 26c). A later high-water event emplaced newly introduced LWD on top of the aeolian accretion layer (Figure 25, profile C-C’ and Figure 26a), and a wave-constructed storm berm evolved about 5 m seaward of the scarp. Morphological changes in the summer of 2017 (Figure 28f) were the same as the summer of 2016 (Figure 28b) with the foreshore building by swell action and relatively little change on the backshore (no significant aeolian activity, consistent with the wind climatology).

Figure 28 – Images from the time-lapse camera looking WNW (see Figure 4 for locations). Panel (c) and (d) show before and after a series of active aeolian transport events that bury nearly all of the LWD. Additional wave-deposited LWD can be seen in panel (e) while

vegetation colonizes the backshore over the summer months (f).

3.5 Discussion

3.5.1 LWD as a Modulator of Aeolian Sediment Transport and Supply to Coastal Dunes

The short-term transport experiments demonstrate that the LWD matrix was highly effective at trapping sediment moving across the backshore toward the dune. The sediment trapping potential of LWD therefore can limit the re-supply of sediment to the foredune, especially after a major wave-scarping event has eroded the dune toe. Depending on the degree to which the LWD matrix has been infilled by aeolian deposition, which alters the aerodynamic roughness and boundary layer turbulence (Grilliot et al., 2018), saltating grains moving across the beach might be trapped at the upwind edge of the LWD (when the matrix accommodation space is empty) or continue to move across the LWD matrix (when the accommodation space is full). The seasonal volumetric survey and TLS profiles (Figure 25 and Figure 26) show examples of all these morphodynamic states because the LWD matrix was progressively in-filled during the seven months of observation. New LWD was deposited atop the former deposit by subsequent storms.

Sand transport and deposition through the matrix decreased with downwind distance from the leading edge. Figure 29 and Figure 30 illustrate the relationship between total sand transport counts and normalized downwind distance within the LWD matrix along T1 and T2, respectively. Gillies and Lancaster (2013) and Gillies et al. (2015) suggested that a negative exponential relationship was appropriate for sand transport reductions within a uniform, artificial roughness array. While our data are not directly comparable (because the LPCs in this study were not calibrated to provide mass transport flux), Gillies et al. (2015, Figure 7, $R^2 = 0.94$) found a similar relationship to the exponential depletion of transport in their uniform array which was located on a flat desert surface. Understanding such decreasing transport trends within a LWD matrix is challenging because the roughness array parameters are irregular and highly complex, unlike the experimentally-emplaced, uniform arrays used by Gillies et al. (2015). The presence of the foredune in altering flow conditions due to pressure effects and topographic steering also complicate matters with natural LWD matrices. Moreover, the

relationships are temporally variable because the accommodation spaces within the LWD matrix will infill or empty and typically be re-arranged by high water events, thereby affecting the aerodynamic roughness and trapping efficiency. While it is possible that the differences in T1 and T2 trends are the result of different LWD coverages and/or roughness effects, it is entirely possible that the differences are a statistical anomaly because of the limited number of data points. In either case, further research is required to attribute the physical cause of the differences in regression trends by transect. The relative agreement with Gillies et al. (2015) demonstrates the similarity between complex natural roughness matrices to those that have tighter experimental control.

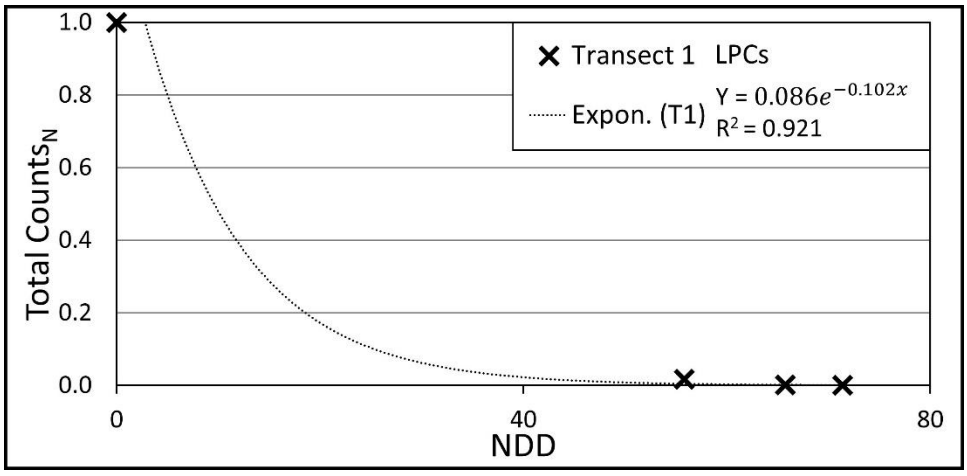

Figure 29 – Total Counts$_N$ (defined as the ratio of total grain counts for all runs at a LPC divided by the total grain counts for all runs at the seaward-most LPC per transect) for all runs on Transect 1 as a function of normalized downwind distance (which is defined as the downwind distance from the seaward most LPC divided by the average height of LWD along T1 and T2 (estimated to be 0.25 m from the TLS scans). 0 marks the upwind extent of the LWD matrix. LPCs 1-4 and 1-5 are excluded as they were on the stoss slope.

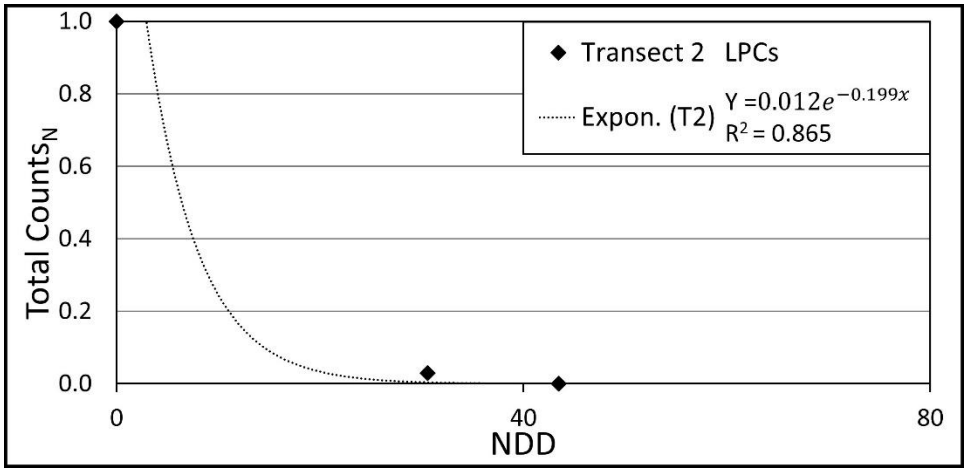

Figure 30 – Total Counts$_N$ for all runs per Transect 2 as a function of normalized downwind distance. 0 marks the upwind extent of the LWD matrix. LPCs 2-2 and 2-3 are excluded due to downwind interference from Transect 1, as is LPC 2-6 which was on the stoss slope.

Despite the enhanced trapping efficiency of a partly filled LWD matrix, there will always be secondary pathways for sediment transport through the zone of LWD, depending on stacking, orientation, and density. Some of these transport corridors are parallel to logs and occasionally underneath logs that are perched on others, where flow can be accelerated through a hollow thereby preventing local deposition. In other instances, grains move over-top the matrix. Although grain suspension was not observed directly during the experiments due to the moderate wind speeds encountered, the 20 – 50 cm height traps 5 m inside the LWD (Trap 1-1) recorded more sand transport than Trap 3-1 on the unimpeded beach (Table 6). This is likely the result of rebounding sand in modified saltation over the LWD at lower heights, such that these grains bounce higher into the flow field than they normally might in the absence of the LWD. For the events observed in this study, this transport mechanism appears limited to the upwind portions of the LWD matrix as it was not documented 10 m into the LWD matrix (trap 1-2). Grilliot et al. (2018) describe shifts in the character of the turbulent boundary layer during the same event that enhanced shear stress over the LWD, which could facilitate continuous transport over the LWD. However, the increase in shear stress was accompanied by a marked reduction in mean flow speed and turbulent kinetic energy immediately above the

LWD, which explains why the rebounding effect was limited to the upwind section of the LWD zone. Experimentation during faster winds is needed to assess if this mechanism can be maintained across the entire LWD matrix, as suggested by Anderson and Walker (2006).

3.5.2 Long-term Impacts of the LWD Matrix on Foredune Recovery and Growth

The long-term impacts of a LWD matrix on a foredune are poorly understood but potentially quite important. A recently deposited matrix of LWD has significant capacity to trap and store sediment, thereby preventing delivery of aeolian sand to the foredune. For example, if a major storm event scarps the foredune and emplaces LWD on the backshore, the presence of the LWD matrix will impede the rapid healing of the foredune scarp by aeolian processes. Without a well-developed sand ramp leading to the stoss slope of the foredune, very little sediment can make its way up the stoss slope toward the crest. Not only can the foredune not grow, the crest can be eroded, especially in the absence of a protective cover of vegetation during intense wind events (as experienced in winter). As the accommodation space in the LWD matrix is infilled with sediment that would otherwise reach the foredune, the matrix will gradually lose its ability to impede sediment transport to the foredune. Such decreasing sand capture capacity has been noted for sand fences (Hotta and Horikawa, 1990; Nordstrom et al., 2006, 2007, 2011; Gillies et al., 2017), 3D roughness arrays (Gillies et al., 2015), and beach wrack (Dugan and Hubbard, 2010; Nordstrom et al., 2011).

While beach wrack is also naturally deposited and may play a similar role to LWD, there are a few primary differences between typical wrack deposits and LWD matrices as transport modulators. The wrack deposits, although important to incipient dune formation (Hesp, 2002), are usually of limited height and width with gentle slopes so they do not protrude as far into the boundary layer as does LWD. Grilliot et al., (2018) showed that the LWD matrix increased vertical mixing and reduced wind speed up to 1.5 m above the surface. These effects resulted in decreased transport recorded to a height of 0.5 m in this study. The LWD matrix in this study was also comprised of a complex network of overlapping pieces that was up to 15 m wide and up to 0.5 m high in places. The scale and shape alone make the LWD matrix far more effective at altering airflow and reducing sediment transport than typical beach wrack deposited in

shallow shore-parallel ridges or scattered across the beach surface. Admittedly, beach wrack (and other deposits of marine vegetation washed on the shore) has been recorded up to a depth of 0.3 m and sometimes higher, but in these instances there is relatively little accommodation space between the individual plants. Given that a LWD matrix can vary in size and density it seems more appropriate to conceptualize the role of the LWD matrix in this study as having properties similar to the artificial roughness arrays studied by Gillies and Lancaster (2013) and Gillies et al. (2015) rather than typical beach wrack.

A beach-dune system offers the potential for understanding cyclical evolutionary relationships between LWD and sand supply because of the combined effects of nearshore and aeolian processes. Waves and currents can erode the beach and thereby exhume, rework, and redeposit buried LWD, which increases the potential for aeolian sand storage on the beach (Komar and Rea, 1976). The March 2016 erosion event exposed a large amount of previously buried LWD, as indicated by the numerous logs protruding out of the established foredune (Figure 31). The sediment liberated from within a LWD matrix during high water events could be stored temporarily in the nearshore zone, only to be returned to the foreshore and backshore during swell wave conditions. Thereafter, aeolian transport is essential to moving sand from the foreshore to the foredune, but this process is mediated by the effectiveness of the LWD matrix in trapping sand moving landward.

Figure 31 – Previously buried logs exhumed from within the established foredune after the 10 March 2016 high water storm event. The scarp in the center of the photo is approximately 1.5 m high.

The temporal phasing of aeolian activity leading to deposition on the backshore and foredune relative to wave reworking events that mobilize sand and LWD is important because it controls how effective the LWD matrix is as a roughness element and sand trapping reservoir. In turn, this will influence sediment delivery to the foredune, despite a seemingly adequate sediment supply in the littoral cell. This confounds the interpretation of cycles of foredune recovery and growth in relation to the magnitude and frequency of storm events. For instance, if a LWD matrix is reworked frequently by waves during storms, then the net effect could be to substantially limit sediment supply to the foredune for rebuilding, even if the aeolian system is otherwise very active. On beach-foredune systems without LWD, most of the aeolian sands could contribute immediately to infilling the scarp and building a sand ramp at the base of the foredune with subsequent contributions to the stoss slope (Ollerhead et al., 2013; Davidson-Arnott et al., 2018). However, with an extensive matrix of LWD, aeolian sediments are trapped

within the LWD and only a fraction reaches the scarp base. Alternatively, if a LWD matrix is reworked infrequently by waves it will experience infilling by aeolian sediment and gradually cease to be an effective modulator of sand delivery to the foredune. Depositional lobes emanating from the LWD matrix will eventually connect to the foredune scarp, and build a sand ramp that re-connects the sediment conveyance from the beach to the stoss slope and beyond. Figure 32 shows the gradual evolution of the sand ramp from very steep avalanche slopes (with sediment derived from the lower stoss slope of the foredune) to an aeolian accretion deposit connecting the backshore to the scarp face. In the foreground is a scour hollow formed by recirculation eddies at the base of the scarp (Piscioneri et al., 2019). LWD can remain buried under these sediments for extensive periods, not playing any role in the overall morphological adjustments of the beach-dune system until exhumed again by a large storm event, if at all.

Figure 32 – Study site on Calvert Island, British Columbia showing a freshly deposited sand ramp almost reconnecting the upper beach and the foredune stoss slope (May 2017).

Sediments that partially bury the LWD matrix provide a protected site for colonizing vegetation, as evidenced in the Aug 2017 TLS scan (Figure 25, profile D – D') and time-lapse camera data (Figure 28f). This evidence supports, in part, the suggested effects of LWD on coastal dune systems identified by Walker and Barrie (2006) and corroborates work by Heathfield and Walker (2011) and Eamer and Walker (2010) on the role of LWD in altering the beach sediment budget, albeit on a shorter, seasonal timescale. If the frequency of erosive water levels and erosive storm events is low enough, relative to aeolian transport events, pioneering vegetation could persist, and a new incipient dune could evolve. If the incipient dune persists, then it is implied that LWD would persist at the base of the dunes on prograding

shorelines. The role of LWD in foredune evolution is explored in more detail in the next chapter.

3.6 Conclusions

The effects of a LWD matrix on aeolian sediment transport potential and subsequent depositional patterns across a beach-dune system were investigated at the scale of single wind events and on a seasonal basis. Sediment traps and laser particle counters were used to quantify transport intensity through the LWD matrix at sampling frequencies of seconds to tens of minutes over a span of hours on multiple days. TLS surveys were spaced many months apart to capture seasonal influences over a span of 16 months. The data were used to investigate resulting erosional and depositional responses of the system to both nearshore and aeolian transporting events. The main findings are:

- LWD had a clear and measurable effect on aeolian sediment transport and acted as a physical barrier to saltating grains moving across the foreshore and toward the foredune. Sediment flux was reduced by 99% at the transition from the unimpeded beach to within the LWD matrix, with most deposition occurring within the first 6 m (NDD=24) of the leading edge. The reduced level of transport within the LWD was similar to that found in other studies dealing with uniform roughness elements, sand fences, and beach wrack.
- Vertical arrays of integrating sand traps showed that about 97% of saltating grains moved in the surface layer below the average height of the LWD (approximately 0.25 m). However, saltating particles rebounding off of the LWD allowed for higher trajectories and farther travel distances than what was measured on a control transect without LWD. It is possible that faster incident wind speeds could facilitate longer particle travel distances and multiple rebounds across the LWD matrix, thereby yielding a direct contribution to the stoss slope of the foredune. This was not observed during this study due to the low mean wind speeds. Such an effect likely depends on the width, height, and composition of the LWD matrix as well as the degree to which the accommodation space has been in-filled.
- The LWD matrix in this study reduced sediment transport similar to a uniform roughness

array. However, transport reduction varied between different LWD concentrations possibly because of the variations in shape, size, structure, orientation, abundance, exposure, and height above the surface. These variations make modeling the effects of LWD on flow and transport across a foredune difficult. More research is needed to understand the relationship between each possible parameter and its effect on flow and transport over time if LWD is to be included as a natural roughness element in flow models.

- Seasonal TLS surveys indicate that the LWD matrix trapped appreciable amounts of sediment on the backshore (0.66 m^3 m^{-2}). The reduced sand delivery to the foredune could increase the time required to re-build a dune ramp after an erosion event. However, observations at this site show that the LWD can be buried over a matter of days by active aeolian transport, quickly restoring sediment delivery to the base of the foredune.
- The ability for a LWD matrix to trap sediment depends on its effectiveness as a flow modifier and as a physical barrier to sediment transport. These properties change over time depending on the magnitude and frequency of nearshore events that periodically erode the beach and re-organize the LWD matrix. In this way, beach-dune systems adjacent to forested terrain may demonstrate cyclical relationships between LWD, sand supply, and foredune growth. LWD can be exhumed by wind and waves and then in the process of being re-buried by aeolian transport, will limit the sand supply to the foredune. How effective a LWD matrix is at modulating sediment supply to the foredune is related to cycles of foredune erosion and recovery from storm events driven by wave and current action. The synoptic regimes of these events requires further study to fully understand the broader geomorphic role of LWD on beach-dune interaction.

4. The role of large woody debris in beach-dune interaction.

Michael J. Grilliot, Ian J. Walker, and Bernard O. Bauer

Submitted to:
Journal of Geophysical Research: Earth Surface (ID: 2019JF005120)

4.1 Abstract

Coastal foredune evolution involves complex processes and controls. Although a great deal is known about the effects of vegetation cover, moisture, and fetch distance on sediment supply to foredunes, and on the effects of topographic forcing on airflow dynamics over beach-dune systems, the role of large woody debris (LWD) as a modulator of sediment supply and a control on foredune development and maintenance is understudied. LWD can alter event-scale sediment budgets by modifying the turbulent boundary layer, reducing the mean shear stress over the sand surface, and causing deposition on the upper beach. Thus, the LWD matrix may serve as sediment storage reservoir on the backshore. To date, no studies have attempted to connect long-term ($\geq$ seasonal) changes in LWD to foredune development and maintenance. Results from a four-year research initiative on a high energy, macrotidal beach and foredune system on Calvert Island, British Columbia, Canada, show that storm events lead to wave-induced erosion of the backshore and reworking of the LWD matrix. The exposed LWD matrix subsequently traps wind blown sand on the upper beach, leading to rapid burial of the LWD. Burial decreases the trapping efficiency of the LWD matrix over time, reconnecting sand transport to the foredune, at least until the next reworking or dune erosion event occurs. The efficient trapping capacity of the LWD matrix implies cessation of sediment delivery to the foredune, which may lead to aeolian erosion of the stoss slope and crest during strong winds. However, interannual observations at this site indicate that infilling of the accommodation

space within the LWD matrix is rapid, so sediment starvation of the foredune is relatively short-lived. The infilled LWD matrix also offers protection to the foredune against wave attack during high water events. Critical to this relationship is the frequency and magnitude of nearshore events that erode the beach periodically and re-organize the LWD matrix, which directly impacts the ability of LWD to modulate onshore sand transport to the foredune, store sediment in the backshore, and act as a buffer against erosive events. An empirically-derived conceptual model explaining these relationships is presented.

Keywords: Foredune; Large Woody Debris; Beach-Dune systems; Sediment Transport; Coastal Erosion.

4.2 Introduction

Foredunes are vegetated shore-parallel ridges of sand built by aeolian sand delivery across beaches. As such, foredunes are unique aeolian features affected by dynamic interactions between a host of marine, terrestrial, biotic, and atmospheric processes (Sherman and Bauer, 1993; Bauer and Sherman, 1999; Hesp and Walker, 2013; Walker et al., 2017). There are many controls on foredune morphology including, vegetation type and growth rate (Hacker et al., 2012; Keijsers et al., 2015), plant density and distribution (Hesp, 2002), roughness elements (e.g., woody debris, wrack, foot prints, bedforms, lag deposits) (Walker and Barrie, 2006; Eamer and Walker, 2010; Nordstrom et al., 2011; Bauer et al., 2013; Grilliot et al., 2018), sand supply (Nickling and Davidson-Arnott, 1990; Bauer and Davidson-Arnott, 2002; Aagaard et al., 2004; Davidson-Arnott and Bauer, 2009; Delgado-Fernandez and Davidson-Arnott, 2011; de Vries et al., 2014a, 2014b; Hoonhout and de Vries, 2017), moisture (Davidson-Arnott et al., 2008; Anthony et al., 2009; Bauer et al., 2009; Namikas et al., 2010; de Vries et al., 2012; Ellis and Sherman, 2013; Smit et al., 2018), fetch (Jackson and Cooper, 1999; Bauer and Davidson-Arnott, 2002; Bauer et al., 2009; Delgado-Fernandez et al., 2012), and topography (Walker et al., 2006, 2009b; Lynch et al., 2010; Hesp et al., 2017).

Research on the influence of roughness elements as a control on boundary layer dynamics and sediment transport has focused primarily on the role of vegetation as a key

control on sedimentation patterns and foredune growth (Hesp, 1989; Arens, 1996; Hesp and Walker, 2013; Keijsers et al., 2015; Hesp et al., 2016). Large woody debris (LWD) and beach wrack can also play an important role in modulating sand transport over beaches (Nordstrom et al., 2011; Bauer et al., 2013; Hesp and Walker, 2013; Houser and Ellis, 2013; Grilliot et al., 2018, 2019) but these roughness elements are less well studied. LWD is common on beaches in the Pacific Northwest of North America (Figure 33) and recent work by Grilliot et al. (2018) and Grilliot et al. (2019) explored the effectiveness of LWD at altering boundary layer airflow and modulating sediment supply to the foredune on an event basis. However, it remains unclear as to how important LWD presence is for seasonal to long-term evolution of the foredune and the overall dynamics of beach-dune systems. This paper addresses this knowledge gap by assessing seasonal to interannual changes in beach-dune morphology in the presence of LWD over the span of four years.

Figure 33 – Beach and foredune system on West Beach, Calvert Island fronted by LWD after a large erosive storm event scarped the foredune, April 2016.

Changes to beach-dune systems are commonly evaluated using cross-shore transects or volumetric surveys taken at monthly, seasonal, or annual intervals (Bascom, 1953; Nordstrom and Inman, 1975; Aagaard et al., 2004; Ollerhead et al., 2013; Brunier et al., 2016). Walker et al. (2017) highlight the importance of considering scale in interpreting such traditional repetitive surveys for the purpose of understanding morphological change and landform evolution through time. The adoption of high-resolution remote sensing techniques such as LiDAR (Montreuil et al., 2013; Feagin et al., 2014; Fabbri et al., 2017; Telling et al., 2017; Guisado-Pintado et al., 2019) and unmanned aerial system (UAS) with Structure-from-Motion Multi-View Stereo methods (James and Robson, 2012; Westoby et al., 2012; Mancini et al., 2013; Carrivick et al., 2016) for coastal monitoring have increased the capacity to detect, quantify,

and assess morphological change. Nevertheless, data collection involves costly field campaigns and significant post-processing time, skill, and computing power that does not easily lend itself to high-frequency (i.e., < daily) observations that could better inform understanding and modelling of seasonal scale processes. In contrast, time-lapse imagery (with hourly or daily capture rates) provides visual data that can be used to contextualize seasonal LiDAR surveys.

This study uses a combination of technological approaches, in an effort to understand the role of LWD in beach-dune processes. Changes in LWD cover, sediment volumetric changes, and morphological responses on a high–energy, embayed, macro-tidal beach-foredune system were monitored over four years. Changes in the system were measured using seasonal terrestrial laser scanning (TLS) surveys and high-frequency (15 min. interval) time-lapse imagery to provide an extensive dataset from which the contextual linkages between short-term processes and long-term morphological adjustments could be examined. The key objectives of the study were to: (1) examine the volumetric changes at the site and determine if there was a correlation to LWD coverage; (2) investigate the frequency and magnitude of the wave-induced erosional (LWD exposing) and aeolian depositional (LWD burying) events to situate the volumetric changes within the overall wave and wind process regimes; (3) determine the principal factors that drive the variability in the study area and how changes in LWD relate to these; and (4) describe the role of LWD in altering beach-dune morphodynamics by proposing a conceptual model based on the volumetric changes and time-lapse data recorded in this study.

4.3 Methods

4.3.1 Study Site

The study site was located on Calvert Island, on the central coast of British Columbia, Canada (Figure 34). The site was located on West Beach, a 1-km wide embayed beach bounded by rocky headlands and relatively open exposure to the Pacific Ocean. The foredune on the north end of the beach is approximately 6.5 m tall and is partially vegetated by native dune grass (*Elymus mollis*). The stoss (seaward) slope of the foredune has slope angles of 23° to 37° and the crestline is oriented SE - NW (128° - 308°). The beach is macro-tidal with a spring tide range of >4 m, a low tide width of ~250 m, and a low tide fetch >500 m in the obliquely

alongshore resultant aeolian sand drift direction (see Fig. 3). Data for 2012 to 2018 from a nearby meteorological station show regional prevailing winds from the SE that are driven dominantly by fall and winter storms. Median grain size (D_{50}) of the beach-dune sediments is 0.198 mm (Eamer, 2017) and the aeolian sand transport potential regime (Figure 35 inset) is unimodal with a resultant drift potential (RDP) of 111 vector units (vu) toward a resultant drift direction, RDD of 322°, as derived using the Fryberger and Dean (1979) model following the approach of Miot da Silva and Hesp (2010).

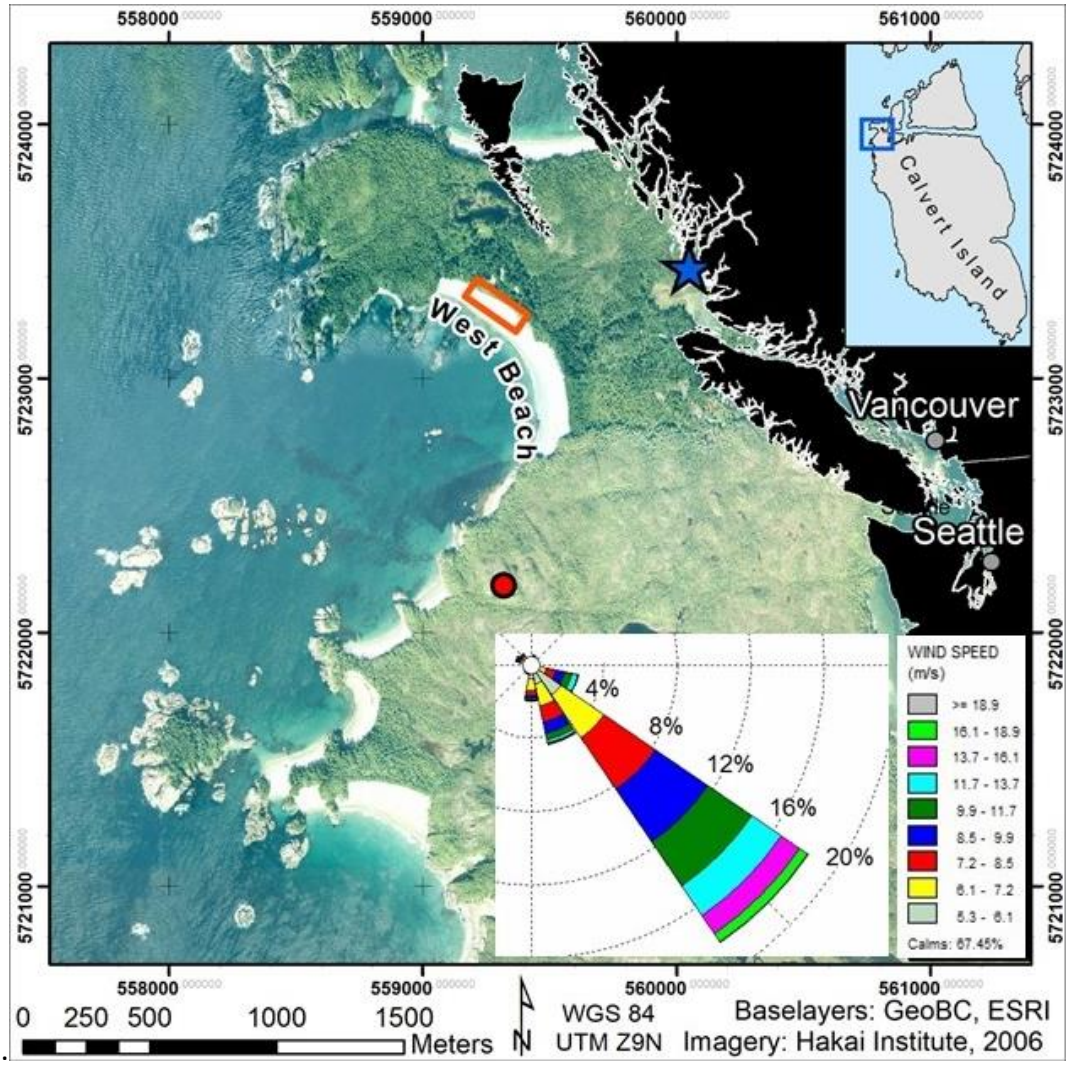

Figure 34 – Location of the study area (orange rectangle) on West Beach, Calvert Island, British Columbia, Canada. The red dot shows the location of the weather station used for drift rose calculations (Figure 35), although at the study site there can be local wind steering effects

that yield an obliquely onshore flow direction under regionally south-easterly winds.

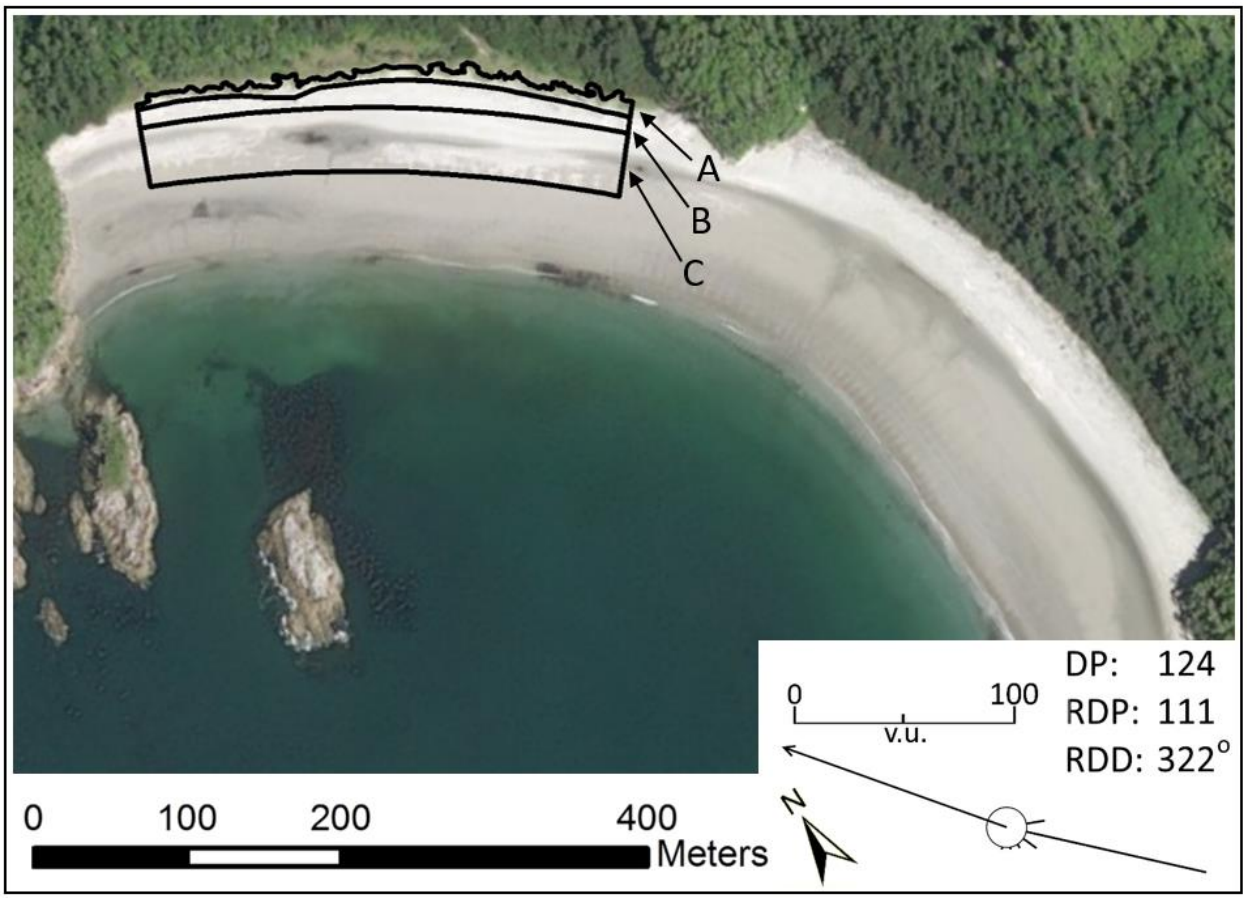

Figure 35 – Morphological units on West Beach, Calvert Island, British Columbia, Canada: A) foredune (2,674 m^2); B) backshore (4,478 m^2); and C) foreshore (13,046 m^2). The extent of the image includes a small island ~250 m offshore, which influences the wave dynamics on the beach. Imagery: ESRI

The study site was divided into three cross-shore morphologic units (Figure 35) to analyze volumetric change. The landward boundary of the foredune (unit A) was delineated by the crest or the start of dense vegetation (i.e., where a terrestrial laser scanner could not penetrate to the ground, as measured by a sharp decline in ground point density). The seaward extent of the foredune unit was the break in slope leading to the fully developed sand ramp, as measured in the first year prior to wave scarping events. The seaward boundary of the backshore (unit B) and landward limit of the foreshore unit included the limit of terrestrial vegetation from all surveys, and thus, covers the majority of LWD measured during each survey.

The seaward limit of the foreshore (unit C) was taken as the maximum extent of all TLS data, which were usually collected at or near low tide. The foredune and backshore units were further subdivided into 20 m zones in the alongshore direction for analysis of local and longitudinal trends (Figure 36). The foreshore was not similarly divided due to the uniform nature of changes in this unit and also to reduce processing time.

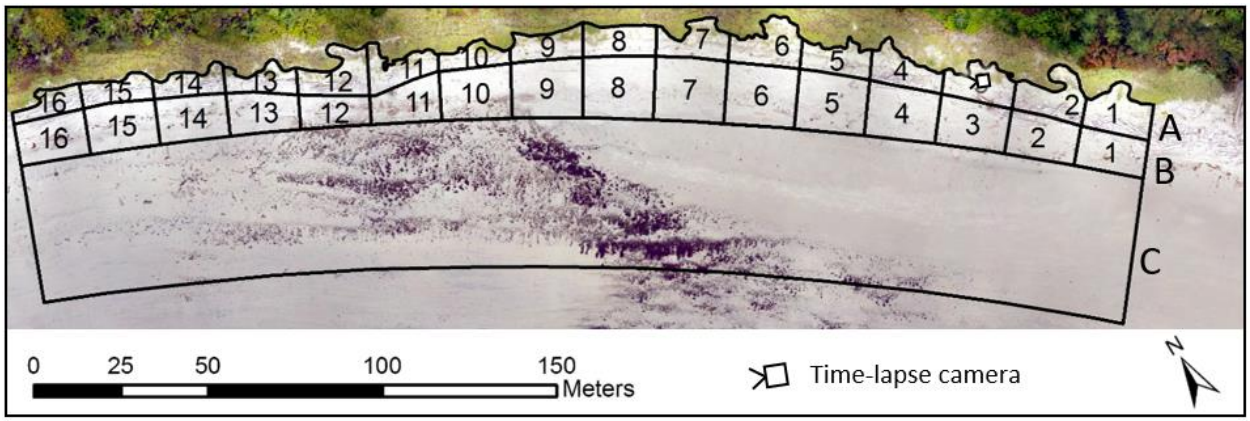

Figure 36 – Study area showing (a) the foredune unit and (b) the backshore unit divided into 20 m zones, numbered 1 to 16, east to west. Each zone is henceforth referred to by its morphological unit and zone number, e.g. backshore 12.

4.3.2 Data Description and Analyses

4.3.2.1 Terrestrial Laser Scanning

The volumetric change analysis considers eight quasi-seasonal intervals spanning four years, from June 2013 to August 2017 (Table 7). Elevation change was measured using a Riegl VZ-1000 TLS with a precision of 8 mm at 100 m distance. Environmental conditions (visibility, temperature, relative humidity, and barometric pressure) are parameterized on the scanner during the time of measurement to account for atmospheric variability in scan accuracy (Wang et al., 2014; Fabbri et al., 2017). Post-processing was completed in Riegl RiScan Pro© software. Individual scan positions were registered using stationary targets (10 cm diameter cylindrical reflectors) sited over benchmarks or using a top-mounted Trimble R10 GNSS receiver in Real Time Kinematic (RTK) mode linked to a network-surveyed base station. Individual scan registration was refined using the Multi-Station Adjustment (MSA) tool in RiScan Pro that

matches similar features between scans to improve accuracy. Relative registration of all scans to the July 2016 survey, which had the smallest registration error, was completed to eliminate possible GNSS errors and the need for repeat RTK ground-truthing surveys. Final registration accuracy for each survey date was less than 1 cm RMSE. A conservative absolute accuracy for each survey was set at 2 cm for digital terrain model (DTM) creation to account for potential inaccuracies associated with vegetation and LWD removal. DTMs were created in Quick Terrain Modeller (QTM) version 8.0.7 using adaptive triangulation at 5 cm^2 raster size. Volumetric analysis was performed in the Geomorphic Change Detection (GCD) 7.0 software plugin for ArcGIS (Wheaton et al., 2010) using the spatially uniform Student's t-test to determine significant volumetric change (p-value of 0.05) (Table 8). Volumetric change is reported as volume per area of change (m^3 m^{-2}) and was normalized temporally by dividing by the number of days between consecutive surveys.

Table 7 – TLS Survey dates. Change detection intervals between adjacent survey dates are indicated as lowercase characters a through h.

TLS Survey Dates							
Jun 10, 2013	← a →	Sep 17, 2014	← b →	Apr 18, 2015	← c →	Oct 28, 2015	← d →
Apr 9, 2016	← e →	Jul 5, 2016	← f →	Sep 21, 2016	← g →	Apr 27, 2017	← h →
Aug 24, 2017							

Table 8 – Normalized volumetric change ($m^3\ m^{-2}\ day^{-1} \times 10^{-3}$) and LWD change (expressed as surface area coverage in $m^2\ day^{-1}$) between each survey interval and morphologic zone (volumetric changes in FD: Foredune, BS: Backshore, FS: Foreshore; areal changes in FD_{LWD}: Foredune LWD, BS_{LWD}: Backshore LWD, FS_{LWD}: Foreshore LWD). Data are normalized temporally by the number of days in each interval. Negative change is highlighted in grey. Omitted values were below the volumetric change error threshold of 0.03 $m^3\ m^{-2}$ and LWD area threshold of 10% classification error added in quadrature between time intervals.

Interval	FD	BS	FS	FD_{LWD}	BS_{LWD}	FS_{LWD}
a	0.82	0.72	1.57	-0.54	-0.40	0.05
b	0.55		-1.67	1.38	0.42	-0.11
c	0.63	0.91	1.27	-0.24	0.80	0.10
d	-3.11	-5.41	-4.24	1.51		-0.14
e		4.23	2.15	2.46	3.47	0.09
f		1.74	7.36	-3.41	-3.28	-0.02
g	1.51	-0.41	-2.89	-0.96	-0.62	-0.02
h	1.17	1.83	4.46	0.77	0.94	0.50
a - h	**0.28**	**0.03**	**0.39**	**0.13***	**0.22***	**2.46***

LWD was isolated from the point clouds using the vegetation filter in RiScan Pro and an iterative refinement method developed by Riegl (2010). The LWD point clouds were converted to 5 cm^2 rasters of presence/absence that were used to calculate the exposed surface area of LWD relative to bare sand. Changes in LWD coverage were calculated between each survey and within each morphological unit and zone, and then normalized by dividing by the number of days in the survey interval.

4.3.2.2 Time-lapse Image Capture

Geomorphic changes to the beach and dune, as well as changes in LWD arrangement, between volumetric surveys was monitored via a RECONYX™ HC500 HyperFire™ camera installed on the dune (location shown in Figure 36 looking WNW. Images had a resolution of 3.1 megapixels and were taken every 15 minutes from 7 am to 6:45 pm ($n=48\ day^{-1}$) local time between Sept 2, 2012 and Aug 22, 2017. Of the 87,322 photos taken, 20,735 photos (23.7%) were excluded from the analysis due to decreased daylight hours in the winter months, fog,

condensation on the lens, or human interference. The photo set was further reduced by using only those images occurring between the TLS survey dates. The photo collection is thus a subsample of the full dynamic regime and, despite a day-time bias, it is believed to be representative of the range of processes active on this beach because of the large sample size spanning multiple years. All candidate images were then analyzed based on categorical or ordinal data structures representative of various processes and landscape changes interpreted from the images, as shown in Table 9 and Figure 37 (c.f., Delgado-Fernandez and Davidson-Arnott, 2011).

Table 9 – Categorical data interpreted from the time-lapse imagery.

Water level	Backshore change	Wave transport	Foredune Change	Aeolian Transport	LWD Change
Not visible	No Change	None	No Change	None	No Change
On beach	Aeolian Accretion	Wave Accretion	Aeolian Accretion	Active	Rearrangement - minor
At the extent of LWD or higher	Aeolian Erosion	Wave Erosion	Aeolian Erosion	Widespread	Rearrangement - major
					Addition - minor
					Addition - major
					Removal - minor
					Removal - major

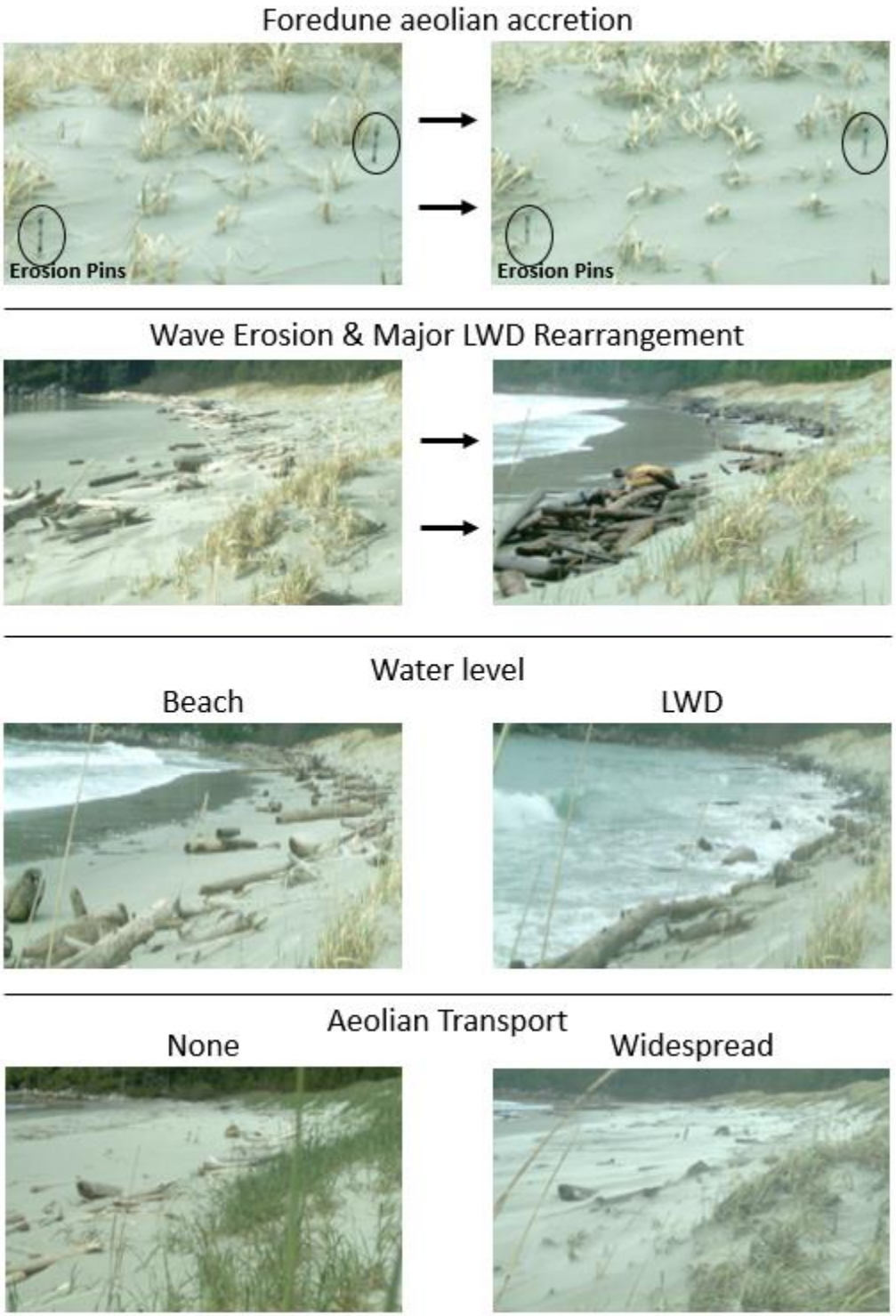

Figure 37 – Examples of time-lapse camera images and associated category assignment. Changes to the dune were categorized by observed changes within the near field of the camera (< 10 m) where resolution is greatest and erosion pins are visible.

The LWD and aeolian transport categories were divided into relative magnitudes that could be determined qualitatively from the photos. The major and minor magnitudes were selected to differentiate between the extreme/less frequent and moderate/more frequent sized events. For example, an assessment of 'major LWD rearrangement' required an almost complete restructuring of the vast majority of LWD in the photo. 'Minor LWD rearrangement' events, which accounted for 93% of the event observations, involved only a small portion of the seaward-most LWD being rearranged. These two types of LWD rearrangement were easy to distinguish visually. LWD additions and removals were utilized only when it was abundantly clear what occurred in order to minimize the potential mis-classification of LWD rearrangement.

Active saltation clouds were clearly visible in some of the images indicating aeolian sand transport. Aeolian transport events were divided into three categories, 1) active saltation on the beach, 2) active saltation on the backshore, and 3) widespread saltation. 'Active saltation' means pockets or streamers of saltation were visible, while 'widespread saltation' means more fully-developed transport that covered most of the visible sand surface and was clearly travelling onto and possibly over the foredune.

Aeolian and wave deposition/erosion categories were designated as either presence or absence because of the inability to resolve small magnitude volumetric changes at the acquired image resolution. Volumetric changes caused by aeolian transport are separated into those visible on the foredune immediately in front of the camera, and those visible in the LWD matrix on the backshore. Water inundation events were classified as those penetrating the seaward margin of the LWD matrix, and the total number of hours was reported for each such event.

Change between photo pairs was assigned to the later photo in the time series. Changes that occurred when the camera was not recording (7 pm to 6:45 am) were assessed on the first photo of the following day, which is a recognized, but inevitable source of uncertainty that is difficult to resolve. The categorical data were evaluated directly and converted to numerical data as hours of observations for use in Principal Components Analysis (PCA) (Table 10).

Table 10 – Total hours per day of time-lapse camera observations for each survey interval[ǂ]. Data are normalized by the number of days in each interval. Zero values are omitted for clarity.

Interval	LWD*	LWD**	LWD+	LWD++	LWD-	LWD--	W+	W-	BA+	BA-	FA+	FA-	AT+	AT++
a	0.37			0.1			0.1		0.113	0.1	0.12	0.21	0.34	0.32
b	0.135		0.12	0.48					0.262		0.56		0.48	0.7
c			0.9						0.141		0.1		0.22	
d	0.52	0.73	0.37	0.21		0.26	0.24	1.433	0.227		0.72	0.34	0.26	0.15
e	0.3		0.3				0.3		0.63					
f														
g	0.158	0.1	0.29				0.8	0.87	0.77		0.3		0.14	0.1
h														
a - h	0.18	0.8	0.11	0.9		0.3	0.4	0.165	0.127		0.52	0.1	0.37	0.13

[ǂ]LWD rearrangement (*: minor, **: major); LWD+: minor LWD addition, LWD++: major LWD addition, LWD-: minor LWD removal, LWD--: major LWD removal, W+: wave deposition, W-: wave erosion, BA+: backshore aeolian deposition, BA-: backshore aeolian erosion, FA+: foredune aeolian deposition, FA-: foredune aeolian erosion, AT+: active aeolian transport (saltation visible on beach), AT++: widespread aeolian transport (saltation visible on beach and dune). LWD-, LWD--, and BA- were not included in the PCA because unit variance could not be calculated on zero or single values.

4.3.2.3 Marine and Meteorological Variables

Data were compiled from multiple sources to include as many marine and meteorological factors as possible into the analysis (Table 11). Mean hourly measurements of wind data were obtained from a weather station near the field site (Figure 34). These data were used to derive a relative indicator of aeolian sand transport potential using the Fryberger and Dean (1979) model per the approach of Miot da Silva and Hesp (2010). Wind data above the predicted transport threshold wind speed measured at 10 m above ground level of 5.3 m s-1 were used to calculate the following wind metrics (DP, RDP/DP, W_S, W_X).

- DP (Drift Potential): The sum of all potential aeolian sand transport events from all possible transport directions in vector units during the survey interval (m^3 m-width^{-1} year^{-1}).
- RDP (Resultant Drift Potential): The vector sum of potential aeolian sand transport events in vector units during the survey interval (m^3 m-width^{-1} year^{-1}).
- RDP/DP: Describes the directional variability in potential aeolian sand transport. Values close to one indicate a strongly unimodal transport regime during the survey interval (dimensionless).

- WS (Wind Speed): The average hourly wind speed during the survey interval (m s^{-1}).
- WX (Max Wind Speed): The average of the hourly maximum wind speed during the survey interval (m s^{-1}).

Table 11 – Marine and meteorological factors calculated for the three morphological units (A - foredune, B - backshore, C - foreshore) during each survey interval‡. Data are normalized by the number of days in each interval. Zero values are omitted for clarity.

Interval	SI	S_H	T_{WL}	$H_{1/3}$	T_S	H_X	T_X	DP	RDP	RDP/DP	W_S	W_X
a	0.593	0.397	0.074	0.004	0.023	0.017	0.006	0.029	0.189	0.176	0.002	0.015
b	2.425	1.484	0.279	0.013	0.050	0.049	0.016	0.062	0.932	0.874	0.004	0.037
c	1.558	0.316	0.009	0.009	0.053	0.037	0.011	0.068	0.254	0.242	0.005	0.035
d	2.271	3.451	0.870	0.020	0.072	0.072	0.025	0.089	1.147	1.064	0.006	0.047
e				0.020	0.125	0.083	0.024	0.157	0.324	0.301	0.011	0.074
f				0.018	0.115	0.088	0.023	0.151	0.388	0.347	0.011	0.082
g	1.867	1.725	0.382	0.012	0.050	0.042	0.016	0.064	1.254	1.138	0.004	0.039
h				0.013	0.077	0.067	0.017	0.099	0.308	0.225	0.006	0.059
a - h	0.251	0.979	0.209	0.001	0.007	0.006	0.002	0.009	0.058	0.054	0.001	0.005

‡SI: Storm Intensity (m^2), S_H: total number of storm hours, T_{WL}: hours of wave influence on the backshore, $H_{1/3}$: average hourly significant wave height (m), T_S: average hourly peak wave period (s), H_X: average daily maximum significant wave height (m), T_X: average daily max peak wave period (s), DP: Drift Potential (m^3 m-width^{-1} year^{-1}), RDP: Resultant Drift Potential (m^3 m-width^{-1} year^{-1}), RDP/DP: Directional Variability Index, W_S: average hourly wind speed (m s^{-1}), W_X: average of the maximum hourly wind speed (m s^{-1}).

High-energy storm events are important drivers of coastal system change (Short and Jackson, 2013). Process-response morphodynamics on wave-dominated coasts depend on the frequency and magnitude of storms and associated wave energy (Wright and Thom, 1977; Davidson-Arnott, 2012). These data were included in the study, as much as possible, from historical wave data from the nearest location, Environment Canada buoy #46204 (West Sea Otter), approximately 53 km SW of Calvert island. For the purposes of this study, a storm was categorized as an event with wave heights exceeding twice the yearly average significant wave height for 6 or more hours (Jiménez et al., 1997; Mendoza and Jiménez, 2005). Significant wave height ($H_{1/3}$) is the mean wave height of the largest one third of the waves, recorded hourly. Relative Storm Intensity (SI) was calculated using equation [19]:

$$SI = \sum_{i=1}^{n} \left(H_{1/3_i}\right)^2 \quad [19]$$

where n is the duration in hours (≥ 6) during which the significant wave height of the event exceeds twice the yearly average significant wave height (Mendoza and Jiménez, 2005; Fabbri et al., 2017). For the study region, the yearly average significant wave height is 2.17 m. Relative water level information was interpreted from the time-lapse imagery and used due to the lack of nearby tide gauge information at this remote site. In addition to SI, the following parameters were calculated for each TLS survey interval and presented in Table 11:

- S_H (Hours of storms): The total number of hours of storm wave conditions, determined by SI, during the survey interval (hrs).
- T_{WL} (Hours of exceedance for threshold water level): The number of hours the water level reached the LWD in the backshore during the survey interval, as recorded by the time-lapse camera (hrs).
- T_A (Average hourly max wave period): The average maximum wave period during the survey interval, measured hourly (s).
- H_X (Average daily max wave height): The average of the daily maximum significant wave heights during the survey interval (m).
- T_X (Average daily max wave period): The average of the daily maximum wave periods during the survey interval (s).

4.3.2.4 Principal Components Analysis (PCA)

In order to evaluate the influence of various controlling factors on geomorphic change, a PCA approach was used (Hotelling, 1933; Jolliffe, 2011). PCA is a dimension-reducing technique used to preserve variability of the internal structure of a dataset while identifying the parameter combinations that maximize the variability between the components (Jolliffe and Cadima, 2016). Reducing dimensionality helps simplify the interpretation of the geomorphic response to the processes identified in the analysis. This study employs a correlation-based PCA because the data have different dimensional units (Jolliffe, 2011). Data from Tables 8, 10, and 11 were used in the PCA analysis to contextualize changes at the study location in relation to

potential drivers of morphologic change. The PCA was performed in R and RStudio (Vu, 2011; Wickham, 2011, 2015, 2018; Bache and Wickham, 2014; RStudio Team, 2016; Kassambara and Mundt, 2017; Kassambara, 2018; R Core Team, 2018; Wickham et al., 2018).

4.4 Results

4.4.1 Changes in Beach-dune Geomorphology and LWD Cover.

TLS scans revealed the magnitude of volumetric and LWD changes at the study site from season to season (Figure 38, Figure 39). Before the winter of 2014-15, all three morphologic units (foredune, backshore, foreshore) experienced moderate deposition (Figure 38, Figure 39a). The winter of 2014-15 brought net erosion to the foreshore, almost no net change to the backshore, and appreciable deposition on the foredune (Figure 38, Figure 39b). The Summer-Fall of 2015 brought minor rebuilding of the foreshore and deposition across all units (Figure 38, Figure 39c). Small parabolic-shaped depositional lobes of sediment were documented forming up the stoss slope of the foredune (Figure 39c, circle 1), while the dune toe experienced minor deflation in some locations (Figure 39c, circle 2). All morphologic units experienced the greatest erosion during a winter 2015-16 storm event (Figure 38), which resulted in 1.5 m tall scarp in some places of the foredune (Figure 39d). The backshore and foreshore were rebuilt in succession after this event, shown by the net deposition peaks in spring and summer of 2016 (Figure 38, Figure 39e-f). Almost immediately after the scarping event, sediment was eroded off the stoss slope by slumping and sand avalanching, thereby initiating the formation of a sand ramp at the foredune toe (Figure 39e, circle 3). At the same time, the backshore was rebuilding by wave action (Figure 39e, circle 4). The backshore experienced net erosion through the following winter (2016-17), but the section of the backshore covered in LWD experienced substantial aeolian deposition (Figure 39g). The peak depositional period on the foredune led to the rebuilding of a sand ramp that eventually infilled the scarp, which then allowed sediment to be delivered continuously across the backshore and onto the foredune (Figure 39g, circle 5). The final survey in the summer of 2017 showed minimal deposition and erosion in the foredune and backshore (Figure 38) but substantial vegetation growth above the buried LWD matrix on the backshore as well as on the foredune

(Figure 39h, circle 6). From Jun 2013 – Aug 2017 there was considerable seasonal sand exchange between the morphologic units and the adjacent nearshore, and yet the overall change in volume was relatively small. There was a slight net positive change in each unit, and the TLS scans revealed that the foredune stoss slope landward of the wave-cut scarp was raised by more than 0.5 m in some areas.

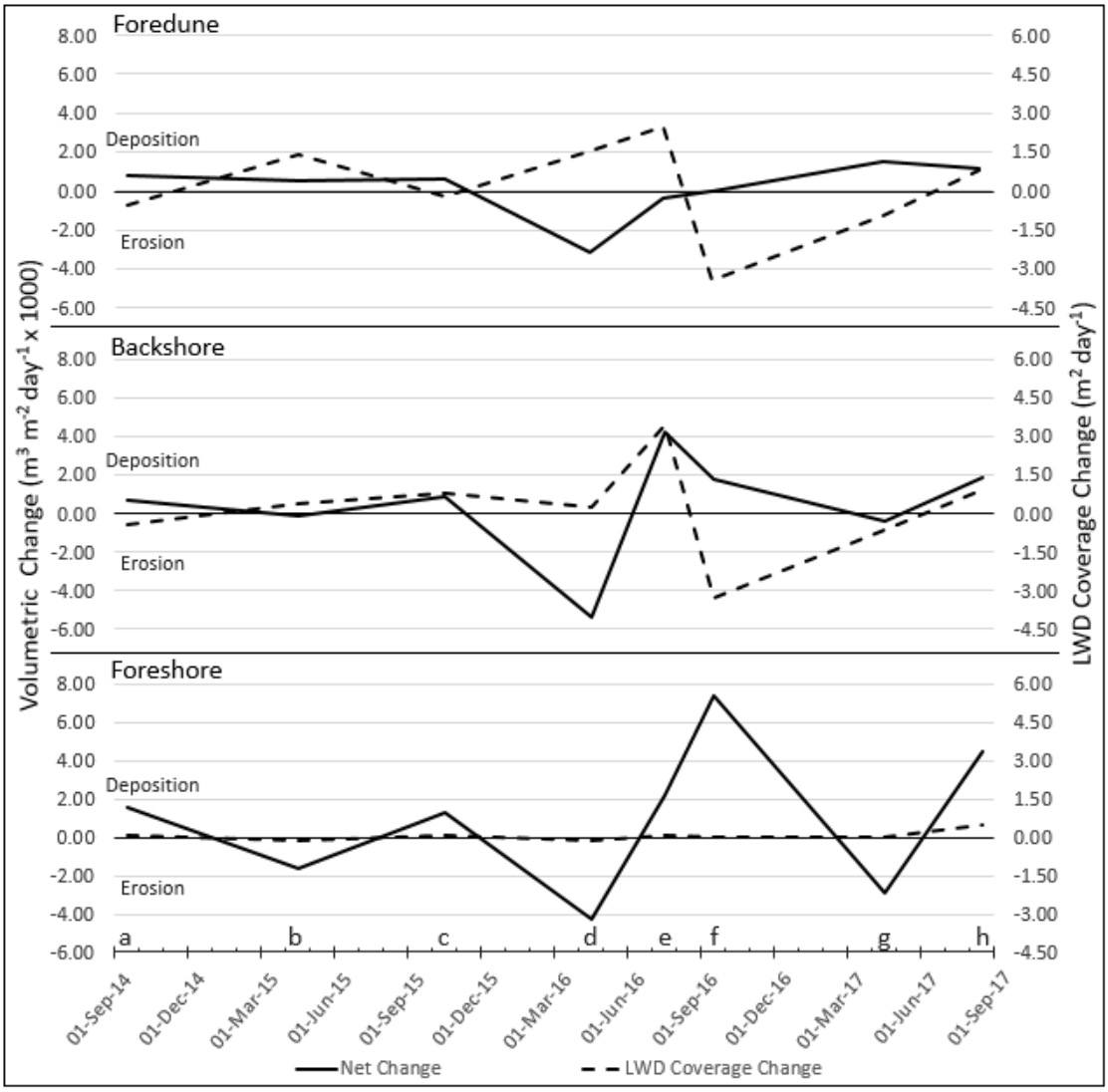

Figure 38 – Changes in normalized sand volume erosion and deposition ($m^3\ m^{-2}\ day^{-1}$ x 10^{-3}) on the left axis and changes in normalized LWD coverage ($m^2\ day^{-1}$) during the study for each morphological unit: foredune, backshore, foreshore (See Figure 35 for unit areas). Data are normalized by the number of days in each interval. Interval IDs (lowercase letters) indicate the last date in the date range and correspond with Figure 39.

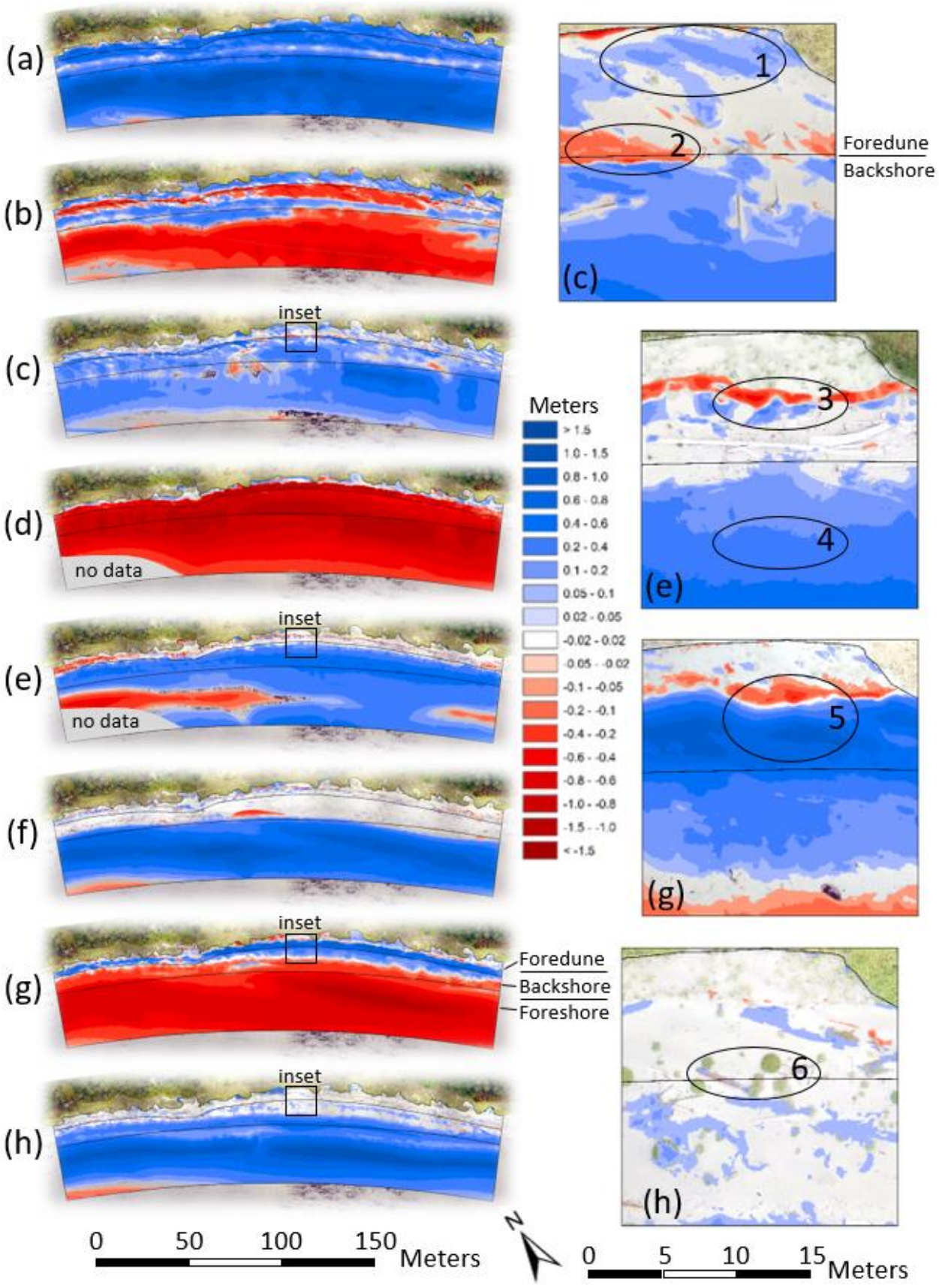
(a)
(b)
(c)
inset
(d)
no data
(e)
inset
no data
(f)
(g)
inset
(h)
inset
Meters
> 1.5
1.0 - 1.5
0.8 - 1.0
0.6 - 0.8
0.4 - 0.6
0.2 - 0.4
0.1 - 0.2
0.05 - 0.1
0.02 - 0.05
-0.02 - 0.02
-0.05 - -0.02
-0.1 - -0.05
-0.2 - -0.1
-0.4 - -0.2
-0.6 - -0.4
-0.8 - -0.6
-1.0 - -0.8
-1.5 - -1.0
< -1.5
1
2
Foredune
Backshore
(c)
3
4
(e)
5
(g)
Foredune
Backshore
Foreshore
6
(h)
0 50 100 150 Meters
N
0 5 10 15 Meters

Figure 39 – Changes in sand surface height (m) for each TLS interval (a-h) on the left with selected areas of detail on the right. Foredune, backshore, and foreshore are shown on TLS interval (g) and inset (c). Missing data in (d) and (e) are due to ground water seepage from recent rainfall and its influence on laser reflection. Orthophotos shown in the insets are from the later date in the survey interval. Numbered ellipses highlight geomorphic features that are described in text.

Changes in LWD coverage revealed a complex relationship between the amount of exposed LWD and the change in sand volume from interval to interval. Table 12 shows the correlations between changes in LWD coverage and volumetric change for each morphologic unit. LWD coverage on the foreshore shows a strong positive relationship with sand deposition, which is consistent with the observation that LWD is emplaced on the foreshore during periods of strong wave action and onshore sediment transport leading to beach building. In contrast, LWD coverage in the foredune unit is negatively correlated with sand deposition events (and positively correlated with erosion events). Camera observations indicate that wave-induced erosion of the foredune toe exhumes previously buried LWD, thereby increasing LWD coverage on the foredune. Aeolian deposition at the foredune toe subsequently buries the LWD, decreasing LWD coverage. The backshore unit shows no apparent relationship between LWD coverage and deposition or erosion. This zone is heavily influenced by both wave and aeolian forces, and the influence of wave action on beach erosion or deposition is not always aligned well with the exhumation and emplacement of LWD.

Table 12 – Pearson product correlation (r) values between changes in LWD coverage and average volumetric change (erosion, deposition) in each morphologic unit.

	Erosion	Deposition
Foredune	0.51	-0.58
Backshore	0.02	0.10
Foreshore	-0.67	0.63

4.4.2 Alongshore Variability in Volumetric and LWD Change

Relative magnitudes (as a fraction of maximum absolute values of change) of volumetric and LWD changes in the alongshore direction between zones 1-16 are shown in Figure 40. The maximum amount of change (value of 1) for all volumetric measurements (erosion, deposition, net change) occurred consistently in the central portion of the site in zones 8 – 10. The maximum change in LWD coverage occurred in zone 2 (along the backshore) and zone 1 (along the foredune), but there was also a locus of large (> 0.9) relative change in the central portion of the study area (zones 8 and 9). These areas coincide with the tallest parts of the dune in zones 6 through 9 (maximum dune height in zone 8 at 9.4 m asl). Figure 41A and Figure 41B show the correlation between volumetric change and LWD coverage for each zone along the backshore and foredune. These data reveal that the central zones of the study area, where the majority of all change activity occurred, are responsible for the overall correlation trends presented in Table 12.

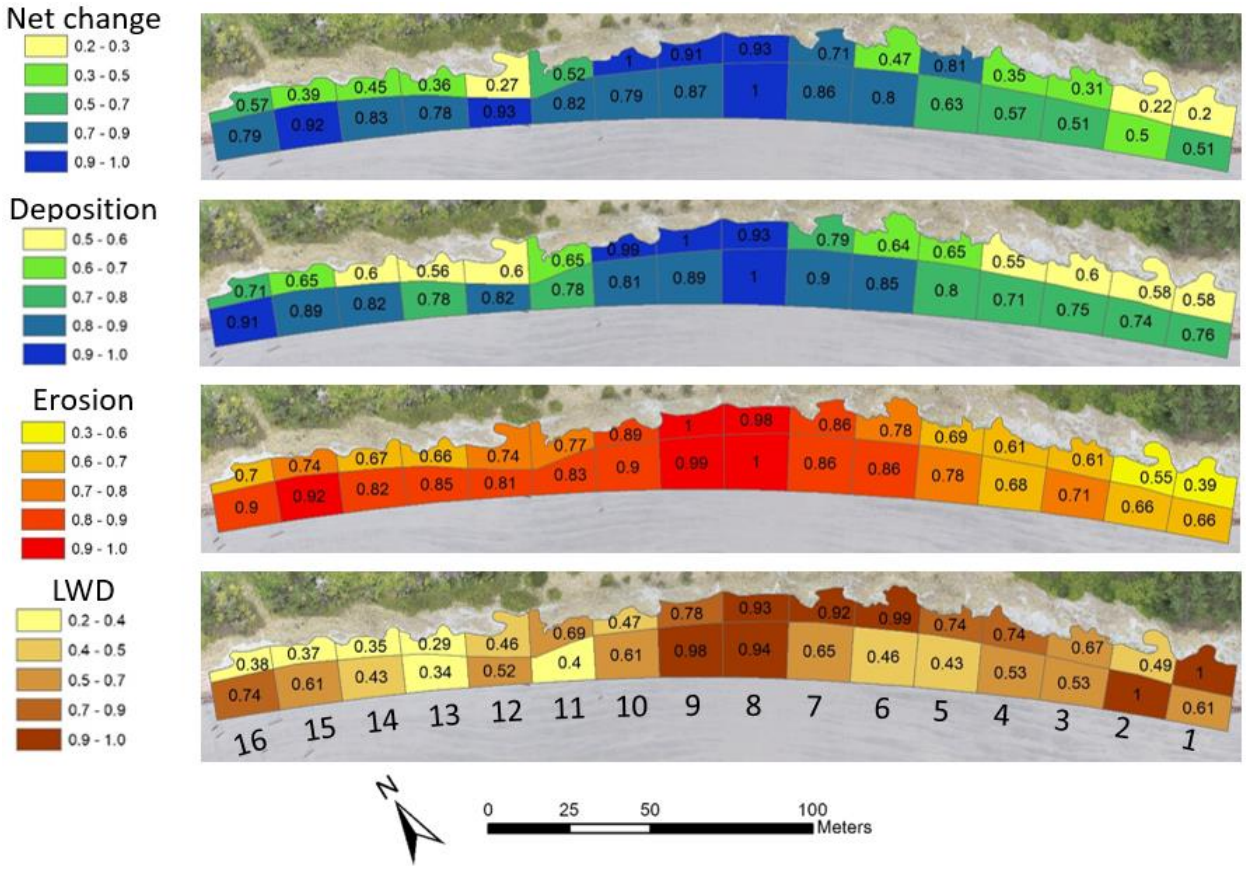

Figure 40 – Relative magnitude of volumetric change (net change, deposition, erosion) and LWD changes on the foredune and backshore by zone. Relative magnitude is expressed as the ratio of the zone sum of change to the maximum change of all zone (1 – 16) sums in each respective morphologic unit (foredune and backshore). A value of 1 indicates the maximum change of any zone in the morphologic unit while values close to zero indicate the least amount of change in the morphologic unit. Zone numbers are shown on the bottom image.

(A)

Foredune Unit:	16	15	14	13	12	11	10	9	8	7	6	5	4	3	2	1
Erosion	0.16	-0.01	0.06	-0.09	0.22	0.59	0.70	0.80	0.87	0.79	0.70	0.66	0.68	0.62	0.44	0.30
Deposition	-0.32	-0.16	-0.35	0.07	-0.37	-0.20	-0.60	-0.55	-0.45	-0.45	-0.40	-0.60	-0.38	-0.42	-0.45	-0.17
Net Change	-0.35	-0.22	-0.29	0.15	-0.42	-0.52	-0.84	-0.88	-0.84	-0.79	-0.65	-0.75	-0.65	-0.58	-0.49	-0.28

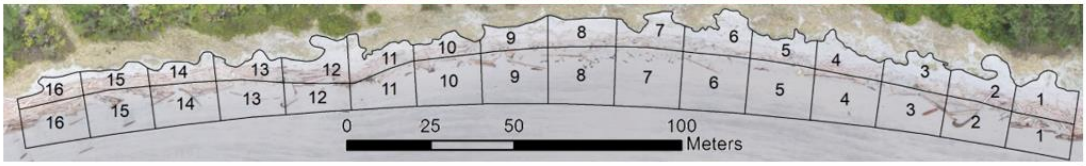

(B)

Backshore Unit	16	15	14	13	12	11	10	9	8	7	6	5	4	3	2	1
Erosion	0.33	-0.12	0.36	-0.60	-0.58	-0.30	0.12	0.18	0.29	-0.02	-0.27	-0.03	-0.02	-0.02	0.24	-0.03
Deposition	-0.33	-0.18	-0.58	0.42	0.33	0.26	0.26	0.07	-0.03	0.33	0.29	0.56	0.21	0.35	0.15	0.22
Net Change	-0.35	0.07	-0.45	0.56	0.60	0.43	0.08	-0.01	-0.18	0.13	0.32	0.26	0.05	0.15	-0.11	0.19

(C)

Shore-normal: Backshore LWD to Foredune Volumetric Change

	16	15	14	13	12	11	10	9	8	7	6	5	4	3	2	1
Erosion	0.37	-0.04	0.28	-0.48	-0.53	-0.16	0.10	0.18	0.30	0.03	-0.25	0.09	0.13	-0.10	0.07	-0.21
Deposition	-0.12	-0.34	-0.29	0.23	-0.20	-0.70	-0.55	-0.63	-0.59	-0.61	-0.36	-0.03	-0.22	0.18	0.50	0.09
Net Change	-0.37	-0.25	-0.36	0.52	0.28	-0.19	-0.39	-0.45	-0.55	-0.41	-0.05	-0.11	-0.22	0.23	0.44	0.15

(D)

Oblique: Backshore LWD to Foredune Volumetric Change

	16	15	14	13	12	11	10	9	8	7	6	5	4	3	2
Erosion	0.02	0.25	-0.37	-0.56	-0.25	0.27	0.19	0.33	0.04	-0.32	0.03	0.17	-0.14	0.17	-0.07
Deposition	-0.20	-0.40	0.09	-0.29	-0.43	-0.63	-0.51	-0.62	-0.50	-0.45	-0.06	-0.22	0.23	0.45	-0.21
Net Change	-0.17	-0.42	0.26	0.38	-0.11	-0.48	-0.44	-0.56	-0.32	-0.02	-0.09	-0.25	0.22	0.18	0.01

Figure 41 – Pearson product correlation (r) between changes in LWD coverage (m^2) and volumetric change ($m^3\ m^{-2}$) (erosion, deposition, net change) in alongshore zones (1 – 16, right to left) for: (A) foredune, (B) backshore, (C) shore-normal backshore LWD to foredune volumetric change, and (D) oblique backshore LWD to foredune volumetric change. Positive correlation values over 0.6 (moderate correlation) are highlighted green while negative correlation values below - 0.6 (moderate inverse correlation) are highlighted pink for ease of viewing.

Figure 41C and Figure 41D show correlation values between neighboring backshore and foredune zones under the assumption of shore-normal onshore or oblique onshore transport directions, respectively, in order to capture the predominant SSE aeolian transport direction. In general, the correlations are weak, suggesting that erosion/deposition tendencies are not associated with LWD coverage in neighboring cells in the cross-shore direction. Interestingly, there is a moderate inverse correlation between LWD change and deposition in some central zones where the majority of activity occurs (Figure 40). This could suggest that there is a

connection between the LWD in the backshore and volumetric changes on the dune in the central zones, but this does not apply elsewhere along the beach.

4.4.3 Frequency and Magnitude of Landscape Altering Events

Figure 42 shows the time-sequencing of different geomorphic events that are thought to be responsible for change on this beach-dune system as determined from the time-lapse camera imagery. There is evident clustering of events (e.g., minor LWD Rearrangement, active aeolian transport) in the winter months when storm activity is greatest. Minor LWD rearrangement events were extremely common during the winter months, but there were few other types of LWD change events. Major LWD rearrangement events occurred only when large waves accompanied extreme high water levels during storms, resulting in significant wave erosion of the entire beach. When compounded with storm surge during high tide, these are the conditions that lead to the mobilization of LWD and erosion of the beach and foredune.

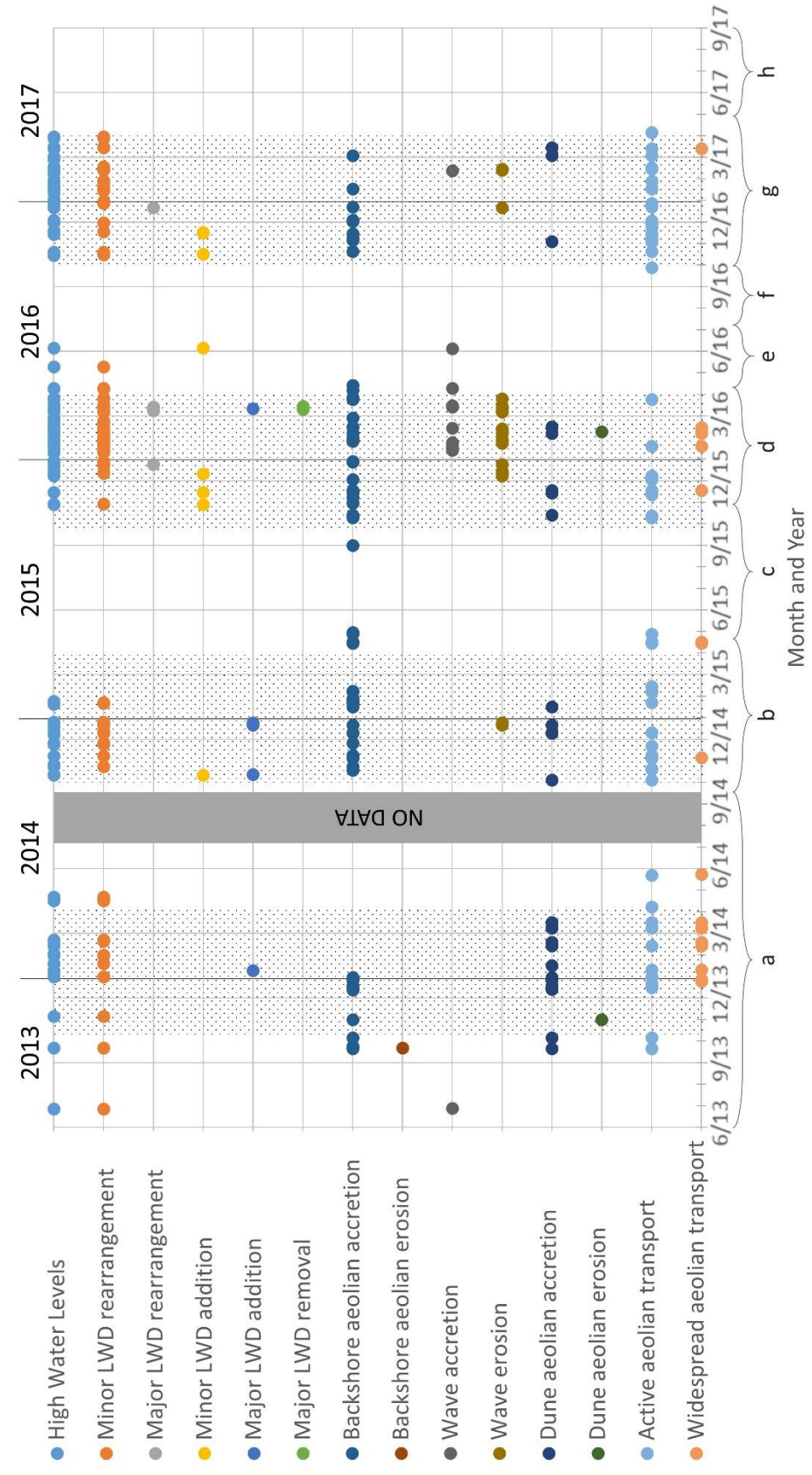
2013
2014
2015
2016
2017
NO DATA
6/13
9/13
12/13
3/14
6/14
9/14
12/14
3/15
6/15
9/15
12/15
3/16
6/16
9/16
12/16
3/17
6/17
9/17
a
b
c
d
e
f
g
h
Month and Year
High Water Levels
Minor LWD rearrangement
Major LWD rearrangement
Minor LWD addition
Major LWD addition
Major LWD removal
Backshore aeolian accretion
Backshore aeolian erosion
Wave accretion
Wave erosion
Dune aeolian accretion
Dune aeolian erosion
Active aeolian transport
Widespread aeolian transport

Figure 42 – Daily occurrences of camera-derived metrics of geomorphic change events. Years are labeled above with yearly boundaries marked by vertical black lines. The shaded background represents winter seasons. TLS intervals a-h (Table 1) are indicated on the bottom of the x-axis.

The most important relationships revealed by the time-lapse camera data are the frequency and magnitude of aeolian-related deposition events compared to erosion events that result from either wave action or aeolian processes. Table 13 shows the number of images for which deposition or erosion was observed during each survey interval for both wave and aeolian activity. Considered together, depositional periods were 3.6 times more numerous than erosive periods over the entire study period (from 2013 to 2017). The totals at the bottom of Table 13 show that aeolian events (n = 1162) were far more numerous than wave-related events (n = 320). In addition, aeolian events leading to deposition (n = 1100) accounted for approximately 99% of all depositional events (n = 1125). Wave-related erosion events (n = 295) acting on the backshore were 12 times more frequent than wave-related deposition events (n = 25). Wave-related erosion accounted for almost 80% of all erosion events (n = 357). Data on the foreshore could not be interpreted from the camera imagery because of the general absence of indicial points.

Table 13 – Number of depositional and erosional images recorded for wave and aeolian forces during each TLS interval a-h (Table 1). The total dataset of useful images over the 4-year observational period was 46,913.

	Backshore, and immediately seaward of scarp				Landward of scarp	
Date Range	Aeolian Deposition	Aeolian Erosion	Wave Deposition	Wave Erosion	Aeolian Deposition	Aeolian Erosion
a) Jun 2013 – Sep 2014	209	1	1	0	222	39
b) Sep 2014 – Apr 2015	223	0	0	41	48	0
c) Apr 2015 – Oct 2015	109	0	0	0	1	0
d) Oct 2015 – Apr 2016	149	0	16	235	47	22
e) Apr 2016 – Jul 2016	22	0	1	0	0	0
f) Jul 2016 – Sep 2016	0	0	0	0	0	0
g) Sep 2016 – Apr 2017	67	0	7	19	3	0
h) Apr 2017 – Aug 2017	0	0	0	0	0	0
Total	**779**	1	25	295	321	61

The data presented in Table 13 demonstrate the relative importance of both wave erosion and aeolian accretion events to the dynamics of the sediment budget even though every event will differ in magnitude and impact. The time-lapse images indicate that aeolian recovery from smaller erosive wave events was typically rapid (less than a month). The period between October 2015 and April 2016 had an unusually large number of geomorphic events, especially wave erosion events, which is associated with the very strong El Niño conditions during this time. However, only one erosive event, the March 10, 2016 storm, was unusual in its overall impact. Foredune scarping and beach surface lowering were pronounced during this storm, and aeolian recovery was relatively slow, given the magnitude of erosion. About one year after, parts of the foredune scarp (< 1 m tall) were rebuilt, but the tallest portions of the scarp (≈1.5 m) had yet to be fully rebuilt. Wave accretion events were significantly less frequent than aeolian deposition events. Wave deposition was largely limited to the foreshore, where there were extreme seasonal volumetric fluctuations by as much as 10×10^{-3} m^3 m^{-2} day^{-1} (Figure 38). Despite this, there were 25 images that showed clear evidence of wave deposition

with 16 of these occurring during the 2015-16 winter. Many of these wave deposition events occurred during the same tidal cycle immediately following an erosive event, which suggests that the nearshore is in a state of dynamic equilibrium. This is enhanced by the highly embayed nature of this beach as wave eroded sediment is typically moved offshore during storms, readily stored in the nearshore for onshore transport during less erosive wave conditions. Aeolian erosion also occurs but mostly as minor deflation of the stoss slope and basal scour around isolated pieces of LWD, and it is of comparatively minor importance to overall dune morphology and volumetric change.

Although the frequency data are interesting regarding how dynamic the system was with regard to wave and wind action, the camera data does not provide quantitative information on the absolute magnitude of change during any specific event. Nevertheless, it is apparent from the images that the more frequent aeolian events moved less sand and caused less volumetric change than single high-water events. Indeed, the high-water event of March 10, 2016 yielded the greatest amount of erosion on the backshore and foredune, while the more frequent and smaller aeolian deposition events ultimately rebuilt the eroded areas. On a number of occasions, aeolian deposition quickly rebuilt the eroded backshore and buried nearly all the LWD on the beach over only a few days. This resulted in rapid re-establishment of a continuous sand transport pathway from the foreshore to the foredune, indicating that the LWD matrix is a highly effective but ephemeral sand-trapping reservoir.

Figure 43 presents a series of images that show typical changes in morphology and LWD coverage during the study. The sequence from (1) to (6) reveals a recurring pattern of LWD additions to the backshore (2-3 and 4-5) followed by aeolian deposition resulting in partial or complete burial of the LWD (1-2, 3-4, and 5-6). In contrast, images (6) to (9) reveal how LWD buried by aeolian activity can be exhumed by wave erosion. In addition, image (7) shows that exhumation events can also result in fresh LWD being deposited on the backshore, while the event prior to image (9) resulted in the removal of the majority of exposed LWD rather than by burial. Without complete data coverage of the embayment at large, it remains unclear whether the LWD additions and removals are simply the result of bay-wide LWD reorganization rather than new influxes of LWD to the embayment. Regardless, the erosive events leading to images

(7) and (9) were followed by aeolian deposition and infilling of the LWD matrix (images not shown). There were numerous events that reworked the LWD, but the time-lapse imagery showed that LWD was usually not removed from the beach, but rather was buried by aeolian accretion. This is important because it places the changes of LWD coverage recorded by TLS in the context of burial instead of removal. Many of the same logs can be seen in the images in Figure 43 and are tracked through time in the accompanying time-lapse video, which better illustrates these types of changes at the study site.

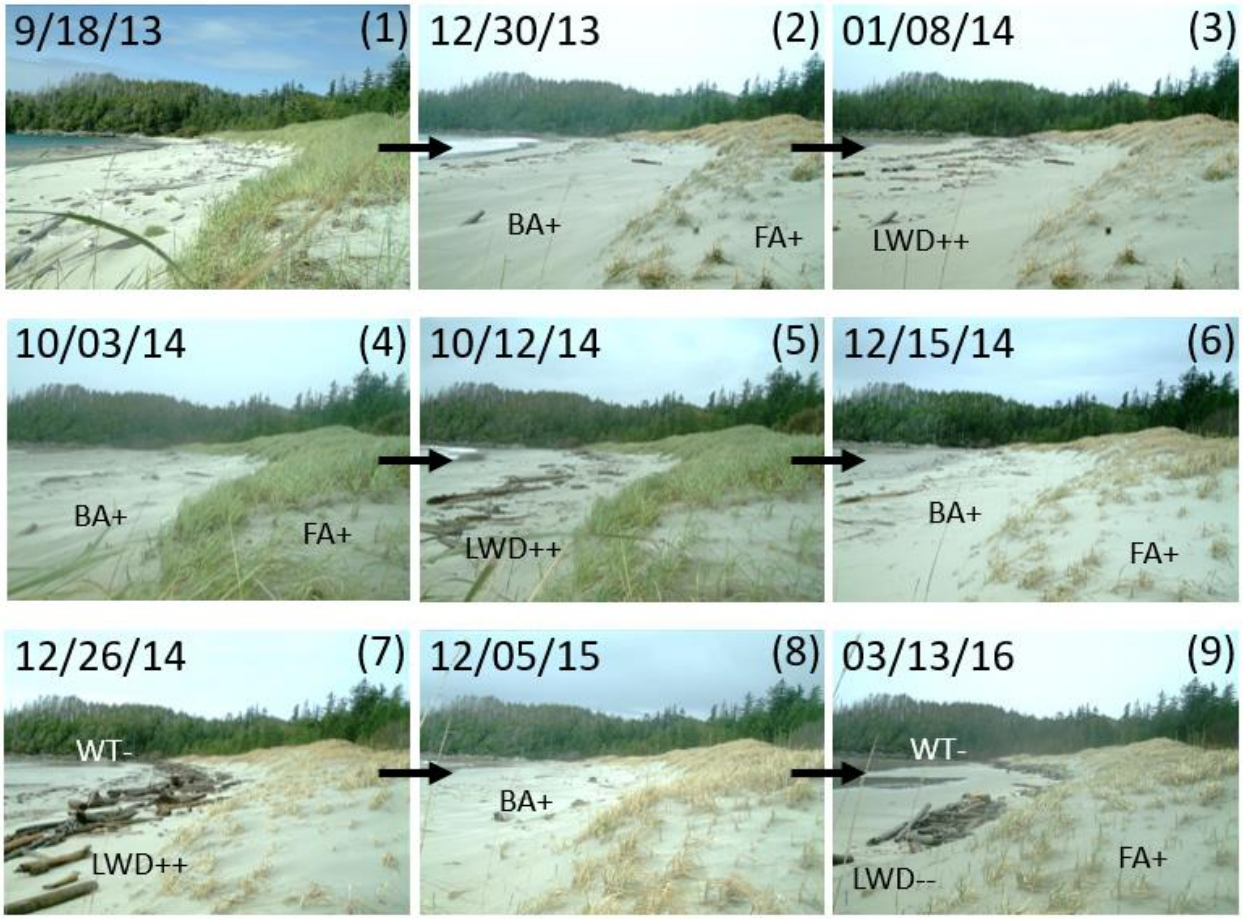

Figure 43 – Panels showing change through time from (1) 9/19/2013 to (9) 3/13/2016, before and after distinctive changes in beach morphology or LWD. Changes are labeled on the images and are represented by: LWD++: major LWD addition, LWD--: major LWD removal, W+: wave deposition, W-: wave erosion, BA+: backshore aeolian accretion, FA+: foredune aeolian accretion.

4.4.4 Principal Components Analysis

Principal components (PCs) are linear combinations of the important variables considered in the analysis, usually centered and normalized (Jolliffe and Cadima, 2016). The variance associated with the PC is called the eigenvalue. The greater the eigenvalue, the greater the contribution a PC has to the overall variance of the dataset. Each eigenvalue has an eigenvector, which is the direction that maximizes the variance. The elements of an eigenvector, known as the loadings, describe the weights of each variable contributing to the maximum variance. Greater absolute values of loadings indicate that a variable had a stronger influence on the corresponding PC.

Table 14 shows that 73% of the total variance in the data was captured by PC1 and PC2. Typical cut-offs for PC consideration are between 70% and 90% (Jolliffe, 2011; Jolliffe and Cadima, 2016), so focus will be restricted to the first two PCs only. Table 15 summarizes the results of the PCA loading values and correlation coefficients, whereas Figure 44 presents the PCA results in bi-plot format. The cosine of the angle between two vectors (each representing a different factor in the analysis) is proportional to the coefficient of correlation between the two variables. In other words, vectors that are near parallel, opposite, or orthogonal are strongly positively, strongly negatively, or not correlated, respectively. Similarly, the cosine of the angle between a vector and a PC (axis) is proportional to the coefficient of correlation between the variable and the PC. Thus, vectors that are near parallel with an axis are strongly correlated to that PC. The terminus position of each vector shows the loading value graphically along the corresponding axis for that variable. Therefore, the longer a vector relative to an axis, the greater that variable contributes to the corresponding PC variance.

Table 14 – Eigenvalues and variance associated with the top 8 principal components arising from the PCA based on the variables listed in Table 8, Table 10, and Table 11.

	PC1	PC2	PC3	PC4	PC5	PC6	PC7	PC8
Eigenvalue	13.36	7.77	3.02	2.29	1.45	0.67	0.45	0.00
Proportion of Variance	0.46	0.27	0.10	0.08	0.05	0.02	0.02	0.00
Cumulative Proportion	0.46	0.73	0.83	0.91	0.96	0.98	1.00	1.00

Table 15 – Summary of the top fourteen variables responsible for the maximized variance in PC1 and PC2. Only loadings within 0.1 of the Rank 1 variable with strong (> 0.6) correlations are shown in the table. Other variables were omitted for clarity. Loadings (L) and correlation coefficients (r) are shown. See Table 10 and Table 11 for acronym descriptions.

Rank	**PC1**	PC1-L	PC1-r	**PC2**	PC2-L	PC2-r
1	**S_H**	-0.27	-0.97	**$H_{1/3}$**	-0.35	-1.00
2	**T_{WL}**	-0.26	-0.94	**H_X**	-0.35	-1.00
3	**LWD***	-0.26	-0.91	**W_X**	-0.32	-0.95
4	**BS**	0.25	0.99	**T_S**	-0.32	-0.93
5	**FS**	0.25	0.98	**T_X**	-0.31	-0.92
6	**LWD+**	-0.24	-0.95	**W_S**	-0.31	-0.91
7	**SI**	-0.23	-0.97	**RDP/DP**	-0.30	-0.90
8	**W-**	-0.23	-0.83			
9	**W+**	-0.23	-0.82			
10	**RDP**	-0.22	-0.95			
11	**BA+**	-0.22	-0.97			
12	**DP**	-0.22	-0.95			
13	**LWD****	-0.22	-0.80			
14	**FA-**	-0.20	-1.00			

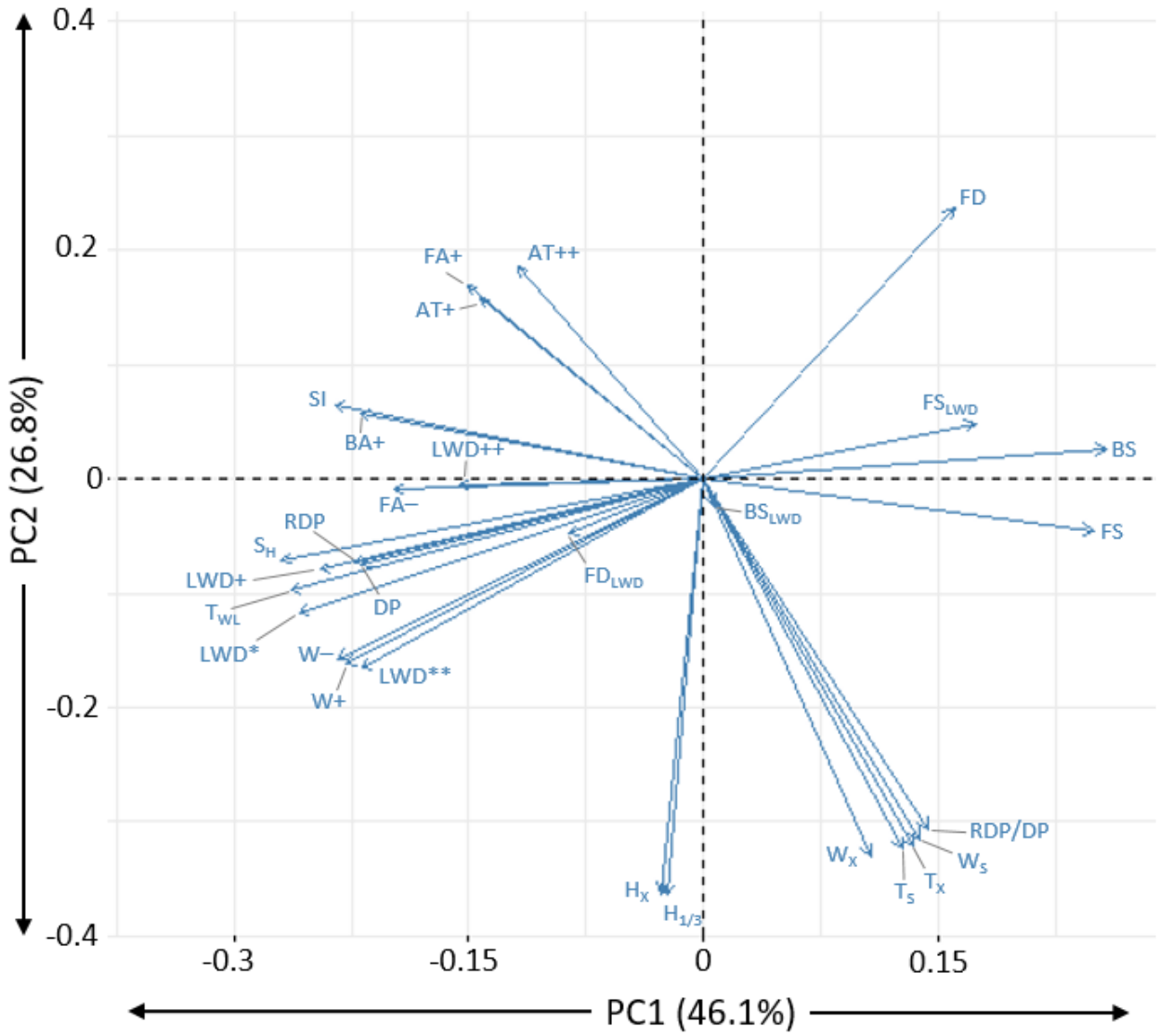

Figure 44 – PCA bi-plot of PC1 and PC2 for all data. See Table 8, Table 10, and Table 11 for acronym definitions.

The PCA revealed that PC1 accounts for 46% of the dataset variability. The strongest explanatory variables aligning with PC1 were the number of storm hours (S_H), hours of wave influence on the backshore (T_{WL}), and minor LWD rearrangement (LWD*), all in the negative direction (Table 15 and Figure 44), although several other variables are only slightly less important (e.g., BS and FS in the positive direction, and LWD+, SI, W- in the negative direction). The first two variables (S_H and T_{WL}) characterize the overall intensity of storm-wave influence on the beach-dune system, and they were identified by other studies as the primary forces driving

geomorphic change on beaches (Pye and Blott, 2016; Fabbri et al., 2017). As these storm-related variables, as well as storm intensity (SI), are in the negative direction, whereas backshore (BS) and foreshore (FS) change are in the positive direction, the interpretation is that enhanced nearshore storminess leads to beach-dune erosion. Winter storms that bring strong winds and high water levels to the beach are strongly implicated in this relationship because the camera imagery showed that such storm events drove the majority of change in the foreshore and backshore, as well as caused minor LWD rearrangements (LWD*) and additions (LWD+). Many of the other variables had slightly smaller positive or negative correlations, demonstrating that beach-dune response involves a complex combination of factors that are interrelated and seasonally mediated.

The remaining 27% of variability in the data set was captured in PC2, which comprised several marine and meteorological factors (Table 15 and Figure 44). Significant and Maximum wave height ($H_{1/3}$, H_X), wave period (T_S, T_X), wind speed (W_S, W_X), and RDP/DP all had prominent loading values in the negative direction. Foredune change (FD), foredune aeolian deposition (FA+) and aeolian transport activity (AT+, AT++) had weak loadings in the positive direction. It seems counter-intuitive to have a negative correlation between wind speed variables (Ws, Wx, RDP/DP) and aeolian activity or accretion on the foredune, until it is recognized that wind speed variables were measured at a regional, higher elevation (63 m asl) and more exposed station several kilometers from the beach site. There is a great deal of evidence from other locations to indicate that topographic steering of regional wind systems can strongly influence and modify the local wind field over beach-dune systems (e.g., Walker et al., 2006, 2009b; Bauer et al., 2012; Hesp et al., 2015). In addition, increased winds are often associated with large wave fields that inundate the beach and shut down the aeolian transport system (Bauer et al., 2009), and potentially erode the foredune toe region. Thus, the correlations between explanatory variables contributing positively and negatively to PC2 are somewhat weaker than those in PC1.

To highlight only the most important explanatory variables and remove clutter from the diagrams, a summary PCA was performed that included change in LWD areal coverage as well as the other system variables with loadings greater than or equal to r = 0.95 based on the previous PCA results (Table 16 and Figure 45). The new $PC1_X$ and $PC2_X$ account for 72.3% of the

variability, similar to the previous PCA, so there is no net loss of explanation and therefore justifies the elimination of other variables. Also included in the diagram are the PCA interval scores and are grouped (color-coded) according to whether the change interval covers the winter/spring or summer/fall season. These points are the sum of the product of the loading value and the centered data value for each PC. They represent how much variability that data interval contributes to each PC. Centroids for each of these seasonal intervals are shown as large dots, with the summer centroid appearing on the positive side of $PC1_x$ and the winter centroid appearing on the negative side of $PC1_x$.

Similar to the previous results, the number of storm hours (S_H) and hours of wave influence on the backshore (T_{WL}) had the strongest (negative) alignment with $PC1_X$ (Table 16). The Resultant Drift Potential (RDP) and Drift Potential (DP) (also negative) became of greater relevance in this simplified analysis. All four of these variables are positively correlated with the winter survey centroid demonstrating that winter storm conditions, which bring strong winds and cause high water levels, are the primary drivers of volumetric change at this site. It is noteworthy that change in LWD on the foreshore (FS_{LWD}) is negatively correlated with these variables but change in LWD on the foredune (FD_{LWD}) is positively correlated with these variables. LWD on the backshore (BS_{LWD}) is poorly correlated with all variables and contributes little explanatory power to the PCA. LWD coverage on the foreshore increased during summer when fair-weather swell wave conditions prevailed, leading to large logs and pieces of driftwood being emplaced on the foreshore and backshore as the beach attains its equilibrium form with the summer wave regime. However, the logs were not buried by this wave deposited sediment. Because the potential for aeolian transport is usually small during the summer, given seasonality in the wind regime, the LWD matrix remains on top of the beach surface in a mostly exposed state with little aeolian infilling. In contrast, LWD coverage on the foredune increased in winter due to increased frequency of high water events that exhume and/or rework LWD that was previously buried or deposited on the upper beach. However, the LWD coverage quickly decreased after such exhumation events because of rapid aeolian deposition within the LWD matrix. These opposing tendencies in rapid succession likely explain the low loading value for FD_{LWD} as evidenced by the markedly shorter vector in Figure 45.

Table 16 – Summary of the top five variables responsible for the maximized variance in $PC1_X$ and $PC2_X$. Only loadings within 0.1 of the Rank 1 variable with strong correlations are considered. Loadings (L) and correlation coefficients (r) are shown. See Table 10 for acronym descriptions.

Rank	$PC1_X$	$PC1_X$-L	$PC1_X$-r	$PC2_X$	$PC2_X$-L	$PC2_X$-r
1	S_H	-0.40	-1.00	W_X	-0.55	-0.99
2	T_{WL}	-0.39	-0.99	H_S	-0.55	-0.98
3	RDP	-0.39	-0.99	H_X	-0.55	-0.98
4	DP	-0.38	-0.99			
5	SI	-0.36	-0.87			

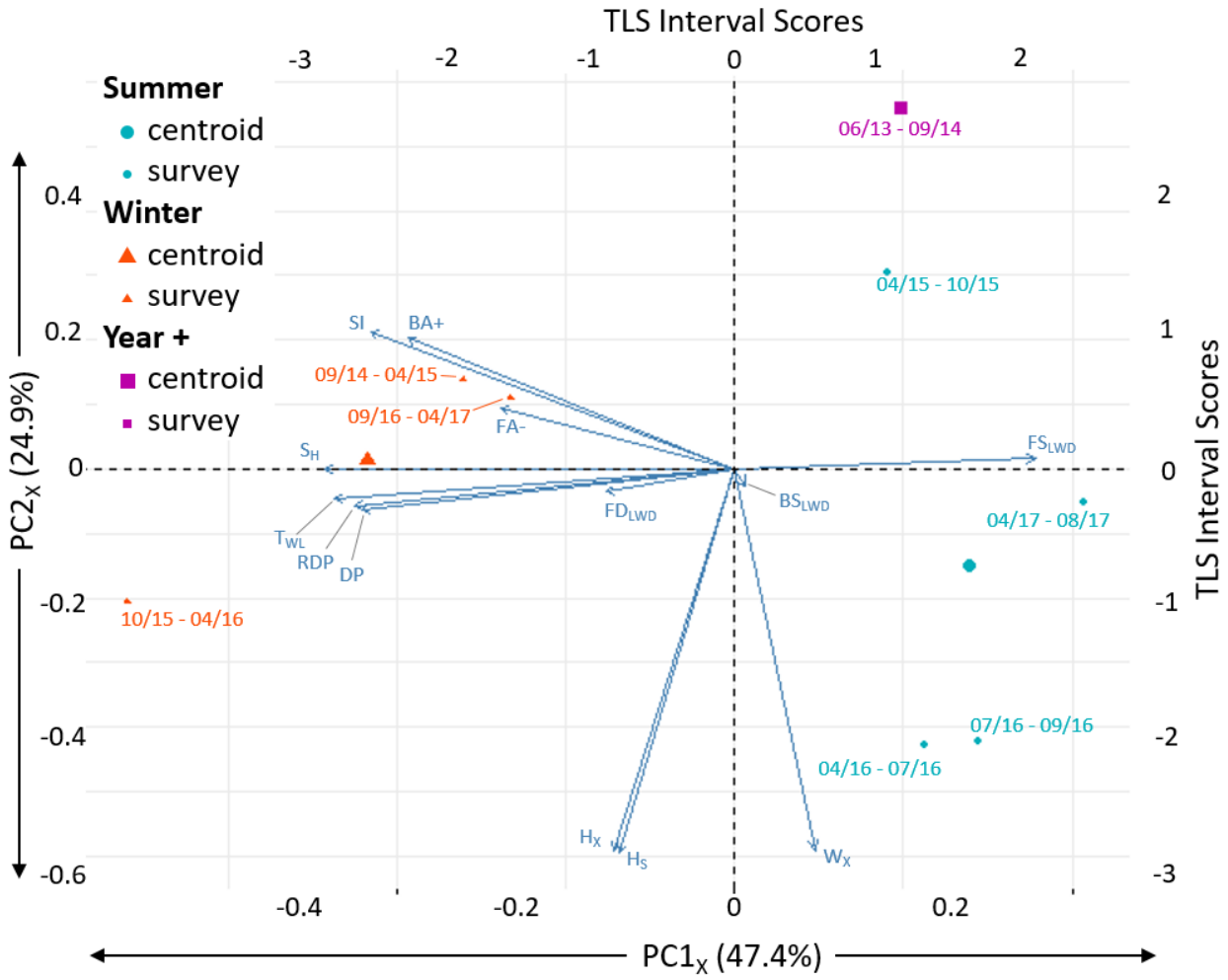

Figure 45 – PCA bi-plot of $PC1_X$ and $PC2_X$ for all data. TLS survey intervals are grouped by seasonality covered during the survey. See Table 10 for acronym definitions.

$PC2_X$ indicates that significant wave height ($H_{1/3}$) and maximum wave height (H_x) during storms, as well as maximum wind speed (W_x), explain around 25% of the variance in the data set, but these variables are not correlated to the other variables in the analysis. This reinforces the conclusion from the first PCA (Figure 44), that the wave statistics embedded in the long-term wave climatology (derived from wave buoy measurements taken 53 km SW away from the study site) are not as relevant as information pertaining to the relative magnitude and duration of events that have the potential to inundate the beach.

4.5 Discussion

4.5.1 The Geomorphic Role of LWD in an Embayed Beach-dune System

The impact that a LWD matrix has on foredune erosion, recovery, and growth depends on the interaction of several variables, which include the characteristics of the LWD matrix, the nature of the wave and water level regimes that favor removal or deposition of sand and LWD on the beach, and the intensity and timing of the aeolian sediment transport regime. An exposed LWD matrix reduces incident wind speeds and alters turbulence characteristics in the boundary layer in a way that may promote sediment deposition in comparison to a flat, open beach (Grilliot et al., 2018). How deposition occurred within the LWD matrix depended on the density of the LWD as well as the size and stacking of the individual logs and debris. A denser matrix imparted greater roughness at the leading edge and therefore reduced transport over a shorter distance than a less dense matrix (Grilliot et al., 2019). While the study results showed that there was a clear relationship between decreasing sand transport with increased LWD density, it was unclear how other LWD matrix characteristics (e.g., size, shape, height above the surface, orientation to incoming flow, structure, apparent porosity) affected sand transport and deposition patterns within, and past, the LWD matrix. These complex inter-relationships evolved over time as the roughness effect changed and the trapping efficiency of the LWD matrix declined with progressive infilling of the accommodation space and ultimate burial.

The sand-trapping efficiency of the LWD matrix at the study site appeared to be seasonally mediated. Winter (Oct – Mar) storms brought high water events that exhumed LWD that was previously buried in the foredune or backshore. The rafted LWD was reworked and deposited as an exposed LWD matrix with considerable accommodation space. Major LWD reworking and addition events occurred about once or twice every winter season. Thus, there were periods of time when the LWD matrix served as a very effective sink for aeolian sediment, thereby limiting continuous sand delivery to the foredune. Accordingly, there is a negative correlation between volumetric change and LWD coverage when the processes are dominated by waves and tides, as in the winter. The PCA results. The PCA results (Table 16 and Figure 45) and volumetric change analyses (Figure 38, Figure 39, and Table 12) confirmed that volumetric

changes on the backshore were inversely correlated with wave processes (i.e., large waves imply erosion). These types of beach-dune interactions have been studied for quite some time (e.g., Sherman and Bauer, 1993; Bauer and Sherman, 1999; Delgado-Fernandez and Davidson-Arnott, 2011; Roelvink and Costas, 2019), but they have never been documented for a beach with a significant cover of LWD.

In contrast to the role of waves during intense storms, aeolian deposition can be pronounced because of strong winds that may not be related to wave activity. This may occur, for example, with obliquely alongshore wind directions that have significant fetch distance across the sand surface but are not capable of generating large waves due to the deeply embayed nature of this beach. Aeolian transport at the study site during the winter was, on average, eight times that during the summer (Figure 42), and any exposed LWD on the backshore was usually partially or completely buried in a matter of days or weeks (see time-lapse video in Supplementary Materials). This meant that aeolian sand was able to travel nearly unimpeded across the buried LWD and onto the foredune, allowing for foredune accretion during the majority of the winter months except directly after particularly large wave events that eroded the beach and exhumed existing LWD. This rapid in-filling effect has been reported for sand fences and beach wrack, consisting of sea weed, kelp and flotsam (Nordstrom et al., 2007, 2011; Grafals-Soto and Nordstrom, 2009; Li and Sherman, 2015), but never before for LWD.

Sand that is trapped in a LWD matrix serves as a buffer that protects the foredune from subsequent wave-induced erosion during storms. This is also the primary purpose of sand fences that are constructed to prevent landward incursion of aeolian sand or to restrict the migration of blowing sand across critical infrastructure such as roads and railway tracks (Nordstrom et al., 2000; Li and Sherman, 2015; Gillies et al., 2017). But LWD matrices can play an additional role in mechanically reducing or enhancing the erosional impact of waves by preventing attack of the foredune toe or rafting the LWD to act as battering rams (Komar and Rea, 1976; Finlayson, 2006). This depends on the degree to which the LWD is stacked and interwoven in a complex geometry that is relatively difficult to mobilize. Floating logs in the swash zone will also extract some wave energy. Thus, the presence of LWD on sandy beaches

may mitigate some of the potential damage done to foredunes during extreme storm events despite localized scour around individual pieces of LWD.

Additional protection to the dune system backing the beach could also be offered by the promotion of incipient dune formation and/or foredune progradation (Walker and Barrie, 2006; Eamer and Walker 2010). Unlike dune-colonizing vegetation such as beach or dune grasses, LWD cannot adapt to increased deposition and continue to grow in pace with the rate of deposition. LWD must be exhumed and reworked in order to regain its role as a significant roughness element that can moderate sand transport to the dune. A completely infilled LWD matrix is limited in its capacity to trap sediment, but it will provide a raised platform where vegetation could establish and remain protected from wave incursions (e.g., Walker and Barrie, 2006; Eamer and Walker, 2010; Heathfield and Walker, 2011). If the vegetation flourishes and traps more sand, an incipient foredune may evolve. This process would lead to foredune progradation, unless disturbed by subsequent storms that have the capacity to erode the incipient foredune entirely (e.g., Walker and Barrie, 2006; Heathfield and Walker, 2011). There is abundant evidence at the study site of buried logs at the base of the foredune, extending well beneath the core of the foredune (Figure 46). These logs were presumably buried during earlier phases of foredune evolution when aeolian deposition prevailed over wave-dominated erosion events. The present foredune is occasionally scarped, but many of the logs remain partially buried and fixed. As the foredune ramp recovers, LWD deposited in the backshore zone then follows the same pattern, potentially facilitating progradation. In terms of the longer-term evolution of the foredune at this site, the system is prograding at an estimated rate of 0.69 m a^{-1} (from 0.4 cal. ka BP – present) based on OSL dating of relict foredunes landward of the modern beach (Eamer et al., 2018), and, therefore, much of the LWD on the present beach will likely become permanently buried as is also evident in the more recent relict foredunes at the site.

Figure 46 – LWD previously buried in the foredune that was exhumed by the March 2016 erosive event. Note large logs sticking out of the beach horizontally, suggesting deposition on a higher beach surface during a phase of foredune growth.

It is important to reiterate the relationship between aeolian deposition events and wave erosion events recorded during the study. Even though the wave erosion events mobilized relatively more sand in one event than several aeolian transport events combined, the much greater number of aeolian transport events had a cumulative re-building effect that equaled or exceeded the destructive impact of the wave-induced erosion events. The maintenance and historical progradation of the foredune at this site attests to such a long-term relationship. As a consequence, it is not unreasonable to conclude that the LWD matrix might not have a longer-term impact (beyond this study) on the overall morphodynamics of this beach. Although, this assumes that the concentrations of LWD would remain the same.

The beach-dune system seems to exist in a state of dynamic equilibrium with annual cycles of net loss and gain that are approximately balanced from year to year, as determined by the severity of storm events in any given year. In this context, it is important to note that the

deeply embayed nature of West Beach with significant headland promontories, as is, commonly found on the BC coast, implies that the sediment budget is, effectively closed to inputs and losses from the marine boundary. More open coast beaches with LWD may have a different morphodynamic response.

A Conceptual Model of the Impacts of LWD on Beach-dune Interaction

Figure 47 shows a simplified model of the cyclical nature of LWD and its relative impact on sand transport in a beach and foredune system based on the observations of this 4-year study. The model presents four states along a spectrum of beach-dune states highlighting the relative prominence of LWD. State 1, for example, aligns with negligible areal coverage of LWD whereas state 4 shows a beach-dune system dominated by the presence of LWD. The latter state evolves when wave-induced exhumation and reworking of the LWD matrix is frequent. Subsequent burial by aeolian deposition leads progressively, and often rapidly, to state 1. The cartoon profiles 1A-4A, and 1B-4B show what each state might look like depending on the trajectory (accretionary or erosional, respectively) of the system. The concept is adapted from (Hesp, 2002).

Progression from one state to another typically occurs rapidly, as documented during this study, although beach-dune systems may exist in only one or two states for extended periods of time depending on wave and wind conditions. Accretionary and stable beach-dune systems likely will experience all states, with the most extreme and rare erosive events infrequently inducing state 4B, followed by recovery to state 3A, 2A and 1A. Accretionary beach-dune systems are likely to have few major events that cause widespread erosion and LWD exhumation/reworking relative to the large number of aeolian transport events that will yield net beach-dune accretion. In contrast, erosional beach-dune systems will experience a greater number of LWD reworking events and relatively ineffective aeolian transport regimes. Thus, states 3 and 4 would be the norm for erosional beach-dune systems with LWD, and rarely if ever would they transition to state 1.

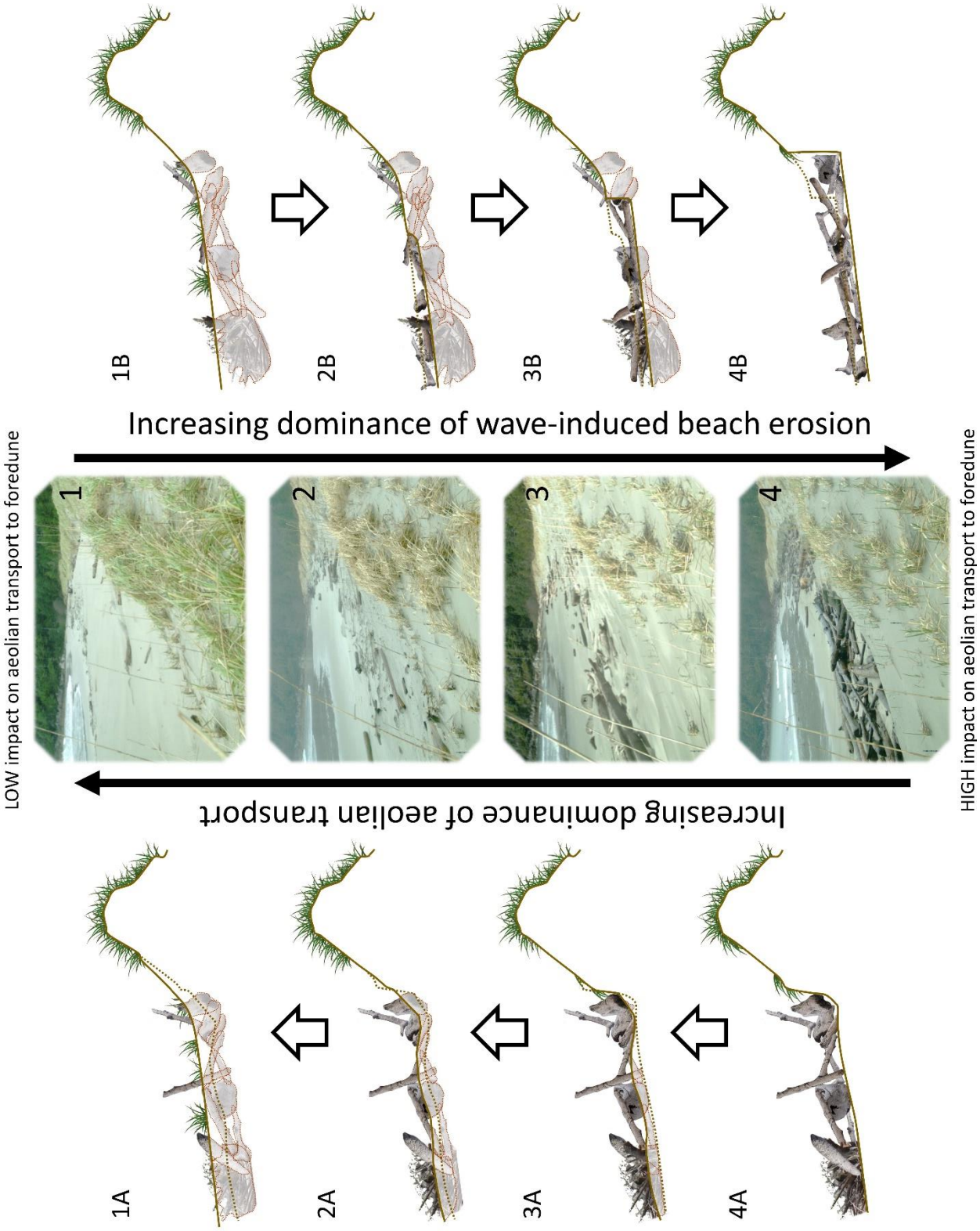

Figure 47 – A conceptual model showing the morphological states of a beach and foredune system fronted by LWD.

LWD additions and removals can occur during any state if new LWD is introduced into the system (i.e., from alongshore or via rivers) or if existing LWD is lost (e.g., offshore transport by nearshore currents). If an addition of LWD occurs, the system state progresses from state 1 or 2 to state 3 or 4, depending on how much LWD is added and whether beach erosion occurs simultaneously. An increase in percent LWD coverage on the surface will have the same net effect of trapping aeolian transport across the beach, regardless of whether existing LWD is exhumed or new LWD is added. The model accommodates both mechanisms of increasing LWD areal cover, but LWD removals are not included explicitly in the model because such events were few in number and magnitude during this study. On a more open coast, LWD removal by a major erosional event could theoretically create a state (5) that is characterized by a large foredune scarp and the absence of LWD. However, along most forested coastlines subject to the presence of LWD, the return of LWD to the beach is inevitable, which requires entering the conceptual model at states 2-4 depending on how effective aeolian processes were in re-building the sand ramp at the base of the foredune.

Four alternative morphological pathways resulting from the presence of LWD on a beach-dune system are suggested in Figure 48, based on the four states shown in Figure 47. It is assumed that these pathways will occur over a decadal timescale keeping relative sea-level remains essentially constant. On a prograding coast (Figure 48 Scenario A), for example, LWD additions to the beach (Figure 48-A2) would be buried by aeolian sand, followed by colonization of pioneering vegetation (Figure 48-A3), leading to the establishment of an incipient dune and eventually a series of stabilized foredune ridges with buried LWD at their core (Figure 48-A4). This assumes a consistently positive onshore sediment budget and dominance of aeolian processes relative to wave-generated erosion events. Existing LWD remains buried while the beach continues to grow, and new LWD needs to be added from elsewhere to enhance aeolian deposition within the LWD matrix.

In the case of an eroding coast (Figure 48 Scenario B), the dominance of wave-induced beach erosion would progressively, but intermittently, scarp the foredune (Figure 16-B2). Depending on the amount of onshore aeolian sand transport, the dune may be eroded completely through time (Figure 48-B3a) or migrate landward (Figure 48-B3b) keeping pace

with seasonal variations in deposition-erosion processes. Extreme high water events could occur during any scenario at any state, leading to total destruction of the foredune, overwash, and landward translation of LWD by hundreds of meters inland (Figure 48-B*).

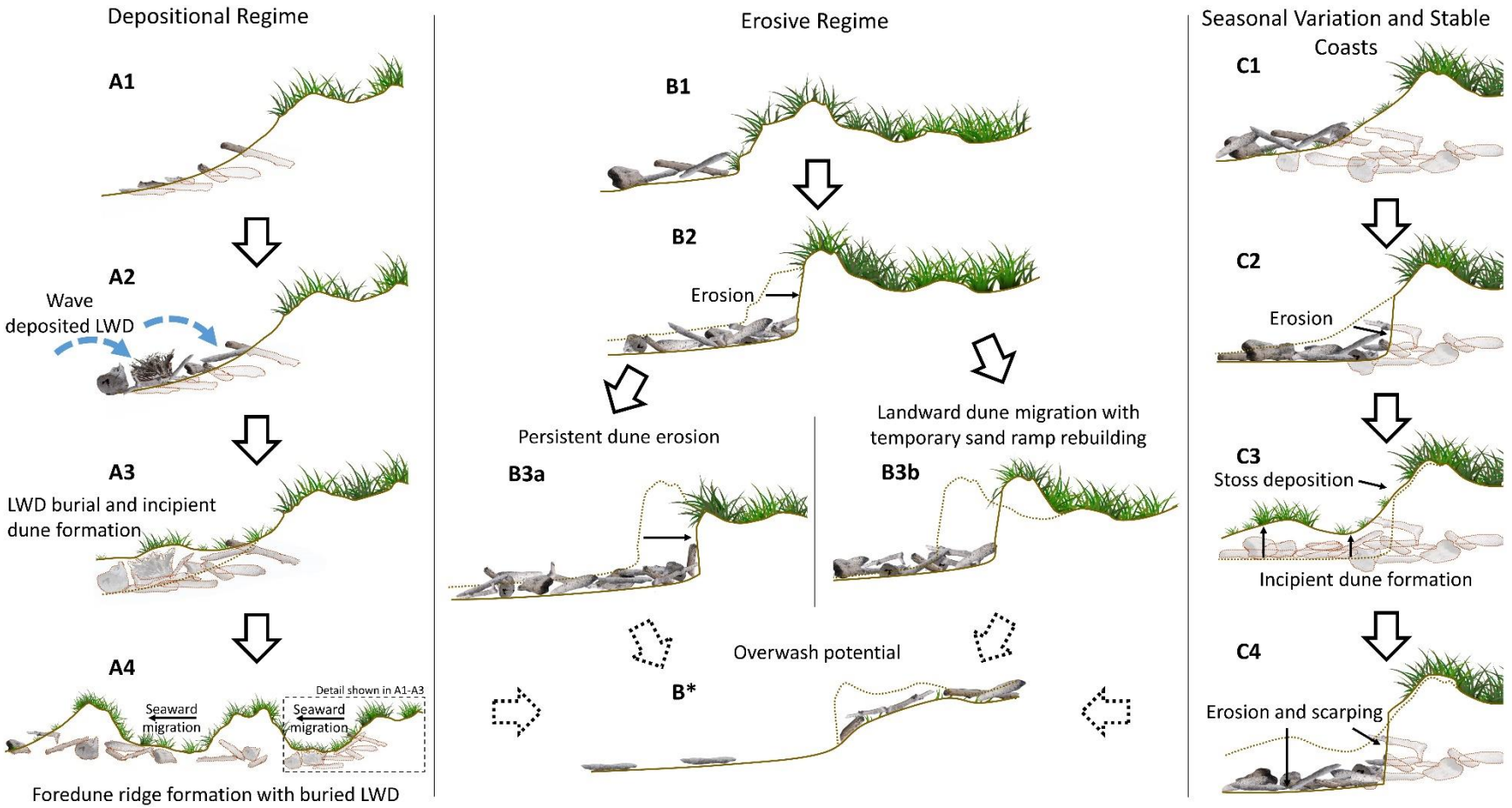
Depositional Regime
A1
A2
Wave
deposited LWD
A3
LWD burial and incipient
dune formation
A4
Detail shown in A1-A3
Seaward
migration
Seaward
migration
Foredune ridge formation with buried LWD
Erosive Regime
B1
B2
Erosion
Persistent dune erosion
B3a
Landward dune migration with
temporary sand ramp rebuilding
B3b
Overwash potential
B*
Seasonal Variation and Stable
Coasts
C1
C2
Erosion
C3
Stoss deposition
Incipient dune formation
C4
Erosion and scarping

Figure 48 – Possible evolutionary states of a beach-dune system with LWD. Scenario A, on the left, shows a prograding coast and seaward migration manifested as a series of foredune ridges with buried LWD. Scenario B, in the middle, shows a receding coast that either maintains persistent dune erosion (B3a) or landward dune migration (B3b) with the potential for overwash (B*) that can occur during any scenario (A, B, C) if water levels are high enough. Scenario C, on the right, shows a seasonal cycle of repeating erosion and LWD burial by aeolian deposition. It is important to understand that seasonal variations in Scenario C could occur in Scenarios A and B with the long-term trend superimposed over the short-term fluctuations. Scenario C would also occur on stable coasts with no long-term migration of the foredune.

In both scenario A and B, seasonal cycles (scenario C) with no migration could occur (Figure 48 Scenario C). Storms scarping the foredune (Figure 48-C2) could occur in Scenario A while periods of sediment accretion (Figure 48-C3) could occur in Scenario B. However, the long-term trend for Scenarios A and B would be as indicated above each scenario. On stable coasts (Figure 48 Scenario C), the system will maintain a balance between the erosion and accretion states with a steady state dune position. Data from this study suggest that the beach-dune system on West Beach matches Scenario C although there is a tendency toward slight progradation.

In order for a LWD matrix to substantially reduce the amount of sediment reaching a foredune, the volume of sand trapped within the LWD must exceed the volume of sand transported into the matrix. The volume of sand a LWD matrix can trap (i.e., accommodation space) can be estimated by calculating average storage ‘depths’ or heights of the matrix above the sand surface using TLS or aerial LiDAR data (Eamer and Walker, 2010). As a LWD matrix is infilled (Figure 49), aeolian transport to the foredune increases, first slowly and then rapidly, until the matrix is ‘effectively buried’, meaning, that it has little to no remaining accommodation space (Figure 47, state 1). The amount of infilling needed in the LWD matrix, relative to the storage depth, to reach this ‘effective’ limit is unknown but it likely does not require complete burial of all LWD elements. A conceptual comparison can be drawn with sand fence research that has shown a significant loss of trapping function when sediment reaches 80% of the fence height (e.g., Hotta and Horikawa, 1990).

Figure 49 – LWD buried to the point where its sand trapping efficiency is substantially reduced, allowing grains to pass over and around logs and into the foredune.

A LWD matrix is most effective at trapping sediment when it is recently exposed or deposited during states 3 and 4. The longer a beach-dune system occupies states 3 and 4, the more effective the LWD would be at impacting sand transport to the foredune. This only applies to saltation transport as some sediment would still be able to reach the foredune during the most extreme wind events that have the capacity to carry sand in suspension over the LWD matrix and foredune (Figure 50) (Hesp, 2002).

Figure 50 – Sand mobilized by saltation and suspension on the West Beach foredune, Calvert Island, April 11, 2015. Credit: Eugene Farrell.

4.5.2 Foredune Evolution on West Beach, Calvert Island

The data collected in this study indicate a relatively minor role for LWD in regard to affecting foredune evolution largely because of the large frequency of aeolian transport events in relation to wave-induced erosion events that cause LWD reworking. As a consequence, LWD is buried rapidly and typical foredune accretion processes are re-established. The lack of significant and consistent correlation between volumetric change on the beach and changes in LWD coverage demonstrate, at the very least, that the TLS survey intervals were not frequent enough to resolve a causal relationship if it exists. Rapid burial of the LWD matrix was clearly captured by the time-lapse imagery, which demonstrated that successive aeolian transport events buried the LWD quickly, thereby reconnecting the foredune to the sediment supply from the foreshore and backshore zones. But the TLS survey intervals were too long to quantify these processes. Over the course of the four years of surveys, from Jun 2013 to Aug 2017, 0.53 m^3 m^{-2} of sediment accumulated on the stoss slope of the foredune above the scarp region. This is

additional evidence in support of the relative ineffectiveness of the LWD matrix in curtailing foredune growth. Nevertheless, more frequent volumetric and sediment transport monitoring would be needed to determine the length of time that the LWD matrix at this study site reduced transport downwind as well as the magnitude of sediment lost to the matrix and not reaching the foredune during wind events that had the capacity to build the foredune had the LWD matrix not existed.

4.6 Conclusions

This study highlights important implications of the presence of LWD on sedimentation pathways and the long term evolution of beach-dune systems on macro-tidal coasts with embayed beaches. Quasi-seasonal TLS surveys were conducted to quantify changes in LWD areal coverage and volumetric changes on the beach and foredune. Time-lapse camera imagery was used to characterize the frequency and magnitude of the nearshore and aeolian transporting regimes and to derive additional qualitative parameters describing beach state. PCA was performed using these derived variables as well as meteorological and marine metrics to better understand the linkages among the primary explanatory variables driving geomorphic change at the study site. The results provided insights into the role that LWD plays in mediating sediment delivery to the foredune. On this basis, a new conceptual model was proposed that includes LWD in the long-term evolution of beach-dune systems.

During the study, the frequency of depositional events outnumbered erosional events by a factor of 3 (Table 13). Infrequent large storms caused wave erosion that was responsible for the vast majority of erosion measured at the site over the four-year study. In contrast, aeolian transport events were responsible for net positive deposition in the backshore and foredune zones. Subsequent to a wave erosion event, a large number of aeolian depositional events that followed in sequence was responsible for quickly burying the exhumed LWD matrix. This allowed sand to rebuild the scarp carved into the foredune toe and reconnect the sediment transport pathway to the foredune. Captured sediment in the LWD matrix was available to be reworked by future storms, but served as a platform for increased vegetation growth at this site, demonstrating how an infilled LWD matrix could serve as a foundation for

incipient and foredune growth.

PCA revealed that most of the variance in the data set was explained by a few variables, including the number of storm hours (S_H), hours of wave influence on the backshore (T_{WL}), Resultant Drift Potential (RDP), and Drift Potential (DP). These variables were positively correlated with TLS survey results during the winter season, demonstrating that storm conditions cause high water levels and high winds that drive volumetric and LWD changes at this site. However, the precise nature of these relationships is nuanced because major wind storms can be associated with either wave-induced erosion or aeolian deposition, which have opposite impacts on LWD matrices (exhumation versus burial, respectively).

A conceptual model is proposed showing the various morphological states of a beach-dune system fronted with LWD. The role that LWD could play in modulating sediment to a foredune depends on the frequency and magnitude of erosive (LWD reworking) and aeolian accretionary events. LWD will have a greater impact on foredune morphology if the LWD is more frequently exhumed and reworked, allowing it to block sand transport and store sediment (Figure 47, state 4). In extreme cases, LWD could starve a foredune of sediment, severely limiting foredune growth; on the other hand, LWD could have little to no effect on foredune growth if it is quickly buried and rarely unearthed. Scenarios are also presented for prograding, recessional, and stable coasts that result in buried LWD at the base of successive foredune ridges, a maintained erosional state where LWD contributes to erosion, or a repeating seasonal cycle of erosion and burial, respectively.

5. Conclusions

5.1 Summary of Findings and Future Directions

The geomorphic role of LWD in sandy beach-dune systems to affect aeolian sediment delivery to the foredune has been understudied compared to other roughness elements like vegetation. This dissertation sought to better understand the role that a LWD matrix has in beach-dune morphodynamics by studying processes at multiple temporal scales, 1) event-scale (10 min) flow and sediment transport patterns, 2) daily frequency and relative magnitude of landscape changing events, 3) seasonal to interannual-scale volumetric changes. An event-based experiment was designed improve our understanding of LWD matrices acting as a rough surface and its role as a modifier of flow dynamics and sediment transport over a beach. Time-lapse camera imagery collected at 15-min intervals over four years revealed the complex cycle of wave scarping of the foredune, LWD exhumation and reworking events, and subsequent LWD burial by aeolian deposition. Seasonal TLS data revealed volumetric changes in sand resulting from the events seen in the time-lapse imagery. Combined, these data provide the basis for a conceptual model of the impact of LWD matrices on beach-dune systems.

The event-based experiment used sonic 3D anemometry to quantify flow and turbulence quantities over and through a LWD matrix while sediment traps and laser particle counters (LPCs) were used to measure relative transport flux. During the experiment, the LWD acted as a highly effective flow modifier over the beach by inducing roughness drag. The LWD deflected the incoming flow upward and away from the surface increasing vertical normal stress. The absolute magnitude of near-surface mean wind speed, turbulent kinetic energy, and Reynolds stress were reduced in the presence of the LWD matrix. However, there was a transfer of energy from the mean flow field to the turbulent fluctuations, such that the overall turbulence intensity increased along with a slight shift in the quadrant geometry toward Q2/Q4 event activity. The reduction in mean energy recorded 10 m inside the LWD matrix resulted in a > 99 % decrease in sand transport close to the surface as compared with the open beach. Similarly, the vertical array of sediment traps 5 m inside the LWD matrix recorded an 89% reduction of in total flux compared to the transect with no LWD at the same location relative to

the scarp. Therefor, the increase in streamwise and vertical turbulent fluctuations would seem to favor sediment transport potential, however in light of the overall reduction in the mean energy of the flow field, the potential is actually reduced.

The increase in turbulent fluctuations, however, contributed to increased transport for grains rebounding off of the LWD. The vertical array of sediment traps 5 m inside the LWD matrix recorded greater proportions of the flux at the 20, 30, 40, and 50 cm heights, yet total flux of all traps was reduced, compared to the trap on the flat beach. This difference is attributed to grains rebounding off the LWD into the higher flow field. The rebounding grains are then exposed to the increased turbulent fluctuations (recorded up to 1.5 m) and greater flow speeds that contribute to the continued transport of these grains farther into the LWD matrix. If flow energy was high enough, it is possible that grains rebounded higher into the flow field could be transported across the LWD matrix entirely, and onto the foredune. Further research is needed to determine if this transport mechanism, during higher wind speeds, would result in greater deposition on the foredune while negating the sand trapping effects of the LWD. This effect would also depend on the width, height, and composition of the LWD matrix as well as the degree to which the accommodation space had been in-filled.

Shore-parallel aligned LWD has the potential to cause alongshore flow steering of oblique onshore winds, although this depends on the incoming flow angle. Unfortunately, the flow steering over the LWD observed in this study cannot be conclusively linked to the presence of LWD because of the unknown effects of the anemometer being placed closer to the dune over the LWD compared to the flat beach. Still, an alongshore flow steering effect of highly oblique incident winds could enhance the decoupling effect of beach and dune sediment transport pathways described by Bauer et al. (2012) minimizing landward transport (Ollerhead et al., 2013). The potential for flow steering over LWD and its impact on sand transport to the foredune is ripe for future research.

Downwind of the LWD, on the stoss slope of the dune, there is evidence of flow compression and streamline concavity that conveys turbulent flow structures toward the bed. The presence of these flow patterns suggests that flow downwind of a LWD matrix responds characteristically to topographic forcing as would be expected in the absence of LWD, thus

providing the potential for sediment transport on the stoss slope of the dune. Sand transport recorded on the stoss slope did not conclusively reflect this though. Only 2 of the 8 runs recorded greater transport on the stoss slope than immediately seaward of the scarp. Most of the runs at these locations recorded fewer than 10 counts, introducing the possibility of false returns (bugs or other debris triggering the sensor). Experiments performed at a wider range of wind speeds with additional sensors on the stoss slope could reveal if sediment transport on the stoss slope does in fact align with the flow patterns recorded in this study.

While the event-based experiment revealed that an exposed LWD matrix was highly effective at limiting transport, the time-lapse footage and TLS scans revealed that this transport limiting effect depends on the frequency of LWD reworking events and infilling of the LWD matrix. This cyclical relationship between LWD, sand supply, and foredune growth is the basis for the conceptual model presented in Section 4.5.2. A LWD matrix is only effective at trapping sediment if it provides enough of a physical barrier to alter flow and thus, sediment transport. These properties change over time depending on the magnitude and frequency of nearshore events that periodically erode the beach and re-organize the LWD matrix. LWD can be exhumed by waves and then in the process of being re-buried by aeolian transport, can limit the sand supply to the foredune. Thus, the conceptual model shows states of wave-induced exhumation and reworking of the LWD matrix thereby impacting sediment transport to the foredune, leading to subsequent burial by aeolian deposition to a state where the LWD matrix no longer has any real impact on transport to the foredune.

Based on this model, possible evolutionary scenarios were presented for prograding, eroding, and stable coasts. Prograding coasts with successive LWD additions can form foredune ridges with buried LWD at their base. On eroding coasts, LWD can contribute to erosion by being rafted, scouring sediments at the toe of the dune or scarp, where they can remain in place or be rafted again with the potential for dune overwashing to distribute the LWD inland. Both of these scenarios can involve portions or all of the cycle shown in the conceptual model but the long-term trend will overtake the seasonal variations. Stable coasts will experience the full range of states in the conceptual model in a form of dynamic equilibrium.

Considering the model on West Beach, Calvert Island, the LWD does trap sediment in

the backshore, helping to protect the dune from scarping, but overall, the LWD at this study site maintains a lower impact on transport to the foredune. One or two major erosive events were counteracted by lower magnitude but more frequent aeolian transport events. So much so that the LWD was typically buried in a matter of days, quickly returning the system to model state 1, where the LWD had close to no impact on transport to the foredune. This cycle allowed aeolian transport to deposit sediment to parts of the foredune stoss slope over the course of four years. Interestingly, the PCA revealed that the factors contributing to the greatest variability in the dataset, i.e., number of storm hours (S_H), hours of wave influence on the backshore (T_{WL}), Resultant Drift Potential (RDP), and Drift Potential (DP), were positively correlated with winter surveys. Thus, nearly all of the model state changes on West Beach, Calvert Island occur during winter storms.

Historically at this site, shoreline progradation has slowed from 1.2 m a^{-1} (over the period 1.8-0.4 cal. ka BP) to 0.69 m a^{-1} (from 0.4 cal. ka BP – present) (Eamer et al., 2018). While current progradation rates are slower than historical rates, the stoss slope of the foredune still grew by as much as half a meter with the presence of LWD and scarping events. Therefore, given the current deposition rates and the observed frequency of sand ramp scarping and rebuilding, it is possible that that the formation of an incipient dune (Figure 48-C3) could be retained long enough to form a new foredune with LWD at its base. LWD visible at the base of the current foredune (Figure 46) and evidence of relic foredunes also support this evolution model (Eamer et al., 2018).

Foredune evolution could also be complicated at this site by log use before written record and the influx of LWD documented in recent history. It is possible that deposition rates on the foredune could increase if LWD was not trapping sand in the backshore. This might have been the case historically before logging and log transportation at an industrial scale led to more logs entering the marine and coastal environment (Edgell and Ross, 1983; Gonor et al., 1988; Heathfield and Walker, 2011). In addition, logs appearing on the beach were valuable sources of fuel, tools, and as artistic media to indigenous peoples and were quickly marked for ownership and collected at high tide (Hebda and Mathewes, 1984; Turner, 1998; Lepofsky et al., 2003; Drabek and Adams, 2004). Firewood collection alone has significantly reduced the

amount of LWD on readily accessed beaches in modern times (Gonor et al., 1988). It is reasonable to assume then that the first peoples on Calvert Island were removing and using LWD from the beaches. This practice would have occurred since the first human occupation of Calvert Island, confirmed as far back as 13 ka cal B.P. (McLaren et al., 2018). The actual amount of LWD removed can never be known, but it is likely that LWD concentrations were reduced by this practice, possibly increasing sand transport to historical foredunes. Conversely, the recent influx of anthropogenically derived LWD into the coastal environment could have contributed to a slowing of foredune progradation by trapping sediment and modulating sand transport to the foredune. However, given how fast the LWD was buried in the backshore and the current foredune deposition rates, any effect that the LWD had on slowing recent progradation rates (0.69 m a^{-1} from 0.4 cal. ka BP – present) reported by Eamer et al., (2018) was likely minimal.

6. References

Aagaard, T., Davidson-Arnott, R., Greenwood, B., Nielsen, J., 2004. Sediment supply from shoreface to dunes: Linking sediment transport measurements and long-term morphological evolution. Geomorphology 60, 205–224. https://doi.org/10.1016/j.geomorph.2003.08.002

Adams, K.R., Ingraham, W.J.J., Ebbesmeyer, C.C., Dickson, J., 2000. Lauan log floats 10,000 miles to Alaska from Asia. Beachcombers' Alert 5, 5–6.

Anderson, J.L., Walker, I.J., 2006. Airflow and sand transport variations within a backshore–parabolic dune plain complex: NE Graham Island, British Columbia, Canada. Geomorphology 77, 17–34. https://doi.org/10.1016/j.geomorph.2005.12.008

Andreoli, A., Comiti, F., Lenzi, M.A., 2007. Characteristics, distribution and geomorphic role of large woody debris in a mountain stream of the Chilean Andes. Earth Surf. Process. Landforms 32, 1675–1692. https://doi.org/10.1002/esp.1593

Anthony, E.J., Ruz, M.H., Vanhée, S., 2009. Aeolian sand transport over complex intertidal bar-trough beach topography. Geomorphology 105, 95–105. https://doi.org/10.1016/j.geomorph.2007.12.013

Arens, S.M., 1996. Patterns of sand transport on vegetated foredunes. Geomorphology 17, 339–350.

Arens, S.M., Slings, Q., de Vries, C.N., 2004. Mobility of a remobilised parabolic dune in Kennemerland, The Netherlands. Geomorphology 59, 175–188. https://doi.org/10.1016/j.geomorph.2003.09.014

Arens, S.M., Van Kaam-Peters, H.M.E., Van Boxel, J.H., 1995. Air flow over foredunes and implications for sand transport. Earth Surf. Process. Landforms 20, 315–332. https://doi.org/10.1002/esp.3290200403

Atha, J.B., 2013. Identification of fluvial wood using google earth. River Res. Appl. https://doi.org/10.1002/rra.2683

Bache, S.M., Wickham, H., 2014. magrittr: A forward-pipe operator for R [WWW Document]. URL https://cran.r-project.org/package=magrittr

Baddock, M.C., Wiggs, G.F.S., Livingstone, I., 2011. A field study of mean and turbulent flow

characteristics upwind, over and downwind of barchan dunes. Earth Surf. Process. Landforms 36, 1435–1448. https://doi.org/10.1002/esp.2161

Barchyn, T.E., Hugenholtz, C.H., Li, B., Neuman, C.M., Sanderson, S.R., 2014. From particle counts to flux: Wind tunnel testing and calibration of the 'Wenglor' aeolian sediment transport sensor. Aeolian Res. 15, 311–318. https://doi.org/10.1016/j.aeolia.2014.06.009

Bascom, W.N., 1953. Characteristics of natural beaches, in: Coastal Engineering Proceedings 1. p. 10.

Bauer, B.O., 2013. Fundamentals of aeolian sediment transport: boundary-layer processes, in: Shroder, J.F., Lancaster, N., Sherman, D.J., Baas, A.C.W. (Eds.), Treatise on Geomorphology, Vol 11: Aeolian Geomorphology. Elsevier Ltd., San Diego, California, pp. 7–22. https://doi.org/10.1016/B978-0-12-374739-6.00295-5

Bauer, B.O., Davidson-Arnott, R.G.D., 2002. A general framework for modeling sediment supply to coastal dunes including wind angle, beach geometry, and fetch effects. Geomorphology 49, 89–108.

Bauer, B.O., Davidson-Arnott, R.G.D., Hesp, P.A., Namikas, S.L., Ollerhead, J., Walker, I.J., 2009. Aeolian sediment transport on a beach: surface moisture, wind fetch, and mean transport. Geomorphology 105, 106–116. https://doi.org/10.1016/j.geomorph.2008.02.016

Bauer, B.O., Davidson-Arnott, R.G.D., Hilton, M.J., Fraser, D., 2018. On the frequency response of a Wenglor particle-counting system for aeolian transport measurements. Aeolian Res. 32, 133–140. https://doi.org/10.1016/j.aeolia.2018.02.008

Bauer, B.O., Davidson-Arnott, R.G.D., Walker, I.J., Hesp, P.A., Ollerhead, J., 2012. Wind direction and complex sediment transport response across a beach-dune system. Earth Surf. Process. Landforms 37, 1661–1677. https://doi.org/10.1002/esp.3306

Bauer, B.O., Sherman, D.J., 1999. Coastal dune dynamics: problems and prospects, in: Goudre, A.S., Livingston, I., Stokes, S. (Eds.), Aeolian Environments, Sediments, and Landforms. John Wiley & Sons Ltd., Chichester, UK, pp. 71–104.

Bauer, B.O., Walker, I.J., Baas, A.C.W., Jackson, D.W.T., McKenna-Neuman, C., Wiggs, G.F.S., Hesp, P.A., 2013. Critical reflections on the coherent flow structures paradigm in aeolian geomorphology, in: Venditti, J.G., Best, J.L., Church, M., Hardy, R.J. (Eds.), Coherent Flow

Structures at Earth's Surface. John Wiley & Sons Ltd., Chichester,West Sussex, UK, pp. 111–134. https://doi.org/10.1002/9781118527221

Bauer, B.O., Yi, J., Namikas, S.L., Sherman, D.J., 1998. Event detection and conditional averaging in unsteady aeolian systems. J. Arid Environ. 39, 345–375. https://doi.org/10.1006/jare.1998.0380

Bilby, R.E., Ward, J.W., 1991. Characteristics and function of large woody debris in streams draining old-growth, clear-cut, and second-growth forests in Southwestern Washington. Can. J. Fish. Aquat. Sci. 48, 2499–2508. https://doi.org/10.1139/f91-291

Bowen, A.J., Lindley, D., 1977. A wind-tunnel investigation of the wind speed and turbulence characteristics close to the ground over various escarpment shapes. Boundary-Layer Meteorol. 12, 259–271.

Bowen, A.J., Lindley, D., 1974. Measurements of the mean wind flow over various escarpment shapes, in: Proc. 5th Australasian Conference on Hydraulics and Fluid Mechanics, University of Canterbury, NZ. pp. 211–219.

Brauns, M., Garcia, X.-F., Walz, N., Pusch, M.T., 2007. Effects of human shoreline development on littoral macroinvertebrates in lowland lakes. J. Appl. Ecol. 44, 1138–1144. https://doi.org/10.1111/j.1365-2664.2007.01376.x

Brown, S., Nickling, W.G., Gillies, J.A., 2008. A wind tunnel examination of shear stress partitioning for an assortment of surface roughness distributions. J. Geophys. Res. Earth Surf. 113, 1–13. https://doi.org/10.1029/2007JF000790

Brunier, G., Fleury, J., Anthony, E.J., Gardel, A., Dussouillez, P., 2016. Close-range airborne Structure-from-Motion photogrammetry for high-resolution beach morphometric surveys: Examples from an embayed rotating beach. Geomorphology 261, 76–88. https://doi.org/10.1016/j.geomorph.2016.02.025

Carrivick, J.L., Smith, M.W., Quincey, D.J., 2016. Structure from motion in the geosciences, Analytical Methods in Earth and Environmental Science. John Wiley & Sons Ltd., West Sussex, England.

Carter, R.W.G., Hesp, P.A., Nordstrom, K.F., 1990. Erosional landforms in coastal dunes, in: Nordstrom, K.F., Psuty, N.P., Carter, R.W.G. (Eds.), Coastal Dunes, Form and Process. John

Wiley & Sons Ltd., West Sussex, England, pp. 217–250.

Chapman, C. a., Walker, I.J., Hesp, P.A., Bauer, B.O., Davidson-Arnott, R.G.D., 2012. Turbulent Reynolds stress and quadrant event activity in wind flow over a coastal foredune. Geomorphology 151–152, 1–12. https://doi.org/10.1016/j.geomorph.2011.11.015

Chapman, C., Walker, I.J., Hesp, P.A., Bauer, B.O., Davidson-Arnott, R.G.D., Ollerhead, J., 2013. Reynolds stress and sand transport over a foredune. Earth Surf. Process. Landforms 38, 1735–1747. https://doi.org/10.1002/esp.3428

Chappell, A., Heritage, G.L., 2007. Using illumination and shadow to model aerodynamic resistance and flow separation: An isotropic study. Atmos. Environ. 41, 5817–5830. https://doi.org/10.1016/j.atmosenv.2007.03.037

Christensen, D.L., Herwig, B.R., Schindler, D.E., Carpenter, S.R., 1996. Impacts of lakeshore residential development on coarse woody debris in north temperate lakes. Ecol. Appl. 6, 1143–1149.

Clague, J.J., Munro, A., Murty, T., 2003. Tsunami hazard and risk in Canada. Nat. Hazards 28, 433–461. https://doi.org/10.1023/A:1022994411319

Cohn, N., Ruggiero, P., de Vries, S., Kaminsky, G.M., 2018. New insights on coastal foredune growth: the relative contributions of marine and aeolian processes. Geophys. Res. Lett. 45, 4965–4973. https://doi.org/10.1029/2018GL077836

Collins, B.D., Montgomery, D.R., Haas, A.D., 2002. Historical changes in the distribution and functions of large wood in Puget Lowland rivers. Can. J. Fish. Aquat. Sci. 59, 66–76. https://doi.org/10.1139/F01-199

Curran, J., Wohl, E., 2003. Large woody debris and flow resistance in step-pool channels, Cascade Range, Washington. Geomorphology 51, 141–157.

Davidson-Arnott, R., 2012. Wave-dominated coasts, Treatise on Estuarine and Coastal Science. Elsevier Inc. https://doi.org/10.1016/B978-0-12-374711-2.00305-3

Davidson-Arnott, R., Bauer, B., 2009. Instantaneous and mean aeolian sediment transport rate on beaches: an intercomparison of measurements from two sensor types. J. Coast. … 2009, 297–301.

Davidson-Arnott, R., Hesp, P., Ollerhead, J., Walker, I.J., Bauer, B., Delgado-Fernandez, I., Smyth,

T., 2018. Sediment budget controls on foredune height: comparing simulation model results with field data. Earth Surf. Process. Landforms. https://doi.org/10.1002/esp.4354

Davidson-Arnott, R.G.D., Bauer, B.O., Walker, I.J., Hesp, P.A., Ollerhead, J., Chapman, C., 2012. High-frequency sediment transport responses on a vegetated foredune. Earth Surf. Process. Landforms 37, 1227–1241. https://doi.org/10.1002/esp.3275

Davidson-Arnott, R.G.D., Yang, Y., Ollerhead, J., Hesp, P.A., Walker, I.J., 2008. The effects of surface moisture on aeolian sediment transport threshold and mass flux on a beach. Earth Surf. Process. Landforms 33, 55–74. https://doi.org/10.1002/esp.1527

Dayton, P.K., 1971. Competition, disturbance, and community organization: the provision and subsequent utilization of space in a rocky intertidal community. Ecol. Soc. Am. 41, 351–389.

de Vries, S., Arens, S.M., de Schipper, M.A., Ranasinghe, R., 2014a. Aeolian sediment transport on a beach with a varying sediment supply. Aeolian Res. 15, 235–244. https://doi.org/10.1016/j.aeolia.2014.08.001

de Vries, S., Southgate, H.N., Kanning, W., Ranasinghe, R., 2012. Dune behavior and aeolian transport on decadal timescales. Coast. Eng. 67, 41–53. https://doi.org/10.1016/j.coastaleng.2012.04.002

de Vries, S., van Thiel de Vries, J.S.M., van Rijn, L.C., Arens, S.M., Ranasinghe, R., 2014b. Aeolian sediment transport in supply limited situations. Aeolian Res. 12, 75–85. https://doi.org/10.1016/j.aeolia.2013.11.005

Delgado-Fernandez, I., Davidson-Arnott, R., 2011. Meso-scale aeolian sediment input to coastal dunes: The nature of aeolian transport events. Geomorphology 126, 217–232. https://doi.org/10.1016/j.geomorph.2010.11.005

Delgado-Fernandez, I., Davidson-Arnott, R., Bauer, B.O., Walker, I.J., Ollerhead, J., Rhew, H., 2012. Assessing aeolian beach-surface dynamics using a remote sensing approach. Earth Surf. Process. Landforms 37, 1651–1660. https://doi.org/10.1002/esp.3301

Dong, Z., Luo, W., Qian, G., Wang, H., 2007. A wind tunnel simulation of the mean velocity fields behind upright porous fences. Agric. For. Meteorol. 146, 82–93. https://doi.org/10.1016/j.agrformet.2007.05.009

Drabek, A.S., Adams, K.R., 2004. The Red Cedar of Afognak: a driftwood journey. Native Village of Afognak, Afognak, Alaska.

Dugan, J.E., Hubbard, D.M., 2010. Loss of coastal strand habitat in Southern California: the role of beach grooming. Estuaries and Coasts 33, 67–77. https://doi.org/10.1007/s12237-009-9239-8

Eamer, J.B.R., 2017. Reconstruction of the Late Pleistocene and Holocene geomorphology of Northwest Calvert Island, British Columbia. University of Victoria. PhD Dissertation.

Eamer, J.B.R., Shugar, D.H., Walker, I.J., Neudorf, C.M., Lian, O.B., Eamer, J.L., Bryce, J., Biln, L., 2018. Late Quaternary landscape evolution in a region of stable postglacial relative sea levels, British Columbia central coast, Canada. Boreas 47, 738–753. https://doi.org/10.1111/bor.12297

Eamer, J.B.R., Walker, I.J., 2013. Quantifying spatial and temporal trends in beach-dune volumetric changes using spatial statistics. Geomorphology 191, 94–108. https://doi.org/10.1016/j.geomorph.2013.03.005

Eamer, J.B.R., Walker, I.J., 2010. Quantifying sand storage capacity of large woody debris on beaches using LiDAR. Geomorphology 118, 33–47. https://doi.org/10.1016/j.geomorph.2009.12.006

Eamer, J.L., McLaren, D., Trant, A., 2017. Late Quaternary vegetation dynamics on Calvert Island, British Columbia, Canada. Unpubl. Res. Dev. 46.

Edgell, M.C.R., Ross, W.M., 1983. Marine log transportation and handling systems in British Columbia; Impacts on coastal management. Coast. Zo. Manag. J. 11, 41–69.

Ellis, J.T., Sherman, D.J., 2013. Fundamentals of aeolian sediment transport: wind-blown sand. Treatise Geomorphol. 11, 85–108. https://doi.org/10.1016/B978-0-12-374739-6.00299-2

Fabbri, S., Giambastiani, B.M.S., Sistilli, F., Scarelli, F., Gabbianelli, G., 2017. Geomorphological analysis and classification of foredune ridges based on Terrestrial Laser Scanning (TLS) technology. Geomorphology 295, 436–451. https://doi.org/10.1016/j.geomorph.2017.08.003

Feagin, R. a., Williams, A.M., Popescu, S., Stukey, J., Washington-Allen, R. a., 2014. The use of terrestrial laser scanning (tls) in dune ecosystems: the lessons learned. J. Coast. Res. 30,

111–119. https://doi.org/10.2112/JCOASTRES-D-11-00223.1

Finlayson, D.P., 2006. The geomorphology of Puget Sound beaches. University of Washington. PhD.

Finnigan, J., 2000. Turbulence in plant canopies. Annu. Rev. Fluid Mech. 32, 519–571. https://doi.org/10.1146/annurev.fluid.32.1.519

Frank, A.J., Kocurek, G., 1996. Airflow up the stoss slope of sand dunes: limitations of current understanding. Geomorphology 17, 47–54. https://doi.org/10.1016/0169-555X(95)00094-L

Fryberger, S.G., Dean, G., 1979. Dune forms and wind regime, in: McKee, E.D. (Ed.), A Study of Global Sand Seas, USGS Professional Paper, Vol 1052. US Geological Survey and United States National Aeronautics and Space Administration, Washington D.C., pp. 137–170.

Furieri, B., Harion, J.L., Milliez, M., Russeil, S., Santos, J.M., 2014. Numerical modelling of aeolian erosion over a surface with non-uniformly distributed roughness elements. Earth Surf. Process. Landforms 39, 156–166. https://doi.org/10.1002/esp.3435

Gillies, J.A., Etyemezian, V., Nikolich, G., Glick, R., Rowland, P., Pesce, T., Skinner, M., 2017. Effectiveness of an array of porous fences to reduce sand flux: Oceano Dunes, Oceano CA. J. Wind Eng. Ind. Aerodyn. 168, 247–259. https://doi.org/10.1016/j.jweia.2017.06.015

Gillies, J.A., Green, H., McCarley-Holder, G., Grimm, S., Howard, C., Barbieri, N., Ono, D., Schade, T., 2015. Using solid element roughness to control sand movement: Keeler Dunes, Keeler, California. Aeolian Res. 18, 35–46. https://doi.org/http://dx.doi.org/10.1016/j.aeolia.2015.05.004

Gillies, J.A., Lancaster, N., 2013. Large roughness element effects on sand transport, Oceano Dunes, California. Earth Surf. Process. Landforms 38, 785–792. https://doi.org/10.1002/esp.3317

Gillies, J.A., Nickling, W.G., King, J., 2007. Shear stress partitioning in large patches of roughness in the atmospheric inertial sublayer. Boundary-Layer Meteorol. 122, 367–396. https://doi.org/10.1007/s10546-006-9101-5

Gillies, J.A., Nickling, W.G., King, J., 2006. Aeolian sediment transport through large patches of roughness in the atmospheric inertial sublayer. J. Geophys. Res. 111, F02006.

https://doi.org/10.1029/2005JF000434

Gillies, J.A., Nield, J.M., Nickling, W.G., 2014. Wind speed and sediment transport recovery in the lee of a vegetated and denuded nebkha within a nebkha dune field. Aeolian Res. 12, 135–141. https://doi.org/10.1016/j.aeolia.2013.12.005

Gippel, C.J., 1995. Environmental hydraulics of large woody debris in streams and rivers. J. Environ. Eng. 121, 388–395. https://doi.org/10.1061/(ASCE)0733-9372(1995)121:5(388)

Goldsmith, V., 1985. Coastal dunes, in: Davis, R.A. (Ed.), Coastal Sedimentary Environments. Springer, New York, New York, pp. 303–378.

Gomi, T., Sidle, R.C., Bryant, M.D., Woodsmith, R.D., 2001. The characteristics of woody debris and sediment distribution in headwater streams, southeastern Alaska. Can. J. For. Res. 31, 1386–1399. https://doi.org/10.1139/x01-070

Gonor, J.J., Sedell, J.R., Benner, P.A., 1988. Chapter 4. What we know about large trees in estuaries, in the sea, and on coastal beaches, in: Maser, C., Terrant, R.F., Trappe, J.M., Franklin, J.F. (Eds.), From the Forest to the Sea: A Story of Fallen Trees. U.S. Department of Agriculture, Portland, pp. 83–112.

Grafals-Soto, R., Nordstrom, K., 2009. Sand fences in the coastal zone: intended and unintended effects. Environ. Manage. 44, 420–9. https://doi.org/10.1007/s00267-009-9331-7

Green, A., Ettya, A., McPhee, S., Ricker, B., Temenos, C., 2014. British Columbia in a global context. BC Campus Open Education, Victoria, B.C.

Gregory, K.J., Gurnell, A.M.A., Petts, G.E.G., 2002. Restructuring physical geography. Trans. Inst. Br. Geogr. 27, 136–154.

Grilliot, M.J., Walker, I.J., Bauer, B.O., 2019. Aeolian sand transport and deposition patterns within a large woody debris matrix fronting a foredune. Geomorphology. https://doi.org/10.1016/j.geomorph.2019.04.010

Grilliot, M.J., Walker, I.J., Bauer, B.O., 2018. Airflow dynamics over a beach and foredune system with large woody debris. Geosciences 8, 147. https://doi.org/10.3390/geosciences8050147

Guisado-Pintado, E., Jackson, D.W.T., Rogers, D., 2019. 3D mapping efficacy of a drone and terrestrial laser scanner over a temperate beach-dune zone. Geomorphology 328, 157–

172. https://doi.org/10.1016/j.geomorph.2018.12.013

Gurnell, A.M., Piegay, H., Swanson, F.J., Gregory, S. V, 2002. Large wood and fluvial processes. Freshw. Biol. 47, 601–619.

Guthrie, R.H., 2002. The effects of logging on frequency and distribution of landslides in three watersheds on Vancouver Island, British Columbia. Geomorphology 43, 273–292. https://doi.org/10.1016/S0169-555X(01)00138-6

Hacker, S.D., Zarnetske, P., Seabloom, E., Ruggiero, P., Mull, J., Gerrity, S., Jones, C., 2012. Subtle differences in two non-native congeneric beach grasses significantly affect their colonization, spread, and impact. Oikos 121, 138–148. https://doi.org/10.1111/j.1600-0706.2011.18887.x

Hara, K., Zhao, Y., Tomita, M., Kamagata, N., Li, Y., 2016. Impact of the great east Japan earthquake and tsunami on coastal vegetation and landscapes in Northeast Japan: findings based on remotely sensed data analysis, in: Urabe, J., Nakashizuka, T. (Eds.), Ecological Impacts of Tsunamis on Coastal Ecosystems. Springer, Tokyo, Japan, pp. 253–269.

Hardisty, J., Whitehouse, R.J.S., 1988a. Evidence for a new sand transport process from experiments on Saharan dunes. Nature. https://doi.org/10.1038/332532a0

Hardisty, J., Whitehouse, R.J.S., 1988b. Effect of bedslope on desert sand transport. Nature. https://doi.org/10.1038/334302b0

Harmon, M.E., Hua, C., 1991. Coarse woody debris dynamics in two old-growth ecosystems. Bioscience 41, 604–610.

Hassan, M., Hogan, D.L., Bird, S., Initiative, M.P.B., 2008. Mountain pine beetle impacts on channel morphology and woody debris in forested landscapes, MPBI Project # 8.40. Canadian Forest Service, Victoria, B.C. URL http://publications.gc.ca/collections/collection_2009/nrcan/Fo143-3-2008-7E.pdf

Heathfield, D.K., Walker, I.J., 2015. Evolution of a foredune and backshore river complex on a high-energy, drift-aligned beach. Geomorphology 248, 440–451. https://doi.org/10.1016/j.geomorph.2015.08.006

Heathfield, D.K., Walker, I.J., 2011. Analysis of coastal dune dynamics, shoreline position, and large woody debris at Wickaninnish Bay, Pacific Rim National Park, British Columbia. Can. J.

Earth Sci. 1198, 1185–1198. https://doi.org/10.1139/E11-043

Hebda, R.J., Mathewes, R.W., 1984. Holocene history of cedar and native Indian cultures of the North American Pacific Coast. Science (80-.). 225, 711–713. https://doi.org/10.1097/IGC.0000000000000658

Herrero, C., Krankina, O., Monleon, V.J.V., Bravo, F., 2013. Amount and distribution of coarse woody debris in pine ecosystems of north-western Spain, Russia and the United States. iForest-Biogeosciences For. e1–e9. https://doi.org/10.3832/ifor0644-006

Hesp, P., 2011. Dune coasts, in: Treatise on Estuarine and Coastal Science. Elsevier, pp. 193–221. https://doi.org/10.1016/B978-0-12-374711-2.00310-7

Hesp, P.A., 2004. Coastal dunes in the tropics and temperate regions: location, formation, morphology and vegetation processes, in: Martínez, M.L., Psuty, N.P. (Eds.), Coastal Dunes: Ecology and Conservation. Springer-Verlag, New York, New York, p. 390.

Hesp, P.A., 2002. Foredunes and blowouts: initiation, geomorphology and dynamics. Geomorphology 48, 245–268.

Hesp, P.A., 1989. A review of biological and geomorphological processes involved in the initiation and development of incipient foredunes, in: Gimingham, C.H., Ritchie, W., Willetts, B.B., Willis, A.J. (Eds.), Coastal Sand Dunes. Proceedings of Royal Society, Edinburgh, Edinburgh, pp. 181–201.

Hesp, P.A., Davidson-Arnott, R., Walker, I.J., Ollerhead, J., 2005. Flow dynamics over a foredune at Prince Edward Island, Canada. Geomorphology 65, 71–84. https://doi.org/10.1016/j.geomorph.2004.08.001

Hesp, P.A., Hilton, M., Konlecher, T., 2017. Flow and sediment transport dynamics in a slot and cauldron blowout and over a foredune, Mason Bay, Stewart Island (Rakiura), NZ. Geomorphology 295, 598–610. https://doi.org/10.1016/j.geomorph.2017.08.024

Hesp, P.A., Pringle, A., 2001. Wind flow and topographic steering within a trough blowout. J. Coast. Res. 597–601.

Hesp, P.A., Smyth, T. a G., Nielsen, P., Walker, I.J., Bauer, B.O., Davidson-Arnott, R., 2015. Flow deflection over a foredune. Geomorphology 230, 64–74. https://doi.org/10.1016/j.geomorph.2014.11.005

Hesp, P.A., Smyth, T.A.G., 2016. Jet flow over foredunes. Earth Surf. Process. Landforms 1735, 1727–1735. https://doi.org/10.1002/esp.3945

Hesp, P.A., Smyth, T.A.G., Walker, I.J., Gares, P.A., Wasklewicz, T.A., 2016. Flow within a trough blowout at Cape Cod. J. Coast. Res. Spec. Issue Coconut Creek SI, 288–292. https://doi.org/10.2112/SI75-XXX.1

Hesp, P.A., Smyth, T.A.G.G., 2017. Nebkha flow dynamics and shadow dune formation. Geomorphology 282, 27–38. https://doi.org/10.1016/j.geomorph.2016.12.026

Hesp, P.A., Walker, I.J., 2013. Coastal dunes, in: Shroder, J.F., Lancaster, N., Sherman, D.J., Baas, A.C.W. (Eds.), Treatise on Geomorphology, Vol 11: Aeolian Geomorphology. Elsevier, San Diego, California, p. 439.

Hesp, P.A., Walker, I.J., Namikas, S.L., Davidson-Arnott, R., Bauer, B.O., Ollerhead, J., 2009. Storm wind flow over a foredune, Prince Edward Island, Canada, in: Journal of Coastal Research, Special Issue No. 56. Proceedings of the 10th International Coastal Symposium ICS 2009. pp. 312–316.

Higman, B., Shugar, D.H., Stark, C.P., Ekström, G., Koppes, M.N., Lynett, P., Dufresne, A., Haeussler, P.J., Geertsema, M., Gulick, S., Mattox, A., Venditti, J.G., Walton, M.A.L., McCall, N., Mckittrick, E., MacInnes, B., Bilderback, E.L., Tang, H., Willis, M.J., Richmond, B., Reece, R.S., Larsen, C., Olson, B., Capra, J., Ayca, A., Bloom, C., Williams, H., Bonno, D., Weiss, R., Keen, A., Skanavis, V., Loso, M., 2018. The 2015 landslide and tsunami in Taan Fiord, Alaska. Sci. Rep. 8, 1–12. https://doi.org/10.1038/s41598-018-30475-w

Hilton, M., Nickling, B., Wakes, S., Sherman, D., Konlechner, T., Jermy, M., Geoghegan, P., 2017. An efficient, self-orienting, vertical-array, sand trap. Aeolian Res. 25, 11–21. https://doi.org/10.1016/j.aeolia.2017.01.003

Hoonhout, B., de Vries, S., 2017. Field measurements on spatial variations in aeolian sediment availability at the Sand Motor mega nourishment. Aeolian Res. 24, 93–104. https://doi.org/10.1016/j.aeolia.2016.12.003

Hotelling, H., 1933. Analysis of a complex of statistical variables into principal components. J. Educ. Psychol. 24, 417–441. https://doi.org/10.1037/h0071325

Hotta, S., Horikawa, K., 1990. Function of sand fence placed in front of embankment. Twenty-

Second Coast. Eng. Conf. 2754–2767.

Houser, C., Ellis, J., 2013. Beach and dune Interaction, in: Shroder, J.F. (Editor in C., Sherman, D.J. (Eds.), Treatise on Geomorphology Vol 10: Coastal Geomorphology. Academic Press, San Diego, California, pp. 267–288.

Hugenholtz, C.H., Barchyn, T.E., 2011. Laboratory and field performance of a laser particle counter for measuring aeolian sand transport. J. Geophys. Res. Earth Surf. 116, 1–13. https://doi.org/10.1029/2010JF001822

Huggett, R.J., 2007. Fundamentals of Geomorphology, 2nd Editio. ed. Routledge, New York, New York.

Hygelund, B., Manga, M., 2003. Field measurements of drag coefficients for model large woody debris. Geomorphology 51, 175–185. https://doi.org/10.1016/S0169-555X(02)00335-5

Iversen, J.D., Wang, W.-P., Rasmussen, K.R., Mikkelsen, H.E., Hasiuk, J.F., Leach, R.N., 1990. The effect of a roughness element on local saltation transport. J. Wind Eng. Ind. Aerodyn. 36, 845–854. https://doi.org/10.1016/0167-6105(90)90081-M

Jackson, D.W.T., Cooper, J.A.G., 1999. Beach fetch distance and aeolian sediment transport. Sedimentology 46, 517–522. https://doi.org/10.1046/j.1365-3091.1999.00228.x

Jackson, N.L., Nordstrom, K.F., 2013. Aeolian sediment transport and morphologic change on a managed and an unmanaged foredune. Earth Surf. Process. Landforms 38, 413–420. https://doi.org/10.1002/esp.3333

Jakob, M., 2000. The impacts of logging on landslide activity at Clayoquot Sound, British Columbia. Catena 38, 279–300. https://doi.org/10.1016/S0341-8162(99)00078-8

James, M.R., Robson, S., 2012. Straightforward reconstruction of 3D surfaces and topography with a camera: Accuracy and geoscience application. J. Geophys. Res. Earth Surf. 117, 1–17. https://doi.org/10.1029/2011JF002289

Jiménez, J.A., Sánchez-Arcilla, A., Valdemoro, H.I., Gracia, V., Nieto, F., 1997. Processes reshaping the Ebro delta. Mar. Geol. 144, 59–79. https://doi.org/10.1016/S0025-3227(97)00076-5

Johannessen, J., Maclennan, A., 2007. Beaches and bluffs of Puget Sound and the northern straits prepared in support of the Puget Sound nearshore partnership. Seattle,

Washington.

Jolliffe, I.T., 2011. Principal component analysis, in: Miodrag, Lovric (Eds.), International Encyclopedia of Statistical Science. Springer-Verlag Berlin Heidelberg, p. 1671.

Jolliffe, I.T., Cadima, J., 2016. Principal component analysis: a review and recent developments. Philos. Trans. R. Soc. A Math. Phys. Eng. Sci. 374, 20150202. https://doi.org/10.1098/rsta.2015.0202

Kail, J., 2003. Influence of large woody debris on the morphology of six central European streams. Geomorphology 51, 207–223. https://doi.org/10.1016/S0169-555X(02)00337-9

Kassambara, A., 2018. ggpubr: "ggplot2" Based Publication Ready Plots [WWW Document]. URL https://cran.r-project.org/package=ggpubr

Kassambara, A., Mundt, F., 2017. factoextra: extract and visualize the results of multivariate data analyses [WWW Document]. URL https://cran.r-project.org/package=factoextra

Keijsers, J.G.S., De Groot, A. V., Riksen, M.J.P.M., 2015. Vegetation and sedimentation on coastal foredunes. Geomorphology 228, 723–734. https://doi.org/10.1016/j.geomorph.2014.10.027

Keller, E., Swanson, F., 1979. Effects of large organic material on channel form and fluvial processes. Earth Surf. Process. 4, 361–380.

Kennedy, D.M., Woods, J.L.D., 2012. The influence of coarse woody debris on gravel beach geomorphology. Geomorphology 159–160, 106–115. https://doi.org/10.1016/j.geomorph.2012.03.009

Komar, P.D., Rea, C.C., 1976. Erosion of Siletz Spit, Oregon. Shore & Beach 44, 9–15.

Kramer, N., Wohl, E., 2015. Driftcretions: The legacy impacts of driftwood on shoreline morphology. Geophys. Res. Lett. 42, 5855–5864. https://doi.org/10.1002/2015GL064441

Kuethe, A.M., 1971. Boundary layer control of flow separation and heat exchange. 3,578,264.

Lancaster, N., 1995. Geomorphology of Desert Dunes, 1st ed. Routledge, New York, New York.

Lancaster, N., Baas, A., 1998. Influence of vegetation cover on sand transport by wind: Field studies at Owens Lake, California. Earth Surf. Process. Landforms 23, 69–82. https://doi.org/10.1002/(SICI)1096-9837(199801)23:1<69::AID-ESP823>3.0.CO;2-G

Langhans, C., Nyman, P., Noske, P.J., Van der Sant, R.E., Lane, P.N.J., Sheridan, G.J., 2017. Post-

fire hillslope debris flows: Evidence of a distinct erosion process. Geomorphology 295, 55–75. https://doi.org/10.1016/j.geomorph.2017.06.008

Le Lay, Y.-F.F., Piégay, H., Moulin, B., 2013. Wood entrance, deposition, transfer and effects on fluvial forms and processes: problem statements and challenging issues. Treatise Geomorphol. 12, 20–36. https://doi.org/10.1016/B978-0-12-374739-6.00320-1

Lee, B.E., Soliman, B.F., 1977. An investigation of the forces on three dimensional bluff bodies in rough wall turbulent boundary layers. J. Fluids Eng. 99, 503–510.

Lee, Z.S., Baas, A.C.W., 2012. Streamline correction for the analysis of boundary layer turbulence. Geomorphology 171–172, 69–82. https://doi.org/10.1016/j.geomorph.2012.05.005

Leenders, J.K., Boxel, J.H. van, Sterk, G., 2007. The effect of single vegetation elements on wind speed and sediment transport in the Sahelian zone of Burkina Faso. Earth Surf. Process. Landforms 32, 1454–1474. https://doi.org/10.1002/esp.1452

Lepofsky, D., Lyons, N., Moss, M.L., 2003. The use of driftwood on the north pacific coast: an example from south east Alaska. J. Ethnobiol. 23, 125–141.

Li, B., Sherman, D.J., 2015. Aerodynamics and morphodynamics of sand fences: A review. Aeolian Res. 17, 33–48. https://doi.org/10.1016/j.aeolia.2014.11.005

Lu, S.S., Willmarth, W.W., 1973. Measurements of the structure of the Reynolds stress in a turbulent boundary layer. J. Fluid Mech. 60, 481–511.

Luo, W., Dong, Z., Qian, G., Lu, J., 2012. Wind tunnel simulation of the three-dimensional airflow patterns behind cuboid obstacles at different angles of wind incidence, and their significance for the formation of sand shadows. Geomorphology 139–140, 258–270. https://doi.org/10.1016/j.geomorph.2011.10.027

Lynch, K., Jackson, D.W.T., Cooper, J.A.G., 2010. Coastal foredune topography as a control on secondary airflow regimes under offshore winds. Earth Surf. Process. Landforms 35, 344–353. https://doi.org/10.1002/esp.1925

Maclennan, A., 2005. An analysis of large woody debris in two Puget Sound salt marshes; Elger Bay, Camano Island, and Sullivan Minor Marsh, Padilla Bay. Western Washington University. MSc Thesis.

Mancini, F., Dubbini, M., Gattelli, M., Stecchi, F., Fabbri, S., Gabbianelli, G., 2013. Using unmanned aerial vehicles (UAV) for high-resolution reconstruction of topography: the structure from motion approach on coastal environments. Remote Sens. 5, 6880–6898. https://doi.org/10.3390/rs5126880

Manga, M., Kirchner, J.W., 2000. Stress partitioning in streams by large woody debris. Water Resour. Res. 36, 2373–2379. https://doi.org/10.1029/2000WR900153

Manners, R.B., Doyle, M.W., Small, M.J., 2007. Structure and hydraulics of natural woody debris jams. Water Resour. Res. 43, 1–17. https://doi.org/10.1029/2006WR004910

Marburg, A.E., Turner, M.G., Kratz, T.K., 2006. Natural and anthropogenic variation in coarse wood among and within lakes. J. Ecol. 94, 558–568. https://doi.org/10.1111/j.1365-2745.2006.01117.x

Marshall, P.L., Davis, G., 2002. Measuring the length of coarse woody debris. Ext. Note EN-011 8.

Maser, C., Cline, S.P., Cromack, K., Trappe, J.M., Hansen, E., 1988. Chapter 2. What we know about large trees that fall to the forest floor, in: Maser, C., Terrant, R.F., Trappe, J.M., Franklin, J.F. (Eds.), From the Forest to the Sea: A Story of Fallen Trees. U.S. Department of Agriculture, Portland, Oregon, pp. 25–45.

May, C.L., Gresswell, R.E., 2003a. Large wood recruitment and redistribution in headwater streams in the southern Oregon Coast. Can. J. For. Res. 33, 1352–1362. https://doi.org/10.1139/X03-023

May, C.L., Gresswell, R.E., 2003b. Processes and rates of sediment and wood accumulation in headwater streams of the Oregon Coast Range, USA. Earth Surf. Process. Landforms 28, 409–424. https://doi.org/10.1002/esp.450

Mayaud, J.R., Wiggs, G.F.S., Bailey, R.M., 2016a. Characterizing turbulent wind flow around dryland vegetation. Earth Surf. Process. Landforms 1436, 1421–1436. https://doi.org/10.1002/esp.3934

Mayaud, J.R., Wiggs, G.F.S., Bailey, R.M., 2016b. Dynamics of skimming flow in the wake of a vegetation patch. Aeolian Res. 22, 141–151. https://doi.org/10.1016/j.aeolia.2016.08.001

McKenna Neuman, C., Bédard, O., 2015. A wind tunnel study of flow structure adjustment on

deformable sand beds containing a surface-mounted obstacle. J. Geophys. Res. Earth Surf. 120, 1824–1840. https://doi.org/10.1002/2015JF003475

McLaren, D., Fedje, D., Dyck, A., Mackie, Q., Gauvreau, A., Cohen, J., 2018. Terminal Pleistocene epoch human footprints from the Pacific coast of Canada. PLoS One 13, e0193522. https://doi.org/10.1371/journal.pone.0193522

McLaren, D., Fedje, D., Hay, M.B., Mackie, Q., Walker, I.J., Shugar, D.H., Eamer, J.B.R., Lian, O.B., Neudorf, C., 2014. A post-glacial sea level hinge on the central Pacific coast of Canada. Quat. Sci. Rev. 97, 148–169. https://doi.org/10.1016/j.quascirev.2014.05.023

Mendoza, E.T., Jiménez, J.A., 2005. Factors controlling vulnerability to storm impacts along the Catalonian coast, in: Smith, J.M. (Ed.), Proceedings of the 29th International Conference Coastal Engineering 2004. World Scientific Publishing Company, pp. 3087–3099. https://doi.org/10.1142/9789812701916_0249

Miot da Silva, G., Hesp, P., 2010. Coastline orientation, aeolian sediment transport and foredune and dunefield dynamics of Moçambique Beach, Southern Brazil. Geomorphology 120, 258–278. https://doi.org/10.1016/j.geomorph.2010.03.039

Montreuil, A.-L., Bullard, J., Chandler, J., 2013. Detecting seasonal variations in embryo dune morphology using a terrestrial laser scanner. J. Coast. Res. 165, 1313–1318. https://doi.org/10.2112/SI65-222.1

Nakamura, F., Swanson, F.J., 1993. Effects of coarse woody debris in morphology and sediment storage of a mountain stream system in Western Oregon. Earth Surf. Process. Landforms 18, 43–61.

Nakamura, F., Swanson, F.J., Wondzell, S.M., 2000. Disturbance regimes of stream and riparian systems - A disturbance-casade perspective. Hydrol. Process. 14, 2849–2860. https://doi.org/10.1002/1099-1085(200011/12)14:16/17<2849::AID-HYP123>3.0.CO;2-X

Namikas, S.L., Edwards, B.L., Bitton, M.C.A., Booth, J.L., Zhu, Y., 2010. Temporal and spatial variabilities in the surface moisture content of a fine-grained beach. Geomorphology 114, 303–310. https://doi.org/10.1016/j.geomorph.2009.07.011

Nickling, W., Davidson-Arnott, R., 1990. Aeolian sediment transport on beaches and coastal sand dunes, in: Proceedings Canadian Symposium on Coastal Sand Dunes.

Nordstrom, C.E., Inman, D.L., 1975. Sand level changes on Torrey Pines beach, California. Fort Belvair, Virginia. URL http://oai.dtic.mil/oai/oai?verb=getRecord&metadataPrefix=html&identifier=ADA019833 (accessed 10.23.13).

Nordstrom, K.F., Jackson, N.L., 1992. Effect of source width and tidal elevation changes on aeolian transport on an estuarine beach. Sedimentology 39, 769–778. https://doi.org/10.1111/j.1365-3091.1992.tb02152.x

Nordstrom, K.F., Jackson, N.L., Hartman, J.M., Wong, M., 2007. Aeolian sediment transport on a human-altered foredune. Earth Surf. Process. Landforms 32, 102–115. https://doi.org/10.1002/esp.1377

Nordstrom, K.F., Jackson, N.L., Klein, A.H.F., Sherman, D.J., Hesp, P.A., 2006. Offshore aeolian transport across a low foredune on a developed barrier island. J. Coast. Res. 225, 1260–1267. https://doi.org/10.2112/06A-0008.1

Nordstrom, K.F., Jackson, N.L., Korotky, K.H., 2011. Aeolian sediment transport across beach wrack. J. Coast. Res. 59, 211–217. https://doi.org/10.2112/SI59-022.1

Nordstrom, K.F., Lampe, R., Vandemark, L.M., 2000. Reestablishing naturally functioning dunes on developed coasts. Environ. Manage. 25, 37–51. https://doi.org/10.1007/s002679910004

Ollerhead, J., Davidson-Arnott, R., Walker, I.J., Mathew, S., 2013. Annual to decadal morphodynamics of the foredune system at Greenwich Dunes, Prince Edward Island, Canada. Earth Surf. Process. Landforms 38, 284–298. https://doi.org/10.1002/esp.3327

Page, N., Lilley, P., Walker, I.J., Vennesland, R.G., 2011. Status report on coastal sand ecosystems in British Columbia. Vancouver, B.C. URL http://www.raincoastappliedecology.ca/wp-content/uploads/2012/09/CSE-Status-Report-2011.pdf

Parise, M., Cannon, S.H., 2017. Debris flow generation in burned catchments, in: Mikoš, M., Casagli, N., Yin, Y., Sassa, K. (Eds.), Advancing Culture of Living with Landslides. Springer, pp. 643–650.

Pattenden, R.J., Turnock, S.R., Zhang, X., 2005. Measurements of the flow over a low-aspect-

ratio cylinder mounted on a ground plane. Exp. Fluids 39, 10–21. https://doi.org/10.1007/s00348-005-0949-9

Perry, A.E., Schofield, W.H., Joubert, P.N., 1969. Rough wall turbulent boundary layers. J. Fluid Mech. 37, 383–413. https://doi.org/10.1017/S0022112069000619

Pethick, J., 1984. An Introduction to Coastal Geomorphology. Edward Arnold, London.

Piscioneri, N., Smyth, T.A.G., Hesp, P.A., 2019. Flow dynamics over a foredune scarp. Earth Surf. Process. Landforms. https://doi.org/10.1002/esp.4555

Pye, K., Blott, S.J., 2016. Assessment of beach and dune erosion and accretion using LiDAR: Impact of the stormy 2013–14 winter and longer term trends on the Sefton Coast, UK. Geomorphology 266, 146–167. https://doi.org/10.1016/j.geomorph.2016.05.011

Pye, K., Tsoar, H., 1990. Aeolian Sand and Sand Dunes. Unwin Hyman, Inc., Cambridge, MA.

Qian, G., Dong, Z., Luo, W., Lu, J., 2011. Mean airflow patterns upwind of topographic obstacles and their implications for the formation of echo dunes: A wind tunnel simulation of the effects of windward slope. J. Geophys. Res. Earth Surf. 116, 1–12. https://doi.org/10.1029/2011JF002020

R Core Team, 2018. R: A language and environment for statistical computing [WWW Document]. URL https://www.r-project.org/

Ralph, S.C., Poole, G.C., Conquest, L.L., Naiman, R.J., 1994. Stream channel morphology and woody debris in logged and unlogged basins of western Washington. Can. J. Fish. Aquat. Sci. 51, 37–51. https://doi.org/10.1139/f94-006

Raupach, M.R., 1992. Drag and drag partition on rough surfaces. Boundary-Layer Meteorol. 60, 375–395. https://doi.org/10.1007/BF00155203

Raupach, M.R., Gillette, D.A., Leys, J.F., 1993. The effect of roughness elements on wind erosion threshold. J. Geophys. Res. 98, 3023–3029.

Ray, G.L., 2005. Invasive marine and estuarine animals of the South Atlantic and Puerto Rico. Aquat. Nuis. Species Progr. Vicksbg. MS 1–14.

Reeves, G.H., Burnett, K.M., McGarry, E. V, 2003. Sources of large wood in the main stem of a fourth-order watershed in coastal Oregon. Can. J. For. Res. 33, 1363–1370. https://doi.org/10.1139/x03-095

Riegl, 2010. How to generate a DTM in RiScan Pro [WWW Document]. URL http://www.riegl.com/media-events/newsletter-archiv/1011-news-from-the-software-side-how-to-generate-a-dtm-in-riscan-pro/

Roberts, B., Ward, B., Rollerson, T., 2004. A comparison of landslide rates following helicopter and conventional cable-based clear-cut logging operations in the Southwest Coast Mountains of British Columbia. Geomorphology 61, 337–346. https://doi.org/10.1016/j.geomorph.2004.01.007

Robertson-Rintoul, M.J., 1990. A quantitative analysis of near-surface wind flow pattern over coastal parabolic dunes, in: Nordstrom, K.F., Psuty, N.P., Carter, R.W.G. (Eds.), Coastal Dunes, Form and Process. John Wiley & Sons Ltd., West Sussex, England, pp. 57–78.

Roelvink, D., Costas, S., 2019. Coupling nearshore and aeolian processes: XBeach and duna process-based models. Environ. Model. Softw. 115, 98–112. https://doi.org/10.1016/j.envsoft.2019.02.010

RStudio Team, 2016. RStudio: integrated development environment for R [WWW Document]. URL http://www.rstudio.com/

Ruiz-Villanueva, V., Díez-Herrero, A., Ballesteros, J.A., Bodoque, J.M., 2014. Potential large woody debris recruitment due to landslides, bank erosion and floods in mountain basins: A quantitative estimation approach. River Res. Appl. 30, 81–97. https://doi.org/10.1002/rra.2614

Sarkar, S., Dey, S., 2010. Double-averaging turbulence characteristics in flows over a gravel bed. J. Hydraul. Res. 48, 801–809. https://doi.org/10.1080/00221686.2010.526764

Scott, D.N., Wohl, E.E., 2018. Natural and anthropogenic controls on wood loads in river corridors of the Rocky, Cascade, and Olympic Mountains, USA. Water Resour. Res. i, 1–17. https://doi.org/10.1029/2018WR022754

Sedell, J.R., Bisson, P.A., Swanson, F.J., Gregory, S. V, 1988. Chapter 3. What We Know About Large Trees That Fall Into Streams and Rivers, in: Maser, C., Terrant, R.F., Trappe, J.M., Franklin, J.F. (Eds.), From the Forest to the Sea: A Story of Fallen Trees. U.S. Department of Agriculture, Portland, pp. 47–81.

Sedell, J.R., Leone, F.N., Duval, W.S., 1991. Water transportation and storage of logs, in:

Meehan, W.R. (Ed.), American Fisheries Society Special Publication 19. Bethesda, Maryland, pp. 325–368.

Shepard, F.P., 1950. Beach cycles in southern California, Beach erosion board technical memorandum. Beach Erosion Board, Corps of Engineers, Washington D.C.

Sherman, D.J., 1995. Problems of scale in the modeling and interpretation of coastal dunes. Mar. Geol. 124, 339–349.

Sherman, D.J., Bauer, B.O., 1993. Dynamics of beach-dune systems. Prog. Phys. Geogr. 17, 413–447. https://doi.org/10.1177/030913339301700402

Short, A.D., Jackson, D.W.T., 2013. Beach morphodynamics, in: Shroder, J.F., Sherman, D.J. (Eds.), Treatise on Geomorphology Vol 10: Coastal Geomorphology. Elsevier Inc., San Diego, California, pp. 106–129.

Shugar, D.H., Walker, I.J., Lian, O.B., Eamer, J.B.R., Neudorf, C., McLaren, D., Fedje, D., 2014. Post-glacial sea-level change along the Pacific coast of North America. Quat. Sci. Rev. 97, 170–192. https://doi.org/10.1016/j.quascirev.2014.05.022

Sidle, R.C., Ziegler, A.D., Negishi, J.N., Nik, A.R., Siew, R., Turkelboom, F., 2006. Erosion processes in steep terrain - Truths, myths, and uncertainties related to forest management in Southeast Asia. For. Ecol. Manage. 224, 199–225. https://doi.org/10.1016/j.foreco.2005.12.019

Smit, Y., Ruessink, G., Brakenhoff, L.B., Donker, J.J.A., 2018. Measuring spatial and temporal variation in surface moisture on a coastal beach with a near-infrared terrestrial laser scanner. Aeolian Res. 31, 19–27. https://doi.org/10.1016/j.aeolia.2017.07.004

Smith, M.W., 2014. Roughness in the earth sciences. Earth-Science Rev. 136, 202–225. https://doi.org/10.1016/j.earscirev.2014.05.016

Smith, R.D., Sidle, R.C., Porter, P.E., Noel, J.R., 1993. Effects of experimental removal of woody debris on the channel morphology of a forest, gravel-bed stream. J. Hydrol. 152, 153–178. https://doi.org/10.1016/0022-1694(93)90144-X

Smyth, T.A.G., Jackson, D., Cooper, A., 2014. Airflow and aeolian sediment transport patterns within a coastal trough blowout during lateral wind conditions. Earth Surf. Process. Landforms 39, 1847–1854. https://doi.org/10.1002/esp.3572

Stembridge, J.E.J., 1979. Beach protection properties of accumulated driftwood, in: Proceedings of the Specialty Conference on Coastal Structures. US Army Corps of Engineers, Alexandria, Virginia, pp. 1052–1068.

Stembridge, J.E.J., 1975. Recent shoreline changes of the Alsea sandspit, Lincoln County, Oregon. Ore Bin 37.

Sterk, G., Jacobs, A.F.G., Boxel, J.H.V.A.N., 1998. The effect of turbulent flow structures on saltation sand transport in the atmospheric boundary layer 887, 877–887. https://doi.org/10.1002/(SICI)1096-9837(199810)23

Stout, J.E., Zobeck, T.M., 1997. Intermittent saltation. Sedimentology 44, 959–970. https://doi.org/10.1046/j.1365-3091.1997.d01-55.x

Strong, C.C., Skolmen, R.G., 1963. Origin of drift-logs on the beaches of Hawaii. Nature 197, 890. https://doi.org/10.1038/197890a0

Sutton, S.L.F., McKenna Neuman, C., 2008. Sediment entrainment to the lee of roughness elements: Effects of vortical structures. J. Geophys. Res. Earth Surf. 113, 1–7. https://doi.org/10.1029/2007JF000783

Svasek, J.N., Terwindt, J.H.J., 1974. Measurements of sand transport by wind on a natural beach. Sedimentology 21, 311–322. https://doi.org/10.1111/j.1365-3091.1974.tb02061.x

Sweet, M.L., Kocurek, G., 1990. An empirical model of aeolian dune lee-face airflow. Sedimentology 37, 1023–1038. https://doi.org/10.1111/j.1365-3091.1990.tb01843.x

Telling, J., Lyda, A., Hartzell, P., Glennie, C., 2017. Review of earth science research using terrestrial laser scanning. Earth-Science Rev. https://doi.org/10.1016/j.earscirev.2017.04.007

Terich, T.A., Milne, S., 1977. The effects of wood debris and drift logs on estuarine beaches of northern Puget Sound. Dept. of Geography and Regional Planning, Western Washington University, Bellingham, Washington. URL http://scholar.google.com/scholar?hl=en&btnG=Search&q=intitle:The+Effects+of+Wood+Debris+and+Drift+Logs+on+Estuarine+Beaches+of+Northern+Puget+Sound#0 (accessed 5.22.14).

Tomita, M., Hirabuki, Y., Kanno, H., Hara, K., 2016. Influences of large, infrequent disturbance

caused by tsunami on coastal forest communities, in: Urabe, J., Nakashizuka, T. (Eds.), Ecological Impacts of Tsunamis on Coastal Ecosystems. Springer, Tokyo, Japan, pp. 383–394.

Tsoar, H., 2001. Types of aeolian Sand dunes, in: Balmforth, N.J., Provenzale, A. (Eds.), Geomorphological Fluid Mechanics. Springer-Verlag, Berlin Heidelberg, pp. 403–429.

Tsoar, H., 1983. Wind tunnel modeling of echo and climbing dunes, in: Developments in Sedimentology. Elsevier, pp. 247–259. https://doi.org/10.1016/S0070-4571(08)70798-2

Tsoar, H., Blumberg, D., 2011. The effect of sea cliffs on inland encroachment of aeolian sand, in: Aeolian Grain Transport. Springer, pp. 131–146. https://doi.org/10.1007/978-3-7091-6703-8_10

Turner, N.J., 1998. Plant technology of First Peoples in British Columbia. University of British Columbia Press, Royal British Columbia Museum, Vancouver, Victoria, B.C.

van Boxel, J.H., Sterk, G., Arens, S.M., 2004. Sonic anemometers in aeolian sediment transport research. Geomorphology 59, 131–147. https://doi.org/10.1016/j.geomorph.2003.09.011

Vandenbruwaene, W., Temmerman, S., Bouma, T.J., Klaassen, P.C., De Vries, M.B., Callaghan, D.P., Van Steeg, P., Dekker, F., Van Duren, L. a., Martini, E., Balke, T., Biermans, G., Schoelynck, J., Meire, P., 2011. Flow interaction with dynamic vegetation patches: Implications for biogeomorphic evolution of a tidal landscape. J. Geophys. Res. Earth Surf. 116, 1–13. https://doi.org/10.1029/2010JF001788

Vu, V.Q., 2011. ggbiplot: A ggplot2 based biplot [WWW Document]. URL http://github.com/vqv/ggbiplot

Waelti, A.E., MacCleod, D.I., 1971. British Columbia forest service log and debris salvage in the Strait of Georgia. Victoria, B.C.

Walker, I.J., 2005. Physical and logistical considerations of using ultrasonic anemometers in aeolian sediment transport research. Geomorphology 68, 57–76. https://doi.org/10.1016/j.geomorph.2004.09.031

Walker, I.J., 1999. Secondary airflow and sediment transport in the lee of a reversing dune. Earth Surf. Process. Landforms 24, 437–448. https://doi.org/10.1002/(SICI)1096-9837(199905)24:5<437::AID-ESP999>3.0.CO;2-Z

Walker, I.J., Barrie, J. V., 2006. Geomorphology and sea-level rise on one of Canada's most sensitive coasts: northeast Graham Island, British Columbia, in: Journal of Coastal Research. Journal of Coastal Research, Itajai, SC, Brazil, pp. 220–226.

Walker, I.J., Davidson-Arnott, R.G.D., Bauer, B.O., Hesp, P.A., Delgado-Fernandez, I., Ollerhead, J., Smyth, T.A.G., 2017. Scale-dependent perspectives on the geomorphology and evolution of beach-dune systems. Earth-Science Rev. https://doi.org/10.1016/j.earscirev.2017.04.011

Walker, I.J., Davidson-Arnott, R.G.D., Hesp, P.A., Bauer, B.O., Ollerhead, J., 2009a. Mean flow and turbulence responses in airflow over foredunes: new insights from recent research. J. Coast. Res. 2009, 366–370.

Walker, I.J., Hesp, P.A., 2013. Fundamentals of aeolian sediment transport: airflow over dunes, in: Shroder, J.F. (Editor in C., Lancaster, N., Sherman, D.J., Baas, A.C.W. (Eds.), Treatise on Geomorphology, Vol 11: Aeolian Geomorphology. Academic Press, San Diego, California, pp. 109–133. https://doi.org/10.1016/B978-0-12-374739-6.00300-6

Walker, I.J., Hesp, P.A., Davidson-Arnott, R.G.D., Bauer, B.O., Namikas, S.L., Ollerhead, J., 2009b. Responses of three-dimensional flow to variations in the angle of incident wind and profile form of dunes: Greenwich Dunes, Prince Edward Island, Canada. Geomorphology 105, 127–138. https://doi.org/10.1016/j.geomorph.2007.12.019

Walker, I.J., Hesp, P.A., Davidson-Arnott, R.G.D., Ollerhead, J., 2006. Topographic steering of alongshore airflow over a vegetated foredune: Greenwich dunes, Prince Edward Island, Canada. J. Coast. Res. 225, 1278–1291. https://doi.org/10.2112/06A-0010.1

Walker, I.J., Nickling, W.G., 2002. Dynamics of secondary airflow and sediment transport over and in the lee of transverse dunes. Prog. Phys. Geogr. 26, 47–75. https://doi.org/10.1191/0309133302pp325ra

Wallerstein, N.P., Thorne, C.R., 2004. Influence of large woody debris on morphological evolution of incised, sand-bed channels. Geomorphology 57, 53–73. https://doi.org/10.1016/S0169-555X(03)00083-7

Wang, W., Zhao, W., Huang, L., Vimarlund, V., Wang, Z., 2014. Applications of terrestrial laser scanning for tunnels: a review. J. Traffic Transp. Eng. (English Ed. 1, 325–337.

https://doi.org/10.1016/S2095-7564(15)30279-8

Weaver, C.M., Wiggs, G.F.S., 2011. Field measurements of mean and turbulent airflow over a barchan sand dune. Geomorphology 128, 32–41. https://doi.org/10.1016/j.geomorph.2010.12.020

Wells, W.G.I., 1987. The effects of fire on the generation of debris flows in southern California, in: Costa, J.E., Wieczorek, G.F. (Eds.), Debris Flows/Avalanches. Geological Society of America.

West, A.J., Lin, C.W., Lin, T.C., Hilton, R.G., Liu, S.H., Chang, C.T., Lin, K.C., Galy, A., Sparkes, R.B., Hovius, N., 2011. Mobilization and transport of coarse woody debris to the oceans triggered by an extreme tropical storm. Limnol. Oceanogr. 56, 77–85. https://doi.org/10.4319/lo.2011.56.1.0077

Westoby, M.J., Brasington, J., Glasser, N.F., Hambrey, M.J., Reynolds, J.M., 2012. "Structure-from-Motion" photogrammetry: A low-cost, effective tool for geoscience applications. Geomorphology 179, 300–314. https://doi.org/10.1016/j.geomorph.2012.08.021

Wheaton, J.M., Brasington, J., Darby, S.E., Sear, D.A., 2010. Accounting for uncertainty in DEMs from repeat topographic surveys: Improved sediment budgets. Earth Surf. Process. Landforms 35, 136–156. https://doi.org/10.1002/esp.1886

White, B.R., Tsoar, H., 1998. Slope effect on saltation over a climbing sand dune. Geomorphology 22, 159–180. https://doi.org/10.1016/S0169-555X(97)00058-5

Wickham, H., 2018. Scales: scale functions for visualization [WWW Document]. URL https://cran.r-project.org/package=scales

Wickham, H., 2015. Elegant graphics for data analysis. Springer-Verlag New York. https://doi.org/10.1007/978-0-387-98141-3

Wickham, H., 2011. The split-apply-combine strategy for data analysis [WWW Document]. J. Stat. Softw. https://doi.org/10.18637/jss.v040.i01

Wickham, H., Hester, J., Chang, W., 2018. devtools: tools to make developing R packages easier [WWW Document]. URL https://cran.r-project.org/package=devtools

Wiggs, G.F.S., Livingstone, I., Warren, A., 1996. The role of streamline curvature in sand dune dynamics: evidence from field and wind tunnel measurements. Geomorphology 17, 29–46.

Williams, G.L., Cooper, D., 2000. Characterization of wood debris in the Lower Fraser River estuary. Burnaby, B.C.

Wohl, E., 2017. Bridging the gaps: An overview of wood across time and space in diverse rivers. Geomorphology 279, 3–26. https://doi.org/10.1016/j.geomorph.2016.04.014

Wolfe, S.A., Nickling, W.G., 1993. The protective role of sparse vegetation in wind erosion. Prog. Phys. Geogr. 17, 50–68. https://doi.org/10.1177/030913339301700104

Wolter, A., Ward, B., Millard, T., 2010. Instability in eight sub-basins of the Chilliwack River Valley, British Columbia, Canada: A comparison of natural and logging-related landslides. Geomorphology 120, 123–132. https://doi.org/10.1016/j.geomorph.2010.03.008

Wright, L.D., Thom, B.G., 1977. Coastal depositional landforms: a morphodynamic approach. Prog. Phys. Geogr. 1, 412–459. https://doi.org/10.1177/030913337700100302

Yuxiang, D., Hesp, P.A., Dequan, H., Namikas, S.L., 2017. Flow dynamics and sediment transport over a reversing barchan, Changli, China. Geomorphology 278, 121–127. https://doi.org/10.1016/j.geomorph.2016.11.004

7. Appendices

7.1 Appendix 1

Summary of observed flow properties for each 10 min run including surface slope angle and incident flow angle (degrees), resultant 3D wind speed (S, m s^{-1}), flow streamline angles (degrees), Normal Reynolds stresses ($\overline{u'^2}, \overline{v'^2}, \overline{w'^2}$, m^2 s^{-2}), total kinetic energy (TKE, m^2 s^{-2}), Horizontal kinematic Reynolds stress (RS_{Hk}, m^2 s^{-2}), and coefficient of variation (CV_u). Flow angle is relative to true north. Streamline angles and surface slope angles are relative to horizontal (0°).

	T1 (LWD)				T2 (No LWD)			
	Beach lower (.5 m)	Beach upper (1.5 m)	Stoss lower (.5 m)	Stoss upper (1.5 m)	Beach lower (.5 m)	Beach upper (1.5 m)	Stoss lower (.5 m)	Stoss upper (1.5 m)
surface slope angle (o)	-4	-4	-23	-23	-4	-4	-37	-37
13 April 2016								
Run 1 (13:35:20-13:45:19)								
Flow angle (o)	151	153	145	148	152	153	159	155
S	2.4	3.2	2.3	2.9	3.5	3.8	2.7	3.2
Streamline angle (o)	-2.94	-2.87	-8.46	-9.79	-0.31	-2.00	-16.09	-15.93
$\overline{u'^2}$	2.03	2.61	1.11	1.61	2.01	2.15	1.41	1.72
$\overline{v'^2}$	0.63	1.24	0.89	1.15	1.21	1.38	1.17	1.52
$\overline{w'^2}$	0.08	0.15	0.18	0.24	0.04	0.10	0.27	0.40
TKE	1.37	2.00	1.09	1.51	1.63	1.82	1.43	1.82
RS_{Hk}	0.11	0.08	1.61	0.31	0.09	0.10	0.47	0.57
CVu	0.67	0.57	0.53	0.50	0.43	0.41	0.52	0.47
Run 2 (13:56:40-14:06:39)								
Flow angle (o)	161	161	162	159	151	151	155	151
S	1.8	2.6	2.0	2.4	3.1	3.3	2.2	2.6
Streamline angle (o)	-7.24	-3.08	-11.62	-9.96	0.19	-1.85	-14.68	-13.74
$\overline{u'^2}$	1.77	2.59	1.48	1.87	2.17	2.27	1.51	1.71
$\overline{v'^2}$	0.70	1.20	1.19	1.20	1.66	1.55	1.12	1.27
$\overline{w'^2}$	0.09	0.21	0.16	0.29	0.06	0.14	0.26	0.37
TKE	1.28	2.00	1.42	1.68	1.95	1.98	1.44	1.68
RS_{Hk}	0.19	0.04	1.87	0.25	0.16	0.13	0.43	0.47
CVu	0.96	0.77	0.87	0.72	0.54	0.51	0.68	0.61
Run 3 (14:43:50-14:53:49)								
Flow angle (o)	155	158	152	150	144	144	155	151
S	2.6	3.5	2.6	3.2	3.9	4.2	3.0	3.5

Streamline angle (o)	-5.50	-3.00	-10.21	-8.15	0.57	-0.86	-15.09	-12.87
$\overline{u'^2}$	2.37	3.86	2.27	3.39	3.46	3.76	2.30	3.02
$\overline{v'^2}$	1.15	1.97	1.91	1.99	2.66	2.82	1.67	1.90
$\overline{w'^2}$	0.13	0.23	0.27	0.49	0.07	0.20	0.39	0.70
TKE	1.83	3.04	2.23	2.94	3.10	3.39	2.18	2.81
RS_{Hk}	0.24	0.14	3.39	0.53	0.23	0.34	0.66	0.81
CVu	0.73	0.66	0.77	0.72	0.54	0.51	0.60	0.56
Run 4 (15:05:50-15:15:49)								
Flow angle (o)	157	159	153	153	141	143	150	146
S	2.1	3.0	2.2	2.7	3.4	3.7	2.6	3.1
Streamline angle (o)	-8.57	-3.28	-10.65	-7.43	0.35	-1.81	-12.09	-11.76
$\overline{u'^2}$	1.88	2.82	1.49	2.06	2.91	3.33	2.09	2.46
$\overline{v'^2}$	0.72	1.13	1.21	1.28	1.46	1.46	1.00	1.19
$\overline{w'^2}$	0.10	0.19	0.23	0.34	0.04	0.14	0.30	0.45
TKE	1.35	2.07	1.47	1.84	2.21	2.47	1.70	2.05
RS_{Hk}	0.27	0.06	2.06	0.30	0.12	0.15	0.45	0.48
CVu	0.75	0.62	0.71	0.61	0.54	0.53	0.62	0.57
15 April 2016								
Run 5 (11:22:00-11:31:59)								
Flow angle (o)	152	161	157	160	170	172	174	172
S	3.3	4.7	3.5	4.4	4.6	5.2	3.6	4.3
Streamline angle (o)	-1.24	-5.18	-8.38	-11.21	-1.17	-4.15	-21.03	-19.78
$\overline{u'^2}$	1.19	1.42	1.11	1.39	1.05	1.29	0.92	1.14
$\overline{v'^2}$	1.02	2.26	1.81	2.30	2.27	2.63	2.17	2.63
$\overline{w'^2}$	0.11	0.14	0.23	0.30	0.03	0.09	0.32	0.42
TKE	1.16	1.91	1.57	2.00	1.67	2.01	1.70	2.10
RS_{Hk}	1.02	2.26	1.81	2.30	2.27	2.63	2.17	2.63
CVu	0.35	0.27	0.32	0.29	0.23	0.23	0.30	0.27
Run 6 (11:43:54-11:52:53)								
Flow angle (o)	147	155	148		157	160	162	161
S	4.0	5.5	4.4		5.4	6.1	4.6	5.4
Streamline angle (o)	-1.26	-5.31	-6.10		-0.66	-3.21	-16.75	-16.11
$\overline{u'^2}$	1.66	2.27	1.86		1.71	2.13	1.74	1.98
$\overline{v'^2}$	1.06	2.69	1.81		2.43	2.80	2.43	3.08
$\overline{w'^2}$	0.11	0.15	0.28		0.03	0.09	0.41	0.49
TKE	1.42	2.56	1.98		2.09	2.51	2.29	2.78
RS_{Hk}	0.14	0.27	0.65		0.18	0.24	0.96	0.97
CVu	0.34	0.29	0.33		0.25	0.25	0.31	0.28
Run 7 (12:09:30-12:19:29)								
Flow angle (o)	149	158	155		167	169	172	171
S	3.6	5.2	4.0		5.7	6.3	4.4	5.2
Streamline angle (o)	-1.11	-5.02	-8.00		-1.23	-4.16	-20.26	-18.99
$\overline{u'^2}$	1.40	1.84	1.57		1.63	1.95	1.33	1.54
$\overline{v'^2}$	1.36	3.45	2.48		3.80	4.49	3.48	4.26

$\overline{w'^2}$	0.13	0.17	0.29	0.04	0.09	0.44	0.56
TKE	1.44	2.73	2.18	2.74	3.27	2.63	3.18
RS_{Hk}	0.12	0.29	0.73	0.24	0.35	1.06	1.22
CVu	0.35	0.28	0.34	0.24	0.23	0.29	0.26
Run 8 (13:31:00-13:40:59)							
Flow angle (o)	144	152	144	152	154	155	155
S	4.1	5.8	4.2	5.6	6.2	4.9	5.7
Streamline angle (o)	-0.87	-4.50	-6.07	-0.26	-2.60	-14.58	-13.84
$\overline{u'^2}$	1.46	2.22	1.78	2.24	2.78	2.23	2.71
$\overline{v'^2}$	1.78	4.09	2.17	2.19	2.59	2.34	2.73
$\overline{w'^2}$	0.14	0.23	0.36	0.03	0.09	0.48	0.58
TKE	1.70	3.28	2.16	2.24	2.73	2.53	3.02
RS_{Hk}	0.15	0.36	0.71	0.14	0.20	1.05	1.15
CVu	0.32	0.27	0.34	0.28	0.28	0.33	0.30